



저작자표시-비영리-변경금지 2.0 대한민국

이용자는 아래의 조건을 따르는 경우에 한하여 자유롭게

- 이 저작물을 복제, 배포, 전송, 전시, 공연 및 방송할 수 있습니다.

다음과 같은 조건을 따라야 합니다:



저작자표시. 귀하는 원저작자를 표시하여야 합니다.



비영리. 귀하는 이 저작물을 영리 목적으로 이용할 수 없습니다.



변경금지. 귀하는 이 저작물을 개작, 변형 또는 가공할 수 없습니다.

- 귀하는, 이 저작물의 재이용이나 배포의 경우, 이 저작물에 적용된 이용허락조건을 명확하게 나타내어야 합니다.
- 저작권자로부터 별도의 허가를 받으면 이러한 조건들은 적용되지 않습니다.

저작권법에 따른 이용자의 권리는 위의 내용에 의하여 영향을 받지 않습니다.

이것은 [이용허락규약\(Legal Code\)](#)을 이해하기 쉽게 요약한 것입니다.

[Disclaimer](#)

**A THESIS
FOR THE DOCTOR OF PHILOSOPHY**

**Development of Flexible SWCNT based Supercapacitors through
Electrohydrodynamic Atomization Technique**

Sridharan Sundharam

Department of Mechatronics Engineering

GRADUATE SCHOOL

JEJU NATIONAL UNIVERSITY

February 2014

Development of Flexible SWCNT based Supercapacitors through Electrohydrodynamic Atomization Technique

Sridharan Sundharam

(Supervised by Professor Kyung Hyun Choi)

A thesis submitted in partial fulfillment of the requirement for the degree of

DOCTOR OF PHILOSOPHY

2014. 2

The thesis has been examined and approved by

Ki Rin Kwon

Thesis Director, Ki Rin Kwon, Professor, Department of Mechanical Engineering

Yang-Hoi Doh

Yang-Hoi Doh, Professor, Department of Electronic Engineering

Jeongda Jo

Jeongda Jo, Professor, Korea Institute of Machinery and Materials

Choi Kyung Hyun

Kyung-Hyun Choi, Professor, Department of Mechatronics Engineering

Hong Dong Peoh

Hong Dong Peoh, Professor, Ph.D., Chonbuk National University

Date

Department of Mechatronics Engineering

GRADUATE SCHOOL

JEJU NATIONAL UNIVERSITY

REPUBLIC OF KOREA



To
My Parents

Acknowledgments

I would like to thank everyone who made a contribution to this work. I thank my parents who raised me with unconditional love and care and supported me in all my endeavors. I would like to express my sincere gratitude to my research advisor, Prof. Kyung Hyun Choi, for providing me the opportunity to pursue my research here. I am grateful for his contributions of time, insightful discussions and his support which made my research experience a constructive one. When I had to go through a harrowing phase in life and decided to quit, he took a magnanimous gesture, gave me time and space to get back on track. I will ever be grateful to him for having faith in me despite the odds.

I would also thank the members of my Ph.D. committee, Prof. Ki Rin Kwon, Prof. Yang-Hoi Doh, Prof. Jeongdai Jo, Prof. Kyung-Hyun Choi, and Prof. Hong Dong Peoh who monitored my work and rendered their time in reading and providing me with valuable suggestions for making this study an appreciable one.

Dr. Ganesh Thangaraj was the first lab mate I got introduced to, who later became one of my close friends. His moral support has always been there through the ups and downs and I would like thank him for that. I thank my seniors in Jeju Dr. Rajneesh, Dr. Shrikanth, and Dr. Gunasekaran for their support.

I also would like to thank my lab mates who have constituted a challenging research atmosphere. Dr. Ahsan, Dr. Nauman, Dr. Khalid, Mr. Saleem, Mr. Arshad, Dr. Naeem, Mr. Zubair, Mr. Kamran, Mr. Adnan, Mr. Murtaza and Mr. Navaneethan made the atmosphere lively. I would like to thank my native colleagues who were there when I needed help. I thank my friends Mr. Saravanakumar, Mr. Anantha kumar, Mr. Thyagarajan, Mr. Sebastian Dr. Dharaneedharan and Dr. Saranya for providing support that I needed. I would like to thank everyone I missed out to mention for contributing to my accomplishments.

Contents

List of Figures	iv
Abstract.....	vi
1. Introduction.....	1
1.1 Motivation.....	1
1.2 Types of energy storage technologies.....	6
1.3 Thin film fabrication techniques.....	24
1.4 Aims and outline.....	31
2. Background.....	33
2.1 Supercapacitors.....	33
2.2 Electrohydrodynamic atomization.....	48
3. ITO Current collector.....	59
3.1 Introduction.....	59
3.2 Experimental.....	60
3.3 Results and discussion.....	64
3.4 Conclusion.....	71
4. Fabrication of flexible SWCNT active layers.....	72
4.1 Introduction.....	72
4.2 Materials and methods.....	74
4.3 Results and discussion.....	81
4.4 Conclusion.....	92

5. Conclusions and future work.....93

 5.1 Summary and major conclusions.....93

 5.2 Future work.....95

References.....96

List of Figures

Figure 2-1 Schematic illustration of charging/discharging process in supercapacitor.....	35
Figure 2-1 Deformation of a pendant drop upon application of electric field and formation of cone-jet transition.....	53
Figure 2-3 EHD spray setup.....	53
Figure 2-4 Electro spray modes.....	54
Figure 2-5 Cone shape, droplet size and electric current depend on the forces acting on liquid and dissolved ions: gravity, electric field, surface tension.....	57
Figure 3-1 ITO ink synthesized at three different concentrations.....	61
Figure 3-2 (a) Operating envelope (b) Stable conjet of 20 wt% ITO ink.....	62
Figure 3-3 (a) Operating envelope (b) Stable conjet of 10 wt% ITO ink.....	63
Figure 3-4 (a) FE-SEM micrograph of ITO thin film deposited with 20wt% ink at 0.5 mm/s.....	65
Figure 3-4 (b) FE-SEM micrograph of ITO thin film deposited with 20wt% ink at 1 mm/s.....	65
Figure 3-5 FE-SEM micrographs of ITO thin films deposited with 10 wt% at substrate speeds of (a) 0.5 mm/s and (b) 1mm/s.....	66
Figure 3-6 X-ray diffraction pattern of ITO thin film.....	67
Figure 3-7 FE-SEM micrographs of ITO thin film at (a)microscale (b)nanoscale magnifications.....	68
Figure 3-8 Transmittance UV-vis spectrum of ITO thin film.....	69
Figure 3-9 I-V characteristics of ITO thin film.....	70

Figure 4-1 Modified SWCNT ink at different combinations (a) SWCNT ink to ethanol, 1:1 (b) SWCNT ink to ethanol to DI water 1:1:1, (c) SWCNT ink to ethanol to DI water 1:2:1, (d) SWCNT ink to ethanol to DI water 1:2:2, (e) SWCNT ink to ethanol to DI water 1:3:2.....	75
Figure 4-2 Schematic diagram of the electrohydrodynamic atomization system.....	78
Figure 4-3 Photograph of electrohydrodynamic atomization system.....	78
Figure 4-4 Close-up photograph of EHDA system.....	79
Figure 4-5 Different modes of atomization of SWCNT, a) Dripping, b) Micro-dripping, c) Unstable cone-jet, d) Stable cone-jet, e) Multijet mode.....	79
Figure 4-6 (a) X-ray diffraction pattern SWCNT thin films on PES substrates. (b) FE-SEM micrographs of SWCNT thin films.....	82
Figure 4-7 (a) Fourier transform infra-red absorption spectra of SWCNTs. (b) UV-vis spectra of SWCNT thin films.....	84
Figure 4-8 (a) I-V characteristics of SWCNT thin films at various temperatures (b) Semi-log of I-V characteristics of SWCNT thin films.....	86
Figure 4-9 CV curves of SWCNT electrode at different scan rates from 25 to 125 mV s ⁻¹ ...	87
Figure 4-10 Galvanostatic charge-discharge curve of SWCNT electrode at a constant current density of 5 mA cm ⁻² in 1 M Na ₂ SO ₄ electrolyte solution.....	88
Figure 4-11 Nyquist plots for SWCNT electrode in 1 M Na ₂ SO ₄ electrolyte solution.....	89
Figure 4-12 SWCNT active layer after (a) 50, (b) 100, (c) 200, (d) 300 flexing cycles.....	90
Figure 4-13 I-V characteristics of flexible SWCNT active layer after (a) 50, (b) 100, (c) 200, (d) 300 flexing cycles.....	91

Abstract

Development of energy storage technologies has become immensely vital for the efficient consumption of energy and reliable utilization of renewable energy as the conventional energy resources pose serious challenges to human health, environment and energy security. Exponential growth of power production through renewable resources like solar, wind, and tidal power to replace enervating fossil fuel has called for implementing environment-friendly, sustainable energy conversion and storage systems. Miniaturized, portable, flexible electronic products demand for the development of new, flexible, lightweight, low-cost and environmentally friendly energy storage devices. With a short cycle life and low power density, rechargeable batteries cannot meet the increasing cycle stability and power demands of the electronic devices. In order to address these issues, energy storage devices with high energy density, flexible design and long lifetime have attracted tremendous research interest. Supercapacitors have been the object of important research in the last decade as they have the potential to provide higher energy density than dielectric capacitors and higher power density than batteries. A wide range of materials and processes have been studied thus far to develop supercapacitors to meet the current and future demands.

In this dissertation, electrohydrodynamic atomization (EHDA) technique has been adopted to fabricate nanostructured functional thin films for applications in supercapacitors. EHDA technique is one of the fast emerging, advanced fabrication technique in the field of printed electronics. This cost-effective, room temperature technique has the potential to process organic, inorganic and polymeric materials.

With the ever growing need for high performance hybrid/composite thin films, EHDA technique promises to meet the aforementioned goals easily compared to conventional technique. Initially, nanostructured ITO have been thin films been deposited through EHDA technique on flexible substrates for transparent current collector applications. The precursor was prepared by the by dispersing the nanoparticles in combination of solvents. Optimization of the process parameters to achieve the crucial Taylor cone is explained. The optical, morphological and electrical studies conducted on the deposited ITO layers have been discussed.

After the deposition of transparent current collectors on flexible substrates, active layers of flexible single walled carbon nanotube (SWCNT) thin films have been fabricated on flexible substrates. The water based precursor has been modified with a combination of solvents in order to lower the surface tension and make it suitable for the EHDA process. The purity, surface morphology, chemical composition, electrical and electrochemical characteristics of the deposited SWCNT electrodes have been studied and discussed.

1. Introduction

1.1 Motivation

Energy storage has become an essential area of strong research interest in the past decade owing to the exponential growth of electronics and transportation industries. To meet their energy requirements, industries have relied on cost-effective fossil fuels for more than two centuries now. As a result of the rapid burning of the fossil fuels, pollution has increased leading to a global environmental change. Electrical energy is mainly produced in large fossil-fuel power plants, whereas nuclear and hydroelectric power plants contribute approximately 30% of the total production. The ever rising demand for energy and the predictable exhaustion of unsustainable fossil fuels are calling for development of technologies that can enhance the efficiency of energy consumption and reliable utilization of renewable energy. However, at present, the eco-friendly renewable energy sources such as solar cells, wind turbines, biomass plants, etc., could only produce up to 4% of the electricity and estimated to grow by 25% in the next decade. In addition to the mitigation of the negative environmental impact of CO₂ emission from fossil fuel combustion, it is immensely important to ensure the security of sustained energy supply when fossil resources either run out or become too expensive to use. Renewable power sources, namely solar, wind and others are intermittent because they produce electrical power according to the time and climatic availability of the resources (Armand et al. 2008, Miller et al. 2008, Alotto et al. 2014 and Chen et al. 2013). While replacing the conventional plants with regenerative energy sources, the grid changes, whereas the demand remains the same. With renewable energy, fluctuation in the production is highly capricious.

Consequently, to compensate for this fluctuation, it is essential to enhance the energy storage efficiency in contemporary technologies which functions as a buffer between generation and use of electricity.

Energy storage technologies ensure efficient utilization of energy produced by existing technologies; enabling us to go green and sustainable by replacing the conventional plants with regenerative energy sources in the future. Electrical energy storage (EES) systems can utilize more renewable energy, making it efficient, by storing the surplus energy produced and thereby reducing the use of fossil fuel. They can maintain supply power voltage and frequency within tolerance improving voltage drops by discharging electricity and reduce voltage rises by charging electricity. Large-scale batteries installed at appropriate substations can make the power distribution network more efficient by mitigating the congestion. The power output from small-capacity generators such as renewable energy must match the power demand. By installing EES the utility can supply stable power to consumers. EES systems such as double-layer capacitors, superconducting magnetic energy storage (SMES) and batteries installed in semiconductor industries provide stable power supply during momentary outages by instantly switching the load off the network to the EES supply thus making sure the quality of products is unaffected.

Portable batteries act as emergency power supplies, providing power to electrical appliances. Electric vehicles (EVs) including plug-in hybrid electric vehicles (PHEVs) are promoted to reduce CO₂ emissions from fossil fuel combustion. High-performance batteries such as nickel cadmium, nickel metal hydride and lithium ion batteries are mounted on EVs/PHEVs and used as power sources. These batteries are also expected to be used to power in-house appliances in combination with solar power and fuel cells; at the same time, studies

are being carried out to see whether they can practically be connected to power networks (IEC report 2011). EES systems can serve at various locations ranging from electricity production plants, transmission/distribution, backup and consumption.

Research and technological development is needed to enable the wider application of many known technologies, and to develop new ones. The main challenges for storage are increasing the capacities and efficiencies of existing technologies, developing new technologies economically for domestic, decentralized/large centralized application, and market deployment. Technologies need to respond according to the energy storage needs and patterns of access. Energy efficiency can be improved in various existing technologies. For example, elevators are the necessity in high buildings. Energy input is needed to raise the elevator against gravity, and the rising process accumulates potential energy. It is obviously desirable to convert the potential energy to a storable and reusable form during the downward course of the elevator. The stored energy can then be released to assist lifting the elevator, and hence improve energy efficiency. Obviously, to match the relatively fast movement of the elevator, the energy storage system must be capable of charging and discharging quickly.

Batteries, supercapacitors, and their hybrid combination are all significant contributing technologies. Capacitors work by storing electrical charge in conducting materials separated by a nonconductor. Capacitors charge and discharge more rapidly than batteries but typically hold much less charge. Supercapacitors can be used instead of rechargeable batteries. Electric double-layer capacitors (EDLCs), also called supercapacitors or ultracapacitors, store charge in the double layer formed at an electrolyte-electrode interface when voltage is applied. The electrodes are generally composed of high-surface-area conductive material, usually activated carbon.

They could potentially increase the density of devices allowing improved functionality, reduced complexity, and enhanced redundancy by removing intricate interconnects to bulk-sized batteries. Currently, advanced rechargeable microbatteries that use thin-film technologies are commercially available, but they suffer from many of the limitations of their larger counterparts, namely limited cycle life, abrupt failure, poor low-temperature kinetics, and safety concerns associated with using lithium. Even three-dimensional (3D) batteries, which are expected to overcome power limitations by further shortening electrolyte path lengths, cannot avoid fast failure because of the inevitable self-discharge caused by electron tunneling through marginally conductive thin dielectric coatings (solid electrolytes) and repeated recharging cycles. Supercapacitors can solve these lifetime and power issues and provide a bridge between devices operating with short charge-discharge times (<0.1 s) and longer discharge times (>0.1 hours) under and over which dielectric or electrolytic capacitors and batteries, respectively, find their slot.

Hybrid systems containing a battery and a supercapacitor have been experimentally demonstrated to exhibit longer operating times when compared to systems with batteries alone under repetitive high load and high current pulse conditions. Electrochemical capacitors (supercapacitors) offer high power density when compared to battery systems and also have a relatively large energy density compared to conventional capacitors. Combining a supercapacitor in parallel with a battery into a hybrid system broadens the applicability of batteries to higher discharge rates due to the high power density of supercapacitors. Such hybrid energy storage devices are more efficient than a battery in supplying the total power for use in digital cellular phones, space communications, power distribution systems, uninterrupted power supplies, electric and hybrid vehicles, portable computers, and military

applications. In many of these applications, the loads are not constant but rather span a range of power levels. Coupling supercapacitors with batteries is more beneficial under pulsed power loads, which are frequently encountered in communication systems.

The outstanding properties reported for new electrode materials may not necessarily be applicable to performance of electrochemical capacitors (ECs). Supercapacitors are not limited by the electrochemical charge transfer kinetics of batteries and thus can operate at very high charge and discharge rates and can have lifetimes of over a million cycles. Unlike batteries, which store large amounts of energy but deliver it slowly, ECs can deliver energy faster (develop high power), but only for a short time. However, recent work has claimed energy densities for ECs approaching or even exceeding that of batteries. There have been notable advances in the supercapacitor field, which were mostly focused on increasing supercapacitor energy density by using different active materials and designs, such as carbon nanotubes (CNTs), activated carbons, polymers, and metal oxides.

1.2 Types of energy storage technologies

Based on the scale and place, storage can be classified large-scale (GW), medium-sized (MW) or micro/local systems (kW). Some of the key technologies are listed below under each category.

- **Large-scale energy storage (GW)**

- Thermal storage, pumped hydro
- Compressed Air Energy Storage (CAES)
- Chemical storage

- **Grid storage systems (MW)**

- Power: Supercapacitors, superconducting magnetic energy storage (SMES), flywheels
- Energy: batteries such as Lead Acid , Li-ion, NaS & Flow batteries
- Energy & Power: Lead Acid & Li-ion batteries
- Hydrogen Energy Storage / CAES / Pumped Hydro Energy Storage (PHES)

- **End-user storage systems (kW)**

- Power: Supercapacitors, flywheels
- Energy: Batteries such as Lead acid and Li-ion
- Energy & Power: Li-ion batteries

Some of the aforementioned technologies are yet to make it to the commercial application stage. Depending on the form of energy used the major technologies of EES system could be classified into mechanical, thermal, electrical, chemical and electrochemical energy storage systems as follows,

- **Mechanical**

- Pumped hydro storage (PHES)
- Compressed air energy storage (CAES)
- Flywheel energy storage (FES)

- **Thermal**

- Sensible heat storage (Molten salt / A-CAES)

- **Electrical**

- Double layer capacitor (DLC)
- Superconducting magnetic coil energy storage (SMES)

- **Chemical**

- Hydrogen energy storage (Electrolyzer / Fuel cell / SNG)

- **Electrochemical**

- Secondary batteries (Lead acid / NiCd / NiMh / Li / NaS)
- Flow batteries (Redox flow / Hybrid flow)

The vast majority of existing large scale energy storage is based on pumped hydro storage. Pumped hydro storage systems were built purely for electricity management. With over 120 GW, pumped hydro storage power plants represent nearly 99 % of world-wide installed electrical storage capacity which is about 3 % of global generation capacity. Conventional pumped hydro storage systems use two water reservoirs at different elevations to pump water during off peak hours from the lower to the upper reservoir (charging). When required, the water flows back from the upper to the lower reservoir, powering a turbine with a generator to produce electricity (discharging). There are different options for the upper and lower reservoirs, e.g. high dams can be used as pumped hydro storage plants. For the lower reservoir flooded mine shafts, other underground cavities and the open sea are also technically possible. Seawater pumped hydro plant was first built in Japan in 1999 (Yanbaru, 30 MW). The first pumped hydro storage plants were used in Italy and Switzerland in the 1890s. By 1933 reversible pump-turbines with motor generators were available. Typical discharge times range from several hours to a few days. The efficiency of PHS plants is in the range of 70 % to 85 %. Advantages are the very long lifetime and practically unlimited cycle stability of the installation. Main drawbacks are the dependence on topographical conditions and large land use. The main applications are for energy management via time shift, namely nonspinning reserve and supply reserve.

Compressed air energy storage is a technology known and used since the 19th century for different industrial applications including mobile ones. Air is used as storage medium due to its availability. Electricity is used to compress air and store it in either an underground structure or an above-ground system of vessels or pipes. When needed the compressed air is mixed with natural gas, burned and expanded in a modified gas turbine.

Typical underground storage options are caverns, aquifers or abandoned mines. If the heat released during compression is dissipated by cooling and not stored, the air must be reheated prior to expansion in the turbine. This process is called diabatic CAES and results in low round-trip efficiencies of less than 50 %. Diabatic technology is well proven and the plants have a high reliability and are capable of starting without extraneous power. The advantage of CAES is its large capacity and the disadvantages are low round-trip efficiency and geographic limitation of locations.

In flywheel energy storage rotational energy is stored in an accelerated rotor, a massive rotating cylinder. The main components of a flywheel are the rotating body/cylinder which comprises of a rim attached to a shaft in a compartment, the bearings and the transmission device with motor/generator mounted onto the stator. The energy is maintained in the flywheel by keeping the rotating body at a constant speed. An increase in the speed results in a higher amount of energy stored. To accelerate the flywheel electricity is supplied by a transmission device. If the flywheel's rotational speed is reduced electricity may be extracted from the system by the same transmission device. Flywheels of the first generation, which have been available since about 1970, use a large steel rotating body on mechanical bearings. Advanced FES systems have rotors made of high-strength carbon filaments, suspended by magnetic bearings, and spinning at speeds from 20 000 to over 50 000 rpm in a vacuum enclosure. The main features of flywheels are the excellent cycle stability and a long life, little maintenance, high power density and the use of environmentally inert material. However, flywheels have a high level of self-discharge due to air resistance and bearing losses and suffer from low current efficiency. Today flywheels are commercially deployed for power quality in industrial and UPS applications, mainly in a hybrid configuration. Efforts are being

made to optimize flywheels for long-duration operation (up to several hours) as power storage devices for use in vehicles and power plants.

Thermal energy storage systems store available heat by different means in an insulated repository for later use in different industrial and residential applications, such as space heating or cooling, hot water production or electricity generation. Thermal storage systems are deployed to overcome the mismatch between demand and supply of thermal energy and thus they are important for the integration of renewable energy sources. Thermal storage can be subdivided into different technologies: storage of sensible heat, storage of latent heat, and thermo-chemical and absorption storage. The storage of sensible heat is one of the best-known and most widespread technologies, with the domestic hot water tank as an example. The storage medium may be a liquid such as water or thermo-oil, or a solid such as concrete or the ground. Thermal energy is stored solely through a change of temperature of the storage medium. The capacity of a storage system is defined by the specific heat capacity and the mass of the medium used.

Latent heat storage is accomplished by using phase change materials (PCMs) as storage media. There are organic (paraffins) and inorganic PCMs (salt hydrates) available for such storage systems. Latent heat is the energy exchanged during a phase change such as the melting of ice. It is also called “hidden” heat, because there is no change of temperature during energy transfer. The best-known latent heat – or cold – storage method is the ice cooler, which uses ice in an insulated box or room to keep food cool during hot days. Currently most PCMs use the solid-liquid phase change, such as molten salts as a thermal storage medium for concentrated solar power (CSP) plants.

The advantage of latent heat storage is its capacity to store large amounts of energy in a small volume and with a minimal temperature change, which allows efficient heat transfer.

Sorption (adsorption, absorption) storage systems work as thermo-chemical heat pumps under vacuum conditions and have a more complex design. Heat from a high-temperature source heats up an adsorbent (e.g. silica gel or zeolite), and vapor (working fluid, e.g. water) is desorbed from this adsorbent and condensed in a condenser at low temperatures. The heat of condensation is withdrawn from the system. The dried adsorbent and the separated working fluid can be stored as long as desired. During the discharging process the working fluid takes up low-temperature heat in an evaporator. Subsequently, the vapour of the working fluid adsorbs on the adsorbent and heat of adsorption is released at high temperatures. Depending on the adsorbent/working fluid pair the temperature level of the released heat can be up to 200 °C and the energy density is up to three times higher than that of sensible heat storage with water. However, sorption storage systems are more expensive due to their complexity.

In the context of EES, it is mainly sensible/latent heat storage systems which are important. CSP plants primarily produce heat, and this can be stored easily before conversion to electricity and thus provide dispatchable electrical energy. State-of-the-art technology is a two-tank system for solar power plants, with one single molten salt as heat transfer fluid and storage medium. The molten salt is heated by solar radiation and then transported to the hot salt storage tank. To produce electricity the hot salt passes through a steam generator which powers a steam turbine. Subsequently, the cold salt (still molten) is stored in a second tank before it is pumped to the solar tower again. The main disadvantages are the risk of liquid salt freezing at low temperatures and the risk of salt decomposition at higher temperatures.

In solar trough plants a dual-medium storage system with an intermediate oil/salt heat exchanger is preferred. Typical salt mixtures such as Na-K-NO₃ have freezing temperatures > 200 °C, and storage materials and containment require a higher volume than storage systems for solar power plants.

Apart from sensible heat storage systems for CSP, latent heat storage is under development by a German-Spanish consortium. The storage system at the pilot facility is based on sodium nitrate, has a capacity of 700 kWh and works at a temperature of 305 °C. In adiabatic CAES the heat released during compression of the air may be stored in large solid or liquid sensible heat storage systems. Various R&D projects are exploring this technology but so far there are no adiabatic CAES plants in operation. As solid materials concrete, cast iron or even a rock bed can be employed. For liquid systems different concepts with a combination of nitrate salts and oil are in discussion. The round-trip efficiency is expected to be over 70 %. Of particular relevance is whether a pressurized tank is needed for the thermal storage, or if a non-pressurized compartment can be used. In liquid systems, a heat exchanger can be used to avoid the need for a large pressurized tank for the liquid, but the heat exchanger means additional costs and increases the complexity. A dual-media approach (salt and oil) must be used to cover the temperature range from 50 °C to 650 °C. Direct contact between the pressurized air and the storage medium in a solid thermal storage system has the advantage of a high surface area for heat transfer. The storage material is generally cheap, but the pressurized container costs are greater.

Electrochemical double-layer capacitors (DLC), also known as supercapacitors, are a technology which has been known for 60 years. They fill the gap between classical capacitors used in electronics and general batteries, because of their nearly unlimited cycle stability as

well as extremely high power capability and their many orders of magnitude higher energy storage capability when compared to traditional capacitors. This technology still exhibits a large development potential that could lead to much greater capacitance and energy density than conventional capacitors, thus enabling compact designs.

The two main features are the extremely high capacitance values, of the order of many thousand farads, and the possibility of very fast charges and discharges due to extraordinarily low inner resistance which are features not available with conventional batteries. Still other advantages are durability, high reliability, no maintenance, long lifetime and operation over a wide temperature range and in diverse environments (hot, cold and moist). The lifetime reaches one million cycles (or ten years of operation) without any degradation, except for the solvent used in the capacitors whose disadvantage is that it deteriorates in 5 or 6 years irrespective of the number of cycles. They are environmentally friendly and easily recycled or neutralized. The efficiency is typically around 90 % and discharge times are in the range of seconds to hours. They can reach a specific power density which is about ten times higher than that of conventional batteries (only very-high-power lithium batteries can reach nearly the same specific power density), but their specific energy density is about ten times lower. Because of their properties, DLCs are suited especially to applications with a large number of short charge/discharge cycles, where their high performance characteristics can be used. DLCs are not suitable for the storage of energy over longer periods of time, because of their high self-discharge rate, their low energy density and high investment costs. A DLC is also ideally suited as a UPS to bridge short voltage failures. A new application could be the electric vehicle, where they could be used as a buffer system for the acceleration process and regenerative braking.

Superconducting magnetic energy storage (SMES) systems work according to an electrodynamic principle. The energy is stored in the magnetic field created by the flow of direct current in a superconducting coil, which is kept below its superconducting critical temperature. 100 years ago at the discovery of superconductivity a temperature of about 4 °K was needed.

Much research and some luck has now produced superconducting materials with higher critical temperatures. Today materials are available which can function at around 100 °K. The main component of this storage system is a coil made of superconducting material. Additional components include power conditioning equipment and a cryogenically cooled refrigeration system. The main advantage of SMES is the very quick response time: the requested power is available almost instantaneously. Moreover the system is characterized by its high overall round-trip efficiency (85 % - 90 %) and the very high power output which can be provided for a short period of time. There are no moving parts in the main portion of SMES, but the overall reliability depends crucially on the refrigeration system. In principle the energy can be stored indefinitely as long as the cooling system is operational, but longer storage times are limited by the energy demand of the refrigeration system. Large SMES systems with more than 10 MW power are mainly used in particle detectors for high-energy physics experiments and nuclear fusion. To date a few, rather small SMES products are commercially available which are mainly used for power quality control in manufacturing plants such as microchip fabrication facilities.

Hydrogen and synthetic natural gas (SNG) as secondary energy carriers could have a significant impact on the storage of electrical energy in large quantities. The main purpose of such a chemical energy storage system is to use “excess” electricity to produce hydrogen via

water electrolysis. Once hydrogen is produced different ways are available for using it as an energy carrier, either as pure hydrogen or as SNG. Although the overall efficiency of hydrogen and SNG is low compared to storage technologies such as PHS and Li-ion, chemical energy storage is the only concept which allows storage of large amounts of energy, up to the TWh range, and for greater periods of time – even as seasonal storage.

Another advantage of hydrogen and SNG is that these universal energy carriers can be used in different sectors, such as transport, mobility, heating and the chemical industry. A typical hydrogen storage system consists of an electrolyzer, a hydrogen storage tank and a fuel cell. An electrolyzer is an electrochemical converter which splits water with the help of electricity into hydrogen and oxygen. It is an endothermal process, i.e. heat is required during the reaction. Hydrogen is stored under pressure in gas bottles or tanks, and this can be done practically for an unlimited time. To generate electricity, both gases flow into the fuel cell where an electrochemical reaction which is the reverse of water splitting takes place: hydrogen and oxygen react and produce water, heat is released and electricity is generated. For economic and practical reasons oxygen is not stored but vented to the atmosphere on electrolysis, and oxygen from the air is taken for the power generation. In addition to fuel cells, gas motors, gas turbines and combined cycles of gas and steam turbines are in discussion for power generation. Hydrogen systems with fuel cells (less than 1 MW) and gas motors (under 10 MW) can be adopted for combined heat and power generation in decentralized installations. Gas and steam turbines with up to several hundred MW could be used as peaking power plants. The overall AC-AC efficiency is around 40 %.

Different approaches exist to storing the hydrogen, either as a gas under high pressure, a liquid at very low temperature, adsorbed on metal hydrides or chemically bonded in complex hydrides. However, for stationary applications gaseous storage under high pressure is the most popular choice. Smaller amounts of hydrogen can be stored in above-ground tanks or bottles under pressures up to 900 bar. For larger amounts of hydrogen, underground piping systems or even salt caverns with several 100 000 m³ volumes under pressures up to 200 bar can be used.

Up to now there have not been any commercial hydrogen storage systems used for renewable energies. Various R&D projects carried out over the last 25 years have successfully demonstrated the feasibility of hydrogen technology.

Synthesis of methane (also called synthetic natural gas, SNG) is the second option to store electricity as chemical energy. Here a second step is required beyond the water splitting process in an electrolyzer, a step in which hydrogen and carbon dioxide react to methane in a methanation reactor. As is the case for hydrogen, the SNG produced can be stored in pressure tanks, underground, or fed directly into the gas grid. Several CO₂ sources are conceivable for the methanation process, such as fossil-fuelled power stations, industrial installations or biogas plants. To minimize losses in energy, transport of the gases CO₂ (from the CO₂ source) and H₂ (from the electrolysis plant) to the methanation plant should be avoided. The production of SNG is preferable at locations where CO₂ and excess electricity are both available. In particular, the use of CO₂ from biogas production processes is promising as it is a widely-used technology.

Nevertheless, intermediate on-site storage of the gases is required, as the methanation is a constantly running process. Recently this concept “power to methane” has been the subject of different R&D projects (e.g. in Germany, where a pilot-scale production plant is under construction). The main advantage of this approach is the use of an already existing gas grid infrastructure. Pure hydrogen can be fed into the gas grid only up to a certain concentration, in order to keep the gas mixture within specifications (e.g. heating value). Moreover, methane has a higher energy density, and transport in pipelines requires less energy (higher density of the gas). The main disadvantage of SNG is the relatively low efficiency due to the conversion losses in electrolysis, methanation, storage, transport and the subsequent power generation. The overall AC-AC efficiency, < 35 %, is even lower than with hydrogen.

Battery is a device that produces electrical energy from chemical reactions. There are different kinds of batteries with different chemicals. The idea behind them is that the two different chemicals within a battery cell have different loads and are connected with a negative (cathode) and the other with a positive electrode (anode). When connected to an appliance the negative electrode supplies a current of electrons that flow through the appliance and are accepted by the positive electrode. For the use of storing energy produced by renewable energy sources only rechargeable batteries are relevant and will be considered.

Lead acid batteries are the world’s most widely used battery type and have been commercially deployed since about 1890. Lead acid battery systems are used in both mobile and stationary applications. Their typical applications are emergency power supply systems, stand-alone systems with PV, battery systems for mitigation of output fluctuations from wind power and as starter batteries in vehicles.

In the past, many lead acid batteries were used for storage in grids. Stationary lead acid batteries have to meet far higher product quality standards than starter batteries. Typical service life is 6 to 15 years with a cycle life of 1 500 cycles at 80 % depth of discharge, and they achieve cycle efficiency levels of around 80 % to 90 %. Lead acid batteries offer a mature and well-researched technology at low cost. There are many types of lead acid batteries available. Costs for stationary batteries are currently far higher than for starter batteries. Mass production of lead acid batteries for stationary systems may lead to a price reduction. One disadvantage of lead acid batteries is usable capacity decrease when high power is discharged. Other drawbacks are lower energy density and the use of lead, a hazardous material prohibited or restricted in various jurisdictions. Advantages are a favorable cost/performance ratio, easy recyclability and a simple charging technology. Current R&D on lead acid batteries is trying to improve their behavior for micro-hybrid electric vehicles.

Nickel cadmium (NiCd) batteries had been in commercial use since about 1915. Compared to lead acid batteries, nickel-based batteries have a higher power density, a slightly greater energy density and the number of cycles is higher many sealed construction types are available. From a technical point of view, NiCd batteries are a very successful battery product; in particular, these are the only batteries capable of performing well even at low temperatures in the range from -20 °C to -40 °C. Large battery systems using vented NiCd batteries operate on a scale similar to lead acid batteries. However, because of the toxicity of cadmium, these batteries are presently used only for stationary applications in Europe. Since 2006 they have been prohibited for consumer use. NiMH batteries were developed initially to replace NiCd batteries.

NiMH batteries have all the positive properties of NiCd batteries, with the exception of the maximal nominal capacity which is still ten times less when compared to NiCd and lead acid. Furthermore, NiMH batteries have much higher energy densities. In portable and mobile applications sealed NiMH batteries have been extensively replaced by lithium ion batteries. On the other hand, hybrid vehicles available on today's market operate almost exclusively with sealed NiMH batteries, as these are robust and far safer than lithium ion batteries. NiMH batteries currently cost about the same as lithium ion batteries.

Lithium ion batteries have become the most important storage technology in the areas of portable and mobile applications (e.g. laptop, cell phone, electric bicycle, electric car) since around 2000. High cell voltage levels of up to 3.7 nominal Volts mean that the number of cells in series with the associated connections and electronics can be reduced to obtain the target voltage. For example, one lithium ion cell can replace three NiCd or NiMH cells which have a cell voltage of only 1.2 Volts. Another advantage of Li-ion batteries is their high gravimetric energy density, and the prospect of large cost reductions through mass production.

Although Li-ion batteries have a share of over 50 % in the small portable devices market, there are still some challenges for developing larger-scale Li-ion batteries. The main obstacle is the high cost of more than USD 600/kWh due to special packaging and internal overcharge protection circuits. Lithium ion batteries generally have a very high efficiency, typically in the range of 95 % - 98 %. Nearly any discharge time from seconds to weeks can be realized, which makes them a very flexible and universal storage technology. Standard cells with 5000 full cycles can be obtained on the market at short notice, but even higher cycle rates are possible after further development, mainly depending on the materials used for the electrodes. Since lithium ion batteries are currently still expensive, they can only compete

with lead acid batteries in those applications which require short discharge times (e.g. as primary control backup). Safety is a serious issue in lithium ion battery technology. Most of the metal oxide electrodes are thermally unstable and can decompose at elevated temperatures, releasing oxygen which can lead to a thermal runaway. To minimize this risk, lithium ion batteries are equipped with a monitoring unit to avoid over-charging and over-discharging. Usually a voltage balance circuit is also installed to monitor the voltage level of each individual cell and prevent voltage deviations among them. Lithium ion battery technology is still developing, and there is considerable potential for further progress. Recent research is focused on the development of cathode materials.

A metal air electrochemical cell consists of the anode made from pure metal and the cathode connected to an inexhaustible supply of air. For the electrochemical reaction only the oxygen in the air is used. Among the various metal air battery chemical couples, the lithium air battery is most attractive since its theoretical specific energy excluding oxygen (oxygen is not stored in the battery) is 11.14 kWh/kg, corresponding to about 100 times more than other battery types and even greater than petrol (10.15 kWh/kg).

However, the high reactivity of lithium with air and humidity can cause fire, which is a high safety risk. Currently only a zinc air battery with a theoretical specific energy excluding oxygen of 1.35 kWh/kg is technically feasible. Zinc air batteries have some properties of fuel cells and conventional batteries: the zinc is the fuel, the reaction rate can be controlled by varying air flow, and oxidized zinc/electrolyte paste can be replaced with fresh paste. In the 1970s, the development of thin electrodes based on fuel-cell research made small button prismatic primary cells possible for hearing aids, pagers and medical devices, especially cardiac telemetry. Rechargeable zinc air cells have a difficulty in design since zinc

precipitation from the water based electrolyte must be closely controlled. A satisfactory, electrically rechargeable metal air system potentially offers low materials cost and high specific energy, but none has reached marketability yet.

Sodium sulphur batteries consist of liquid (molten) sulphur at the positive electrode and liquid (molten) sodium at the negative electrode; the active materials are separated by a solid beta alumina ceramic electrolyte. The battery temperature is kept between 300 °C and 350 °C to keep the electrodes molten. NaS batteries reach typical life cycles of around 4500 cycles and have a discharge time of 6.0 hours to 7.2 hours. They are efficient (AC-based round-trip efficiency is about 75 %) and have fast response. These attributes enable NaS batteries to be economically used in combined power quality and time shift applications with high energy density. The main drawback is that to maintain operating temperatures a heat source is required, which uses the battery's own stored energy, partially reducing the battery performance. In daily use the temperature of the battery can almost be maintained by just its own reaction heat, with appropriately dimensioned insulation.

Since around 1990 NaS batteries have been manufactured by one company in Japan, with a minimum module size of 50 kW and with typically 300 kWh to 360 kWh. It is not practical for the present to use only one isolated module. Because 20 modules are combined into one battery the minimal commercial power and energy range is on the order of 1 MW, and 6.0 MWh to 7.2 MWh. These batteries are suitable for applications with daily cycling. As the response time is in the range of milliseconds and NaS batteries meet the requirements for grid stabilization, this technology could be very interesting for utilities and large consumers.

The sodium nickel chloride (NaNiCl) battery, better known as the ZEBRA (Zero Emission Battery Research) battery, is like the NaS battery, a high-temperature (HT) battery, and has been commercially available since about 1995. Its operating temperature is around 270 °C, and it uses nickel chloride instead of sulphur for the positive electrode. NaNiCl batteries can withstand limited overcharge and discharge and have potentially better safety characteristics and a higher cell voltage than NaS batteries. They tend to develop low resistance when faults occur and this is why cell faults in serial connections only result in the loss of the voltage from one cell, instead of premature failure of the complete system. These batteries have been successfully implemented in several electric vehicle designs and are an interesting opportunity for fleet applications. Present research is in developing advanced versions of the ZEBRA battery with higher power densities for hybrid electric vehicles, and also high-energy versions for storing renewable energy for load-levelling and industrial applications.

In conventional secondary batteries, the energy is charged and discharged in the active masses of the electrodes. A flow battery is also a rechargeable battery, but the energy is stored in one or more electroactive species which are dissolved in liquid electrolytes. The electrolytes are stored externally in tanks and pumped through the electrochemical cell that converts chemical energy directly to electricity and vice versa. The power is defined by the size and design of the electrochemical cell whereas the energy depends on the size of the tanks. With this characteristic flow batteries can be fitted to a wide range of stationary applications. Originally developed by NASA in the early 70s as EES for long-term space flights, flow batteries are now receiving attention for storing energy for durations of hours or days with a

power of up to several MW. Flow batteries are classified into redox flow batteries and hybrid flow batteries.

In redox flow batteries (RFB) two liquid electrolyte dissolutions containing dissolved metal ions as active masses are pumped to the opposite sides of the electrochemical cell. The electrolytes at the negative and positive electrodes are called anolyte and catholyte respectively. During charging and discharging the metal ions stay dissolved in the fluid electrolyte as liquid; no phase change of these active masses takes place. Anolyte and catholyte flow through porous electrodes, separated by a membrane which allows protons to pass through it for the electron transfer process. During the exchange of charge a current flows over the electrodes, which can be used by a battery-powered device. During discharge the electrodes are continually supplied with the dissolved active masses from the tanks; once they are converted the resulting product is removed to the tank. Theoretically a RFB can be recharged within a few minutes by pumping out the discharged electrolyte and replacing it with recharged electrolyte. That is why redox flow batteries are under discussion for mobile applications.

In a hybrid flow battery (HFB) one of the active masses is internally stored within the electrochemical cell, whereas the other remains in the liquid electrolyte and is stored externally in a tank. Therefore hybrid flow cells combine features of conventional secondary batteries and redox flow batteries: the capacity of the battery depends on the size of the electrochemical cell. Typical examples of a HFB are the Zn-Ce and the Zn-Br systems.

In both cases the anolyte consists of an acid solution of Zn^{2+} ions. During charging Zn is deposited at the electrode and at discharging Zn^{2+} goes back into solution. As membrane a microporous polyolefin material is used; most of the electrodes are carbon-plastic composites.

Various companies are working on the commercialization of the Zn-Br hybrid flow battery, which was developed by Exxon in the early 1970s. In the United States, ZBB Energy and Premium Power sell trailer-transportable Zn-Br systems with unit capacities of up to 1 MW / 3 MWh for utility-scale applications. 5 kW / 20 kWh systems for community energy storage are in development as well.

Compact batteries and supercapacitors are newly developed miniaturized electrochemical energy storage devices. They offer power densities that are several orders of magnitude larger than those of conventional batteries due to the short ion diffusion length. They are important on-chip micro-power sources for miniaturized electronic devices. The performance of supercapacitors has been significantly advanced by fabricating nanostructured materials, developing thin-film manufacture technologies and device architectures.

1.3 Thin film fabrication techniques

Thin film is a microscopically thin layer of any material with thickness ranging from fractions of a nanometer to few micrometers. There are many thin film fabrication techniques which are classified into two categories, namely physical methods and chemical methods. Physical methods exploit mechanical, electromechanical or thermodynamic means to deposit thin films, whereas chemical methods use fluid precursors to get solid thin films.

Chemical methods include chemical vapor deposition (CVD), chemical bath deposition (CBD), spin coating, plating and atomic layer deposition (ALD). Sputtering, thermal evaporation, electron beam evaporation, molecular beam epitaxy (MBE), pulsed laser deposition, cathodic arc deposition and electrohydrodynamic atomization (EHDA) are the most important physical methods to fabricate thin films.

In chemical vapor deposition, the substrate is placed inside a reactor to which a number of gases are supplied. The fundamental principle of the process is that a chemical reaction takes place between the source gases. The product of that reaction is a solid material with condenses on all surfaces inside the reactor. The two most important CVD technologies are the low pressure CVD (LPCVD) and plasma enhanced CVD (PECVD). The LPCVD process produces layers with excellent uniformity of thickness and material characteristics. The main problems with the process are the high deposition temperature (higher than 600°C) and the relatively slow deposition rate.

The PECVD process can operate at lower temperatures (down to 300° C) with the extra energy supplied to the gas molecules by the plasma in the reactor. However, the quality of the films tends to be inferior to processes running at higher temperatures.

Chemical bath deposition (CBD), also known as chemical solution deposition (CSD) is a chemical process through which a thin film of material is deposited. This method is one of the cheapest methods to deposit thin films and nanomaterials, as it does not depend on expensive equipment and is a scalable technique that can be employed for large area batch processing or continuous deposition. Typically, a liquid solution containing precursors to the eventual film is prepared and a substrate is exposed the solution. Over the course of time, the precursors react to produce a solid material that grows, atom by atom, on all the surfaces exposed to the bath. The growth of thin films strongly depends on growth conditions, such as duration of deposition, composition and temperature of the solution, and topographical and chemical nature of the substrate. However, it is, not always an option for thin film growth, as a suitable precursor solution does not exist for every material. Chemical bath deposition is

regularly used in the photovoltaic industry to deposit thin films. A notable drawback of this method is the wastage of solution after every deposition.

Spin Coating involves the acceleration of a liquid puddle on a rotating substrate. The coating material is deposited in the center of the substrate either manually or by a robotic arm. The physics behind spin coating involve a balance between centrifugal forces controlled by spin speed and viscous forces which are determined by solvent viscosity. The variable process parameters involved in spin coating are,

- Solution viscosity
- Solid content
- Angular speed
- Spin Time

Spin coating technique consists of the following four basic stages,

- Deposition of the coating fluid onto the wafer or a flat substrate
- The substrate is accelerated up to its final, desired, rotation speed
- The substrate is spinning at a constant rate and fluid viscous forces dominate the fluid thinning behavior
- The substrate is spinning at a constant rate and solvent evaporation dominates the coating thinning behavior. After evaporation of the whole solvent, a solid film is generated.

The range of film thicknesses easily achieved by spin coating is 1-200nm. For thicker films, high material viscosity, low spin speed, and a short spin time are needed. However, these parameters can affect the uniformity of the thin films produced.

Plating is a surface covering in which a metal is deposited on a conductive surface. Plating has been done for hundreds of years which is also critical for modern technology. Plating is used to decorate objects, for corrosion inhibition, to improve solderability, to harden, to improve wearability, to reduce friction, to improve paint adhesion, to alter conductivity, to improve IR reflectivity, for radiation shielding, and for other purposes. Thin-film deposition has plated objects as small as an atom and therefore plating finds uses in nanotechnology. In electroplating, an ionic metal is supplied with electrons to form a non-ionic coating on a substrate. A common system involves a chemical solution with the ionic form of the metal, an anode (positively charged) which may consist of the metal being plated (a soluble anode) or an insoluble anode (usually carbon, platinum, titanium, lead, or steel), and finally, a cathode (negatively charged) where electrons are supplied to produce a film of non-ionic metal.

Electroless plating, also known as chemical or auto-catalytic plating, is a non-galvanic plating method that involves several simultaneous reactions in an aqueous solution, which occur without the use of external electrical power. The reaction is accomplished when hydrogen is released by a reducing agent, normally sodium hypophosphite, and oxidized, thus producing a negative charge on the surface of the part. The most common electroless plating method is electroless nickel plating, although silver, gold and copper layers can also be applied in this manner.

Atomic layer deposition works on the principle similar to chemical vapor deposition (CVD) except the ALD reaction breaks the CVD reaction into two half-reactions, keeping the precursor materials separate during the reaction. This is accomplished through sequential pulsing of special precursor vapors, each of which forms about one atomic layer during each pulse (reaction cycle). Reaction cycles are then repeated until the desired film thickness is achieved. During coating, two or more chemical vapors or gaseous precursors react sequentially on the substrate surface, producing a solid thin film. Most ALD coating systems utilize a flow-through traveling wave setup, where an inert carrier gas flows through the system and precursors are injected as very short pulses into this carrier flow. The carrier gas flow takes the precursor pulses as sequential waves through the reaction chamber, followed by a pumping line, filtering systems and, eventually, a vacuum pump. Atomic layer deposition (ALD) offers precise control down to the atomic scale.

Sputter deposition is a physical vapor deposition (PVD) method of depositing thin films by sputtering, i.e. ejecting atoms from a source material, which then deposits onto a substrate. Gaseous plasma is created and then the ions from this plasma are accelerated towards some source material also known as target. The source material is eroded by the arriving ions via energy transfer and is ejected in the form of neutral particles - either individual atoms, clusters of atoms or molecules. As these neutral particles are ejected they will travel in a straight line unless they come into contact with something other particles or a nearby surface and get deposited on the substrates as thin film. In reactive sputtering, a small amount of some non-noble gas such as oxygen or nitrogen is mixed with the plasma-forming gas. After the material is sputtered from the target, it reacts with this gas, so that the deposited film is a different

material, i.e. an oxide or nitride of the target material. Resputtering is reemission of the deposited material during the deposition process by ion or atom bombardment.

Magnetron sputtering involves the application of both electric and magnetic fields to the conventional DC sputtering cathode. The magnetic field is usually provided by the arrangement of permanent magnets behind the target. The magnetic field provided is oriented parallel to the target and perpendicular to the electric field. This enhances the ionizing efficiency. DC sputtering of insulators is not possible because of the built up of positive surface charge which would repel the energetic ions. This surface charge can be neutralized by ejecting electron from a gun or by placing a metal filter. These methods are not suitable for thin film deposition either because of thin film-uniformity problem or because of thin film contamination. Applying alternating current instead of DC rectifies this problem. Of all the conventional PVD techniques sputtering has been reported to produce high quality thin films.

Thermal evaporation is done inside a vacuum chamber where the material, usually in a boat is heated typically to its melting point and the substrate to be deposited on is positioned facing the source a couple feet away. A high current flowing through the boat heats it up and causes evaporation. A crystal monitor is mounted close to the substrate, which provides an estimate of how much and how fast the material is being deposited. The distance between the source and the substrate is wide to prevent solid particles reaching the substrate.

Electron beam evaporation is a typical physical vapor deposition (PVD) process that is also performed in a vacuum chamber. A high dc voltage is applied to a tungsten filament that causes electrons to be discharged. The stream of electrons emitted excites the targeted

solid and turns it into vapor, which travels to the substrate. As they reach the surface, they condense and form a thin film coating.

Pulsed laser deposition systems work by an ablation process. Pulses of focused laser light vaporize the surface of the target material and convert it to plasma; this plasma usually reverts to a gas before it reaches the substrate.

In Molecular beam epitaxy (MBE), slow streams of an element can be directed at the substrate, so that material deposits one atomic layer at a time. Compounds such as gallium arsenide are usually deposited by repeatedly applying a layer of one element (i.e., Ga), then a layer of the other (i.e., As), so that the process is chemical, as well as physical. The beam of material can be generated by either physical means (that is, by a furnace) or by a chemical reaction (chemical beam epitaxy).

Cathodic arc deposition (arc-PVD) which is a kind of ion beam deposition where an electrical arc is created that literally blasts ions from the cathode. The arc has an extremely high power density resulting in a high level of ionization (30–100%), multiply charged ions, neutral particles, clusters and macro-particles (droplets). If a reactive gas is introduced during the evaporation process, dissociation, ionization and excitation can occur during interaction with the ion flux and a compound film will be deposited.

Electrohydrodynamic atomization is a relatively new process of thin film deposition. The liquid to be deposited, either in the form of nano-particle solution or simply a solution, is fed to a small capillary nozzle (usually metallic) which is connected to a high voltage. The substrate on which the film has to be deposited is connected to ground. Through the influence of electric field, the liquid coming out of the nozzle takes a conical shape (Taylor cone) and at

the apex of the cone a thin jet emanates which disintegrates into very fine and small positively charged droplets under the influence of Rayleigh charge limit. The droplets keep getting smaller and smaller and ultimately get deposited on the substrate as a uniform thin layer. Electrohydrodynamic atomization (EHDA) is a promising materials deposition technique as it allows uniform and regular deposition, and offers a range of other advantages, such as low cost compared with other current techniques, easy set-up, high deposition rate, ambient temperature processing and the capability to generate specific surface topographies. The limitations of the above stated techniques can be overcome by the direct printing technique of electrohydrodynamic atomization (EHDA) which is a unique, cost-effective, room-temperature process and can be incorporated with roll-to-roll system for mass production. Consequently, this developing direct printing technique has the potential to play a crucial role in the field of printed electronics.

1.4 Aims and Outline

This research primarily aims to understand the fundamentals of electrohydrodynamic atomization and optimize the process parameters to achieve a stable cone jet. In addition, the research also aims at synthesizing nanomaterial precursor to successfully fabricate thin films on flexible and stretchable substrates leading to the development of printed supercapacitors. Studies conducted at each stage of the materials processing through EHDA will aid in understanding the processing of nanomaterials through EHDA to produce cost-effective, eco-friendly thin films for a wide range of applications in electronics including supercapacitors, sensors, solar cells, OLEDs and more.

Chapters 2 will give the background for EHDA and supercapacitors. The evolution of the process over the years and the governing parameters of the EHDA process will be discussed. Furthermore, the need for supercapacitors and their consequent developments in the past will also be described.

Chapter 3 will discuss the deposition of transparent ITO current collectors by EHDA. The experimental observation of ITO nanoparticles through EHDA to deposit transparent, conducting thin films will be explained. The structural and electrical studies of the deposited ITO thin films will also be presented.

Chapter 4 will focus on the fabrication of flexible SWCNT thin films through electrohydrodynamic atomization process. Synthesis of SWCNT precursor and the optimization of process parameters are discussed. The structural, optical and electrical properties of the fabricated SWCNT layers are also explained.

Chapter 5 will synopsise the conclusions and the possible future work.

2. Background

2.1 Supercapacitors

Supercapacitors also known as ultracapacitors or double-layer capacitors were invented in order to meet the requirements of several specific applications that needed quick burst of energy. They provide several order of magnitude higher energy densities than conventional dielectric capacitors, while demonstrating higher power density than batteries and thus bridge the gap between rechargeable batteries and capacitors (Miller et al. 1995, Service et al. 2006).

Capacitors are grouped into three family types and the most basic is the electrostatic capacitor, with a dry separator. This capacitor has a very low capacitance and is used to filter signals and tune radio frequencies. The size ranges from a few pico-farad (pf) to low microfarad (uF). The next member is the electrolytic capacitor, which is used for power filtering, buffering and coupling. Rated in microfarads (uF), this capacitor has several thousand times the storage capacity of the electrostatic capacitor and uses a moist separator. The third type is the supercapacitor, rated in farads, which is again thousands of times higher than the electrolytic capacitor. Conventional capacitors consist of two conducting electrodes separated by an insulating dielectric material. When a voltage is applied to a capacitor, opposite charges accumulate on the surfaces of each electrode. The charges are kept separate by the dielectric, thus producing an electric field that allows the capacitor to store energy.

Supercapacitors store energy by forming a double layer of electrolyte ions on the surface of conductive electrodes. Supercapacitors are not limited by the electrochemical charge transfer kinetics of batteries and thus can operate at very high charge and discharge rates and can have lifetimes of over a million cycles.

The supercapacitor is ideal for energy storage that undergoes frequent charge and discharge cycles at high current and short duration. Engineers at General Electric first experimented with the electric double-layer capacitor, which led to the development of an early type of supercapacitor in 1957. There were no known commercial applications then. In 1966, Standard Oil rediscovered the effect of the double-layer capacitor by accident while working on experimental fuel cell designs. NEC marketed the technology 1978 as “supercapacitor” for computer memory backup.

In the 1990s advances in materials and manufacturing methods led to improved performance and lower cost. The modern supercapacitor is not a battery per se but crosses the boundary into battery technology by using special electrodes and electrolyte. Several types of electrodes have been tried and the major focus is on the double-layer capacitor. Rather than operating as a stand-alone energy storage device, supercapacitors work well as low-maintenance memory backup to bridge short power interruptions. Supercapacitors have also made critical inroads into electric powertrains. The virtue of ultra-rapid charging and delivery of high current on demand makes the supercapacitor an ideal candidate as a peak-load enhancer for hybrid vehicles, as well as fuel cell applications. The charge time of a supercapacitor is about 10 seconds. The charge characteristic is similar to an electrochemical battery and the charge current is, to a large extent, limited by the charger. The initial charge can be made very fast, and the topping charge will take extra time.

Provision must be made to limit the initial current inrush when charging an empty supercapacitor. The supercapacitor cannot go into overcharge and does not require full-charge detection; the current simply stops flowing when the capacitor is full.

The supercapacitor can be charged and discharged virtually an unlimited number of times. Unlike the electrochemical battery, which has a defined cycle life, there is little wear and tear by cycling a supercapacitor. Nor does age affect the device, as it would a battery. Under normal conditions, a supercapacitor fades from the original 100 percent capacity to 80 percent in 10 years. Applying higher voltages than specified shortens the life.

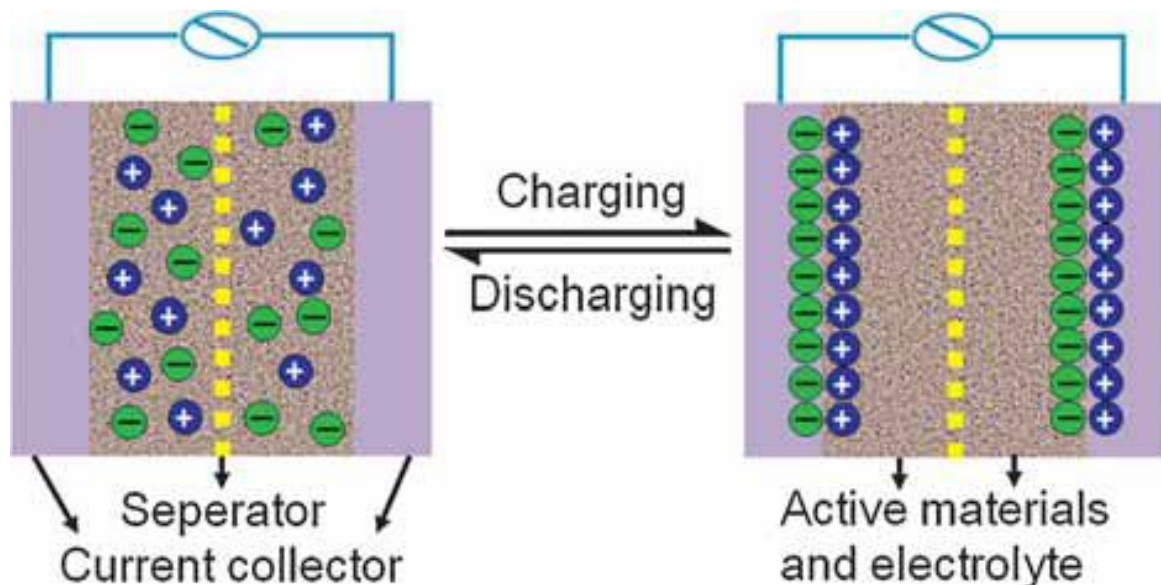


Figure 2-1 Schematic illustration of the charging/discharging process in a supercapacitor (Chen et al)

Supercapacitor functions well at hot and cold temperatures. The self-discharge of a supercapacitor is substantially higher than that of an electrostatic capacitor and somewhat higher than the electrochemical battery. The organic electrolyte contributes to this. The stored energy of a supercapacitor decreases from 100 to 50 percent in 30 to 40 days.

- **Advantages of supercapacitors**

- Virtually unlimited cycle life - can be cycled millions of time
- High specific power - low resistance enables high load currents
- Charges in seconds - no end-of-charge termination required
- Simple charging - draws only what it needs; not subject to overcharge
- Safe - forgiving if abused
- Excellent low-temperature charge and discharge performance

High power electrochemical capacitors based on carbon nanotube electrodes have been developed in 1997. Carbon nanotube sheet electrodes have been prepared from catalytically grown carbon nanotubes of high purity and narrow diameter distribution, centered around 80 Å.

The study showed that the electrodes are free-standing mats of entangled nanotubes with an open porous structure almost impossible to obtain with activated carbon or carbon fiber. These properties are highly desirable for high power and long cycle life electrochemical capacitors. Specific capacitances of 102 and 49 F/g were measured at 1 and 100 Hz, respectively, on a single cell device with 38 wt % H₂SO₄ as the electrolyte with a power density of 8000 W/kg (Niu et al. 1997). Researchers from the United States and France reported that by carefully controlling the nanoscale structure of a carbon-based supercapacitor, the amount of electrical charges it can hold have been increased by about 50%. The power storage capacity of supercapacitors has been increasing ever since their invention with the development of nanostructured materials.

Three types of materials are used in the recent past to develop supercapacitors, namely, metal oxides, conducting polymers and carbon based active materials. Metal oxide supercapacitors provide the highest specific peak power ($>5 \text{ kW kg}^{-1}$), but the high cost of the active material (RuO_2) makes it too expensive for some applications. Conducting polymer-based supercapacitors can reach specific power values of approximately 2 kW kg^{-1} with a specific energy of more than 10 W h kg^{-1} . But up to now, this technology is less developed industrially than the others. Specific power delivered by carbon/carbon supercapacitors can reach 3 kW kg^{-1} , with maximum specific energies of 5 W h kg^{-1} . In this latter type, the cost of the active materials (high-surface activated carbons) is very cheap. This makes this type of supercapacitor interesting for many applications, such as mobile telecommunications, back-up power for engine starting, etc.

Carbon/carbon supercapacitors also called Double Layer Capacitors (DLC), function on the basis of the Helmholtz double layer. There is no charge transfer, as the energy is stored in the double layer near the carbon surface. The use of an organic electrolyte allows a voltage of 2–3 V to be reached with this design.

Nanostructured electrode materials have a short electron diffusion path and very large surface to volume ratio to contact with the electrolyte, which can improve the capacity and cycle life to serve as electrode for supercapacitors. However, in the ordinary nanostructured electrodes, owing to the high surface energy, nanomaterials often self-aggregate, which reduces the effective contact areas of active materials, conductive additives, and electrolyte. Keeping the effective contact areas large and fully realize the advantage of active materials at nanometer scale is still a challenge.

It is noted that electrode materials play a key role in the development of high performance supercapacitors in terms of the morphology, size, porosity and so forth. Recent attention has been focused on the preparation and application of complex hierarchical nanostructured arrays on Ni foam, when applied as an electrode, which can show superior electrochemical performance than single-structured materials.

With the multi-dimensions and large surface area, the hierarchical complex nanostructures can avoid many drawbacks and improve the electrochemical performance for supercapacitors. The electrochemical performance can be improved by the hierarchical nanostructural design, integrating the high conductivity of the inner core and large surface area of the outer branch, which shorten electron diffusion path and increase electron transfers. Among various electrode materials, mixed metal oxides and binary metal oxide/hydroxides were a kind of promising electrode material since it offered many intriguing advantages such as low-cost, abundant resources and environmental friendliness.

More significantly, it is reported that some binary metal oxides possesses a much better electronic conductivity and higher electrochemical activity than single component metal oxide. On the other hand, it is well known that the rate capability of electrode materials is mainly determined by the kinetics of ion diffusion and electronic conductivity.

In recent years, metal sulfides have been also proposed for the electrochemical capacitor and cathodes of lithium batteries, due to their excellent electroactive ability. In order to further enhance the electrochemical ability of metal sulfide, its nanostructures with various morphologies were synthesized, such as three-dimensional nanospheres and two-dimensional nanoflakes.

Wang et al. synthesized three-dimensional cobalt sulfide hierarchitectures through a mechanism similar to Ostwald ripening. Yang et al. fabricated hierarchical MoS₂/PANI nanowires in a mild condition and showed remarkably improved electrochemical performance. Bhandavat et al. produced large-area, few-layer WS₂ sheets by a superacid treatment and the surface energy of WS₂ sheets was relatively high. However, research on the synthesis of multidimensional hierarchical mixed metal sulfides which keep the effective contact areas large at nanometer scale is still a challenge and of great importance.

A recent study reported a cost-effective and simple strategy for the growth of novel multidimensional hierarchical CoNi₂S₄ arrays (MDH- CoNi₂S₄ arrays) on Ni foam. Free-standing CoNi₂S₄ arrays were prepared via a hydrothermal method in aqueous solution without any template. Then, the MDH-CoNi₂S₄ nanostructures were readily obtained by increasing the reaction time. Both of the CoNi₂S₄ arrays were investigated as the supercapacitor electrode materials. Electrochemical measurements showed that the MDH-CoNi₂S₄ arrays electrode exhibited excellent areal capacitance as high as 9.1 F cm⁻² at a scan rate of 5 mV s⁻¹ and 5.21 F cm⁻² at a current density of 20 mA cm⁻².

During 3000 cycles at room temperature with a current density of 100 mA cm⁻², the MDH-CoNi₂S₄ arrays electrode can retain 2.98 F cm⁻² capacitance, showing excellent long-term cycle stability. Compared to traditional electrodes, graphene-like CoNi₂S₄ nanosheets covered the top of arrays not only increased the specific surface area, but also protect the structure of electrode materials at a high current density. The large surface areas of the outer branches on the arrays permit homogeneous interface/chemical distributions at the nanoscale and fast ion and electron transfers.

In carbon-based supercapacitors with organic electrolytes, electrochemical reactions that can be modelled as a diffusion process cause significant loss of stored energy over a period of the order of 1 or 2 h. The nature of the reactions was not known, but the probable presence of water in the organic electrolyte could have been a factor. The processes which lead to excess ionic concentration appear to occur only when a supercapacitor was charged to more than 1 V. When a supercapacitor was charged above 1 V, energy was stored by this mechanism in addition to energy stored by electrostatic charging of the double-layer of the capacitor. During the first 8 h of self-discharge, the energy stored by the ionic concentration mechanism was largely lost. For times longer than 8 h, the voltage during self-discharge decayed exponentially. There was some dependence of the self-discharge time constant on the initial voltage to which a capacitor is charged. This showed that the self-discharge rate for times greater than about 8 h cannot be simply represented by a constant leakage resistance in parallel with the capacitance of the double-layer at the electrolyte–carbon interface.

A study focused on the electrode composition for carbon/carbon power supercapacitor showed that electrode performances were improved by using a mixture of two binders, PTFE and CMC. Laboratory cells containing such electrodes exhibited lower values of resistivity and the mechanical properties of the electrodes were improved. Best results were obtained with the following electrode composition: 90% activated carbon/5% SFG44/5% binder 'b' (a mixture of PTFE and CMC). A supercapacitor containing large electrodes was then assembled with electrodes made of 95% activated carbon/5% binder 'b'. A maximum specific power of 1 kW kg⁻¹ and a maximum specific energy of 1.6 W h kg⁻¹ (based on the total weight of the

cell) were reached at 25°C. When lowering the temperature from +25 to 18°C, the loss of maximum specific energy was 12% while the loss of maximum specific power was 28%.

Polythiophene based supercapacitor study demonstrated: 500 cycles without loss of capacity; 7 mAh g⁻¹ for PFPT, 40 mAh g⁻¹ for Pth were obtained during cyclic voltammetry at 20 mV s⁻¹ between -2 V/ref and +1 V/ref. Studies of the electrode composition have led to the selection of acetylene black as the electronically conducting additive in the electrode and of a new binder for the active materials on the aluminium expanded grids. The best electrode composition selected was 65% polymer, 30% acetylene black, 5% binder A. Preliminary devices have been built, showing the power capabilities of such systems. 260 F g⁻¹ of PFT and 110 F g⁻¹ of PFPT were obtained from un-optimized supercapacitors. Full capacity was delivered between 3 V and 2.3 V. Nevertheless, work has still to be done to decrease the internal resistance of the systems and to improve their cyclability.

Flexible solid-state supercapacitors have attracted great attention as promising energy storage device due to increasing energy demands for the portable and wearable electronics. Compared with conventional supercapacitors, they have significant advantages such as light-weight, ease of handling, excellent reliability and wider range of operation temperature, which make them very promising for laptops, roll-up displays, cell phones, etc. Among various electrode materials, MnO₂ have been intensively investigated as electrode materials for supercapacitors because of its ultrahigh theoretical capacitance (1370 F g⁻¹), low cost, abundance and environmentally friendly.

However, owing to its poor conductivity (10^{-5} – 10^{-6} S cm $^{-1}$), the reported capacitance for MnO $_2$ is still far away from its theoretical capacitance, especially at high mass loading (> 0.1 mg/cm 2). In general, there are two major strategies to improve the capacitance of MnO $_2$ electrodes. The first one is to develop the MnO $_2$ nanostructures with rational morphology and large surface area. A large number of MnO $_2$ nanostructures including nanorods, nanotubes, nanowires and nanoflowers have been reported for supercapacitors. The other one is to develop MnO $_2$ -based composites by incorporating with high conductive materials. Recently, various composites such as MnO $_2$ /graphene, MnO $_2$ /TiO $_2$, MnO $_2$ /Ni(OH) $_2$, and Zn $_2$ SnO $_4$ /MnO $_2$, have been widely studied as electrode materials for supercapacitors and exhibited enhanced electrochemical performances. Despite these achievements, it is still important but challenging to rationally design and prepare high-performance MnO $_2$ -based composites for supercapacitors. Recently, graphene has drawn considerable interest for its fascinating properties and wide applications. As a two-dimensional (2D) structure of sp 2 -bonded carbon materials, graphene has an ultrahigh surface area of up to 2630 m 2 g $^{-1}$, and excellent conductivity. Up to now, composites of graphene and MnO $_2$ have been used to improve their capacitance, and remarkable advances have been achieved.

However, most of the previous studies have mainly focused on single electrodes or aqueous electrolyte supercapacitors. A recent study on flexible supercapacitor reported the facile synthesis of MnO $_2$ /reduced graphene oxide (RGO) composites and their implementation as high-performance electrode for flexible solid-state supercapacitors. Carbon fabric was here chosen as the substrate mainly due to its cost-effectiveness, high conductivity, and excellent chemical stability. On the other hand, the flexible nature of carbon fabric is also preferable for designing a flexible device. The as-fabricated solid-state device based on these MnO $_2$ /RGO

composite electrodes has a good electrochemical performance with an area capacitance of 14 F cm^{-2} at 2 mV s^{-1} and excellent stability.

Recently, great efforts have been dedicated to develop advanced electrode materials, mainly using carbon nanotubes (CNTs) networks or graphene as flexible electrodes, for high-performance flexible supercapacitors. So far, most of the flexible supercapacitors utilized liquid electrolyte, which is usually hazardous to the environment; and good sealing of the electrolyte and housing of the devices are needed. The sealing and housing materials increase the volume and weight of the supercapacitor devices, making them unsuitable for thin and light-weight applications. In addition, the component parts of the devices with liquid electrolyte are not well-integrated and will decrease the electrochemical performance and stability of the devices. Therefore, developing flexible all-solid-state supercapacitors (FASSSs) is highly desired for flexible, wearable and miniaturized electronics. Several aspects should be mainly considered to develop advanced FASSSs which include the design high-performance electrode materials, strengthen the interfacial integrate of electrode and electrolyte, enhance the flexibility of the device, and simplify the device configuration.

Graphene, as a new form of carbon-based materials, has been extensively used as electrode materials for a variety of energy conversion and storage applications such as fuel cells, supercapacitors and batteries. Graphene-based materials have been utilized to replace the conventional carbon electrodes in supercapacitor devices with high performance due to their unique physical and chemical properties. Graphene and graphene derivatives with various morphologies have been demonstrated to be potential electrode materials for supercapacitor applications. For examples, Wu et al. successfully prepared three-dimensional boron and nitrogen co-doped graphene as efficient electrode materials for supercapacitors.

A highly porous graphene on carbon cloth (denoted as PG/CC) was prepared via an electrophoretic deposition (EPD) process for use as efficient flexible electrode materials in FASSS devices. With the EPD process, in order to obtain high porous graphene on carbon cloth, fine-size graphene should be used. In contrast, when large-size graphene was used in the EPD process, carbon cloth was only covered/wrapped by graphene (denoted as G/CC) without porous surface observed. The as-prepared PG/CC was used as flexible and binder-free electrodes for the high-performance FASSS device. The device possesses an electrode–separator–electrolyte integrated structure, in which PG/CC functions as binder-free electrodes and a polyvinyl alcohol (PVA)/H₂SO₄ gel as solid-state electrolyte and separator. The porous structure of graphene in the PG/CC electrode significantly increased the surface area of graphene and thus the specific capacitance. The macroscopic porous morphology of carbon cloth (CC) as the electrode matrix enhanced the integration between electrodes and electrolytes, which is favorable for the ion diffusion and electron transport in the bulk electrode phase. The excellent mechanical stability and flexibility of CC ensures the device with good flexibility. The resultant PG/CC based FASSSs showed high specific capacitance, good cycling stability, and enhanced energy density and power density with respect to G/CC and pristine CC.

The interfacial region between an electrode and an electrolyte, customarily referred to as the ‘electrical double layer’ (EDL) has always been regarded as an active field of interest for comprehending the behavior of ions and dipoles under the influence of an electric field. Thus, the choice of adsorption isotherms, dipolar states of molecules, discreteness of charge effects, etc. became a focus of attention in this context.

Hence, the elucidation of the structure of the electrical double layer using experimental data of differential capacitance and theoretical modeling appeared to be a domain of interest with a singular objective of analyzing the equilibrium properties of electrified interfaces.

The estimation of electrostatic and non-electrostatic interaction energies of adsorbed species at diverse electrochemical interfaces is in itself a challenging issue. Amidst this scenario, a patent by Becker demonstrated that this interfacial region, spanning a few Å thickness has the ability to store ‘charges’, the quantification of which leads to the ‘double layer capacitance’. Thus, the notion of Electrical Double Layer Capacitor (EDLC) arises wherein high values of the specific capacitance are anticipated in view of the distance being $\sim 10^{-8}$ cm since the capacitance and interfacial thickness are inversely related. In contrast, the

conventional capacitors consist of positive and negative electrodes immersed in a dielectric with the physical separation being a few millimeters. Consequently, the field of supercapacitors (also called ultracapacitors) became a frontier area of research in chemistry, physics and materials science and technology.

The systems wherein the capacitance arises from redox processes are often termed as ‘pseudocapacitors’ the associated capacitance being the pseudocapacitance. In the case of pseudocapacitors, the electrodes are metal oxides or polymer-coated metals, the charge storage being associated with faradaic processes. Apart from the pseudocapacitors and true (EDLC) capacitors, there exist hybrid capacitors too wherein pseudocapacitors are combined

with EDLC capacitors. The entire supercapacitor assembly is chosen such that it is voltammetrically stable as inferred from the cyclic voltammograms at a wide range of scan rates, capable of yielding large power densities and charge–discharge cycles as evinced from the galvanostatic studies and has lowest Equivalent Series Resistance (ESR).

It is this combination of factors in conjunction with the versatility of the synthetic protocols of diverse materials that has led to the rapid progress and excitement in the design of supercapacitors. The field of electrochemical supercapacitors has witnessed phenomenal growth during the past few decades not only on account of the impending energy crisis but also due to rapid strides being witnessed in synthesis of novel functional materials of diverse genre. In view of the large surface area, diverse carbon based materials are the preferred substrates for the EDLC. While such EDLC's were being investigated, pseudocapacitors whose redox behavior is 'perfectly reversible' came into prominence in view of their possessing $\sim 10^5$ charge–discharge cycles and specific capacitance of $\sim 10^3$. The essential

criteria to be satisfied by these pseudocapacitors are as follows: (i) reversibility of faradaic reactions; (ii) large capacitances and (iii) satisfactory charge–discharge cycles. Diverse metal oxides such as RuO_2 , Fe_2O_3 , MnO_2 , etc. and conducting polymers such as polypyrrole (Ppy), polyaniline (PANI), polythiophene, polyindole etc. are typical prototype materials for pseudocapacitors. In particular, conducting polymers are especially suitable in view of their ease of fabrication and flexibility.

The ability to store charges in the case of conducting polymers arises from a doping process. In the case of PANI and Ppy, the conductivity arises from p-doping (also known as oxidative doping) wherein the removal of pi-electrons from the conjugation leads to a net positive charge. It is customary to postulate the existence of ‘polarons’ and ‘bipolarons’ in this context so as to imply the creation of the charge carriers in the polymer chain. The mechanism of charge storage may also arise from n-doping as in the case of polyacetylene, wherein net negative charges arise.

Since the magnitude of the specific capacitance is influenced by the extent and efficiency of the charge storage, the quantification of doping becomes essential; hence, extensive investigations on the choice of dopants are being carried out.

The charge storage in pseudocapacitors may also involve intercalation which increases the specific capacitances. It is appropriate to mention here that in the rapidly advancing field of electrochemical supercapacitors, an exhaustive critical review encompassing various features such as (i) the choice of electrode materials (metals, metal oxides, carbon nanotubes, graphene and related materials, metal-polymer composites, etc.); (ii) their structural characterization using spectroscopic and microscopic studies; (iii) the influence of ionic liquids on specific capacitance; (iv) the fabrication of supercapacitor devices and their marketability/cost effectiveness; (v) the efficacy of hybrid supercapacitors and (vi) theoretical modeling of supercapacitors is rendered almost impossible.

A variety of nanostructures of conducting polymers at liquid–liquid interfaces has been obtained by different protocols. These can be coated onto electrodes using methods such as spin-coating, drop casting, electrospinning etc. Their usefulness as capacitor materials has not yet been extensively investigated.

A recent study reported the fabrication of high energy density flexible micro supercapacitors based on CoO nanoflowers woven by CNTs through the screen printing technology. The CoO/CNT based MSCs exhibited improved cycling stability (retaining ~85% after 1700 cycles) and higher energy density ($\sim 3.48 \text{ mWh/cm}^3$) than those of pristine CoO or CNTs. In addition, the CoO/CNT MSCs showed excellent mechanical flexibility with a bending angle of 0–180°. Due to the eco-friendly nature of materials synthesis and device fabrication process, CoO/CNT MSCs could be integrated into many power-on-chip systems, roll-up display panels or solar energy harvesters. In yet another study, flexible and high capacitance electrochemical capacitors were fabricated using CNTs, MnO₂, and papers, and their supercapacitor properties were characterized in a three-electrode system. CNT ink was prepared by dispersing CVD-grown CNTs using SDBS as a surfactant in DI water and by drop-drying it on papers. Subsequently, MnO₂ was electrochemically deposited on the CNT-coated papers. The MnO₂/CNT/paper supercapacitors showed a high specific capacitance of 540 F/g, which was attributed to fine nanostructure of the MnO₂, low resistivity of CNT films, and good adhesion properties between different materials. Specific energy and specific power were 20 Wh/kg and 1.5 kW/kg, respectively, at current density of 5 A/g. Owing to the high capacitance, flexibility, robustness, low-cost, and low environmental impact, the MnO₂/CNT/paper supercapacitors may have a great potential for diverse flexible energy storage applications.

2.2 Electrohydrodynamic atomization

Printed electronics which aims at developing flexible and stretchable electronic devices require accurate processing of a wide range of materials including organic semiconductors, polymers, metal oxides, etc., Direct deposition techniques provide an easy

and cheap way of controlling the structure and position of materials. Current direct deposition techniques involve inkjet printing, direct write fabrication, dip pen nanolithography, and thermal imaging. Inkjet printing technology is by far the most frequently used one among all direct deposition techniques. It is based on break up and ejection of liquid droplets by generating a well-controlled pressure in the nozzle. In general, inkjet printers are divided into two classes: continuous and drop on demand. In the continuous type, droplets break up from a continuous flow of liquid.

The method used to generate pressure in the nozzle varies and defines the type of the drop on demand inkjet printer. Piezoelectric type printers eject droplets upon contraction of their nozzle through activation of piezoelectric crystal as a response to an applied voltage.

Thermal printers utilize heating to generate a bubble which supplies the required pressure to eject a droplet. The typical size of a droplet generated from an inkjet printer is $\sim 10\text{-}15\ \mu\text{m}$. However, using complex wave patterns can reduce droplet size down to $2.5\ \mu\text{m}$. Frequency can be up to 1 MHz in continuous and 6-12 kHz in drop on demand type printers. This translates to 10 m/s and 0.12 m/s printing speeds when printing of continuous lines with $10\ \mu\text{m}$ diameter droplets for continuous and drop on demand operations, respectively. Deposition speed and well established technology are the two most important advantages of inkjet printers. Its biggest disadvantage is inability to print small features. For example, recently inkjet printers are used to produce organic transistors and cell arrays. However, because of its large feature size, researchers have to combine inkjet printing with other techniques such as modification of surface chemistry in order to reach the desired resolution.

In addition to the limited resolution, inkjet printing is problematic when used for colloidal suspensions due to clogging in the nozzle. Although inkjet printing of 3D structures

is possible, resulting structures show wavy interfaces as fingerprints of the merged droplets. In direct write fabrication, special pastes with tailored rheological properties are extruded from cylindrical nozzles. Pastes used in direct write fabrication ‘solidify’ because of their increased viscosity as soon as they leave the high shear nozzle. The biggest advantage of this technique is its applicability to 3-dimensional structures through layer by layer building.

A 3-dimensional network that aids mixing in micro capillaries has already been produced using direct write fabrication. However, the resolution of the technique is determined by the nozzle size and the smallest one achieved so far is 10 μm .

Thermal imaging technique utilizes a laser beam to heat a specific area on a metal film. Organic film, which is below the metal film, separates from the metal upon heating and deposits on the substrate. The process, also used by DuPont, is suitable for large area patterning with a throughput of 1000 cm^2/min ., and its resolution is typically $\sim 5 \mu\text{m}$. Its major advantage is solvent-free operation; on the other hand its disadvantages are lower resolution, the requirement to make a thin film, and large amount of wasted material on the donor film, which can be important if the deposited material is precious.

Dip pen nanolithography (DPN) was developed by Mirkin and co-workers in 1999. The technique is based on delivery of molecules from a solution to a substrate by an Atomic Force Microscope (AFM) tip. In this technique delivered molecules should have affinity for the substrate, so that once delivered, they will bind to the surface. One common example of ‘ink’ and ‘paper’ are molecules with thiol groups and gold substrate.

Hong *et al.* showed that resolutions as low as 5 nm is possible. However the technique requires affinity between the ‘ink’ and ‘paper’ and is not applicable to colloidal suspensions,

and hence is not suitable for building 3D structures. Another major drawback is the low printing speed. DPN is done with $\sim 1 \mu\text{m/s}$ or less velocity. Although Hong *et al.* developed a DPN plotter with eight parallel AFM tips to increase the patterning speed, such an attempt is clearly insufficient to make DPN suitable for large area patterning.

As an alternative to existing patterning techniques, Poon introduced electrohydrodynamic (EHD) printing. EHD printing uses electrohydrodynamic jets for achieving sub micron scale resolution and meter per second patterning velocity. Application of a high enough electric field (1-10 kV/cm) to a pendant droplet deforms the droplet into a conical shape. With a continuous supply of liquid and a sufficient electric field, a thin, steady and charged jet (EHD jet) is emitted at the tip of the cone under appropriate conditions. Moving this EHD jet with respect to a substrate creates patterns on the surface, analogous to writing with a pen.

The diameter of EHD jet, hence the resolution of the pattern, is set by cone dynamics rather than diameter of the nozzle. The cone reduces the diameter of the liquid jet two to three orders of magnitudes compared to the diameter of the nozzle. Evaporation of volatile solvents that are in the printing mixture decreases the feature sizes further. Patterns less than $10 \mu\text{m}$ can be produced routinely and under appropriate conditions feature sizes can be in the nanometer scale with EHD printing.

Velocity of the EHD jet is typically on the order of several meters per second, which allows patterning wall size areas. For example it would take ~ 1.5 hours to decorate 1 m^2 area with $10 \mu\text{m}$ lines using 10 parallel nozzles.

An important feature of EHD printing is its applicability to colloidal suspensions. Using millimeter scale nozzles helps prevent clogging and, upon combination of printing and evaporation driven self assembly, parallel lines of colloidal crystals can be manufactured through a single printing step. Once built in multiple layers, such lines have the potential to lead to 3D ordered structures which would be useful for photonic band gap and micro-electro-mechanical systems (MEMS) applications.

The advantages of using cone-jet transition for printing were also recognized by other researchers. Czaplewski et al. produced nanofluidic channels with 100 nm radii using EHD printed polymer nanofibers as templates. Liu et al. printed nanofibers for chemical sensing application. Chen et al. utilized cone-jet transition for precise delivery of 10 μm diameter droplets in an array. Park et al. used a pulsed cone to print a field effect transistor with a channel length of 1 μm . Lee et al. EHD printed inductors by using a silver nanoparticle suspension.

Electrohydrodynamic atomization (EHDA) utilizes electric force to overcome the surface tension of the liquid and called electrostatic as well. The two terms are used exchangeable in literature. Here the acceleration and droplet breakup is induced by the electric field acting onto the droplet surface. Lord Rayleigh (1879) found that an electrically charged droplet is becoming unstable when the outward electrostatic forces are balancing the surface tension forces. When a pendant drop is subject to an electric field that is high enough to overcome surface tension, the drop changes its shape to a conical one (Figure 2-2). Taylor theoretically demonstrated that for the conducting conical surface to be equipotential, the cone angle should be 49.3° in the absence of any flow. Taylor's prediction of the cone angle was verified through the observation of water drops subject to electric field in oil. In the presence

of liquid supply, a steady jet can be emitted from the tip of this cone and this phenomenon is referred to as the cone-jet transition. The unique feature of cone-jet transition is that the diameter of the jet can be adjusted dynamically, typically to values two or three orders of magnitude smaller than that of the nozzle. This is major advantage in printing applications when nozzle clogging becomes a limiting factor due to the presence of colloidal particles in the solution.

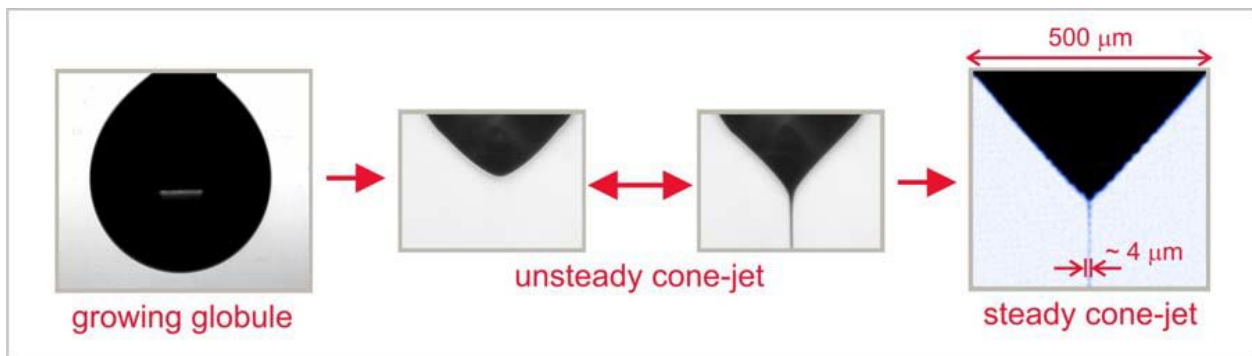


Figure 2-2 Deformation of a pendant drop upon application of electric field and formation of cone-jet transition (Korkut 2008)

A typical electrohydrodynamic spray setup consists of an electrically conducting capillary to which a high potential is applied and a grounded counterplate. The liquid is fed through the capillary and is atomized by the electric field at the capillary exit.

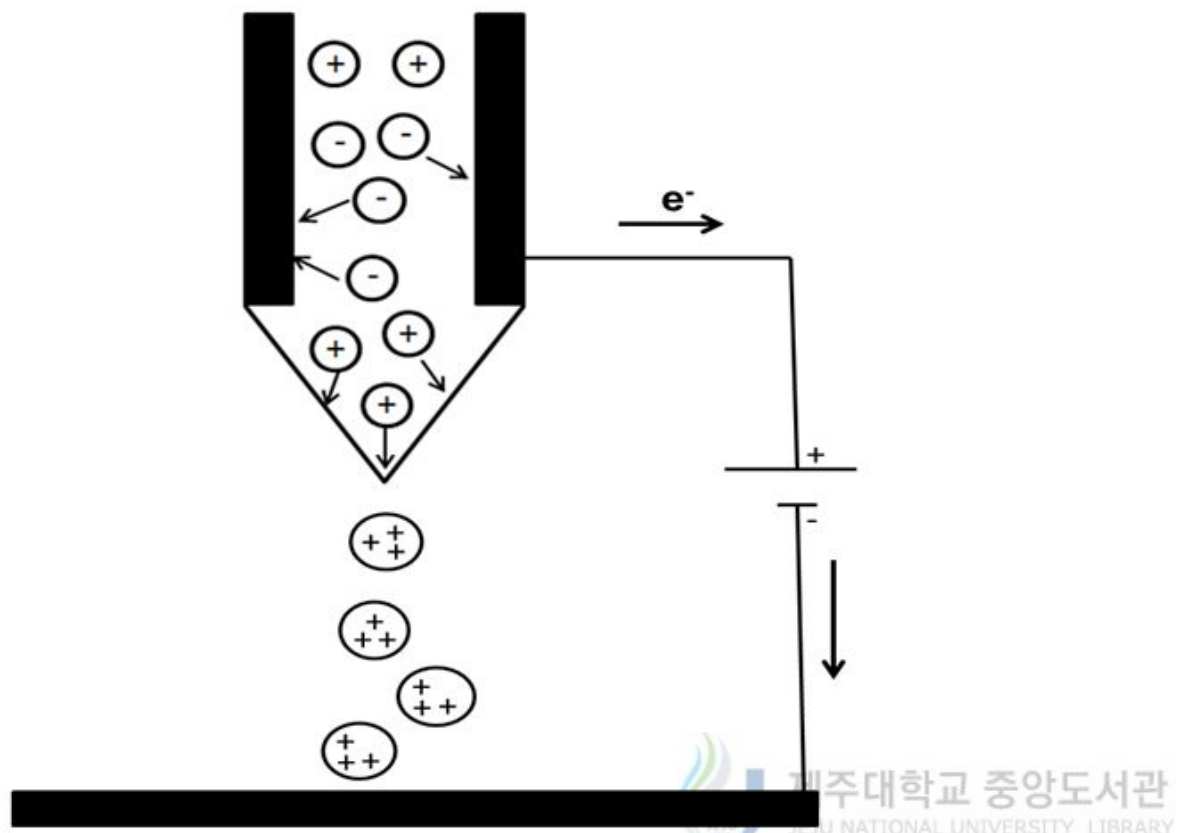


Figure 2-3 EHD spray setup

Cloupeau and Prunet-Foch (1990) describe the different spraying modes that can appear depending on setup geometry (e.g. distance between capillary and plate or capillary radius), volume feed rate, liquid properties (surface tension, electrical conductivity) and applied potential as seen in figure 2-4.

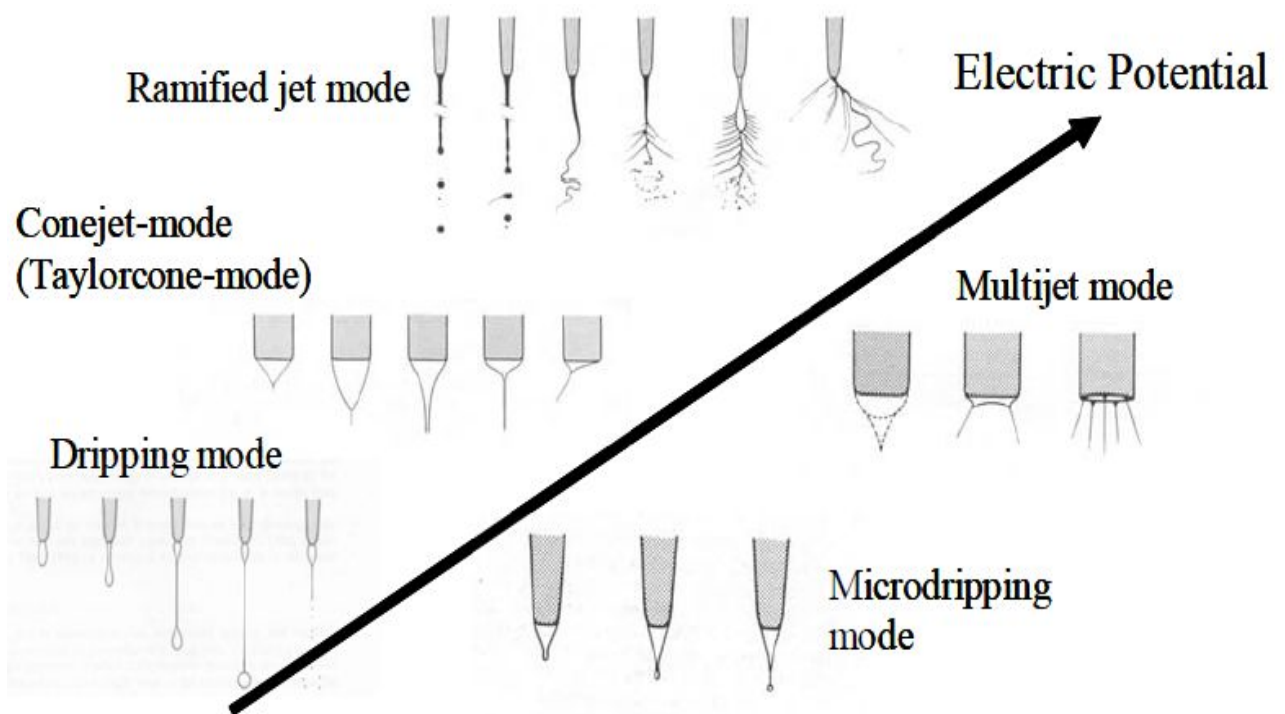


Figure 2-4 Electro-spray modes (Cloupeau and Prunet-Foch, 1990)

In the absence of an electric field, the liquid flows drop by drop at the outlet of the capillary, the application of a DC voltage between the capillary and the plate causes a rise in the emission frequency and a reduction in drop size. This is caused by the attraction of liquid

towards plate due to the action of electric field on the charges located at the end of the hanging drop and apparent reduction in the surface tension of the liquid due to the fact that electric charges on the surface create an electrostatic pressure opposite to the capillary pressure (Ogata et al. 1976, Takamatsu et al. 1981).

This electrostatic pressure is at its maximum at the end of the pendent drop but it is also exerted in the drop detachment zone. It would appear that in several theoretical studies this has not been taken into account in the calculation of the force retaining the drop on the capillary, whereas it is obviously taken into account for calculating the profile of the electrified pendent drops (Borzabadi and Bailey, 1978). In the dripping mode, the emission of drops may occur at regular time intervals, without the creation of satellites, so that all the drops have the same size. In general, drop diameter remains greater than that of the capillary, thus leading to the emission of large drops at low frequencies. For a given flow rate, the maximum emission frequency may increase (and the minimum drop diameter decrease) significantly if the diameter of the capillary is reduced. The electric field at the end of the pendent drop is sometimes sufficient to create a jet following the same process as for the cone-jet mode described below. A multitude of small droplets are then emitted during the formation cycle of each main drop.

In the conejet mode the cone is extended by a jet which is breaking up into droplets. Clopeau and Prunet-Foch (1989) show that the breakup of the jet is comparable to the uncharged jet-breakup investigated by Lord Rayleigh. Lord Rayleigh's theory proposes a droplet diameter to jet diameter ratio of 1.89. This ratio is also found for the conejet-breakup for moderately charged jets. The jet-breakup process leads to micrometer sized droplets as even with the capillary outlet being in the order of millimeters the diameter of electrospray

jets are in the order of micrometers. Consequently the electrospray mechanism serves as jet miniaturization apparatus. Variations of the conejet appear at the lower and upper potential limit of the stable version. If the potential is slightly under the necessary potential for a permanent jet the intermittent or pulsed conejet is observable. The shape of the liquid at the capillary exit is alternating between the form of a cone and a rounded drop.

At increased potential the conejet becomes unstable and two or more jets appear. This is the multijet. The number of jets increases with increasing potential. Simple jet, ramified jet and spindle mode are modes that appear at even higher electric potentials. Here the jets emitted by the capillary are highly charged and unstable. They branch into sub-jets or start wiping. The difference to conejet and multijet mode is mainly the high charge density on the jets. Whereas for conejet and multijet the breakup is still purely of mechanical nature, the charge density for ramified jet is so high that the jet gets torn apart by the mutual repulsion of these charges. Zeleny (1917) was the first to investigate electrosprays systematically in the capillary plate configuration. He examined the dripping mode, conejet and multijet of ethanol and glycerine and was the first to take photographic images of the process. Vonnegut and Neubauer (1952) investigated electrosprays with D.C. and A.C. voltage and were also able to see different spraying modes. They produced a monodisperse conejet spray with droplet sizes around 1 μm . Like Zeleny (1917) they found that it is hard to establish conejets with undistilled water for its high electrical conductivity. But they were successful with alcohol, lubricating oil and distilled water.

There are a number of works dealing with the stability limits of conejets but it is hard to give general rules for boundary values of single parameters like conductivity or surface tension of the liquid as the values are not independently influencing the spray formation

process. For the lower limit of the conductivity the estimates range from 10^{-8} to 10^{-11} S/m (Cloupeau and Prunet-Foch, 1989). The estimates for the upper limit also vary heavily. According to Mutoh et al. (1979) the upper conductivity limit is 10^{-5} S/m, but Smith (1986) could establish a conejet at 10^{-1} S/m. The situation is similar with the surface tension parameter. Conejets could be established with glycerin ($\gamma = 0.063$ N/m) and even with water ($\gamma = 0.073$ N/m).

The current in the cone is transported in two ways. There is ion conduction through the liquid due to the electric field and ion transportation due to fluid convection. When applying an electric field to a pending droplet it is deformed to a cone. The cone liquid surface is accelerated towards the apex due to a tangential electric stress on the free ions in the liquid and a jet is formed which is breaking up into droplets. Cone and jet shape, electric current and droplet size therefore depend on viscosity and conductivity of the liquid.

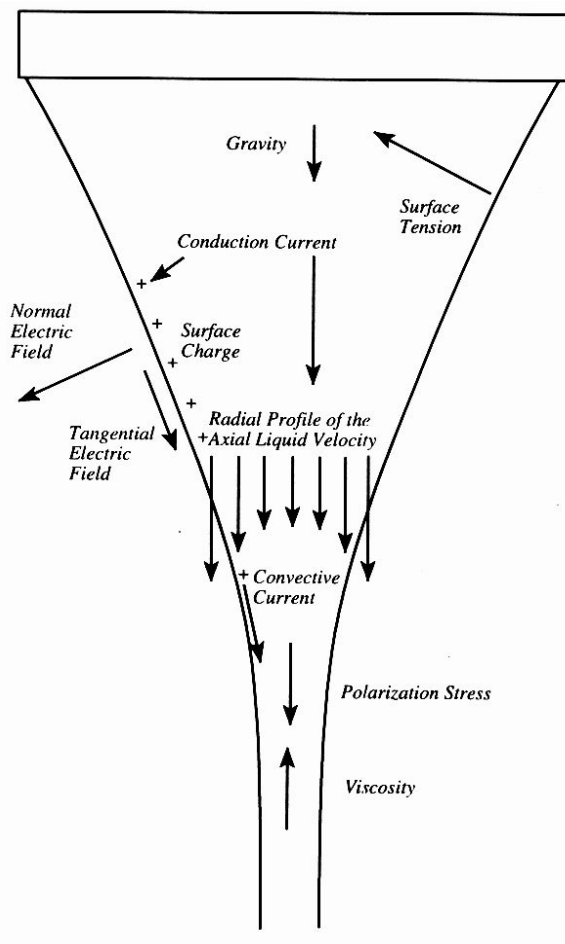


Figure 2-5 Cone shape, droplet size and electric current depend on the forces acting on liquid and dissolved ions: gravity, electric field, surface tension (Hartman, 1998)

Theoretical description of the conejet started with Taylor (1964) who was the first to explain the cone shape of the pending droplet at the capillary exit. He calculated the cone angle to be 49.3° . In his honor the conejet is often called Taylor-cone. Joffre et al. (1982) proposed a numerical model for shape calculation of a stable droplet at the capillary exit under the influence of an electric field. Their equations are balancing the inner liquid pressure with the electrical potential distribution between the capillary and a plate. The model results show good agreement with the experimental data and are not restricted to a purely conical shape as Taylor's analysis. Hartman et al. (1999) presented a model that is able to calculate the shape of cone and jet. They are also able to give values for the electric field inside and outside the cone and the surface charge density at the cone surface.

The intermittent multijet mode finds hardly any attention in literature. It is a variation of the continuous multijet mode and has the same visual appearance. But the breakup process and droplet size distribution are significantly different. One or several jets are emitted in an intermittent fashion from the capillary rim. In contrast to the cone and stable multijet it shows a broad polydisperse droplet size distribution. Jaworek and Kruppa (1996) investigated the stability regimes of continuous and intermittent multijet mode in the capillary-plate configuration regimes with respect to volume flow rate and electric potential. The intermittent conejet mode showed that small quantities of liquid are ejected in the form of short thick jets alternating at distinct locations of the capillary rim. The intermittent mode could be established from the continuous multijet by increasing external electric field and volume flow

rate. In this work, an advanced electrohydrodynamic atomization (EHDA) technique developed on this background has been adopted to fabricate nanostructured thin films and subsequently develop printed supercapacitors.

3. ITO Current Collector

3.1 Introduction

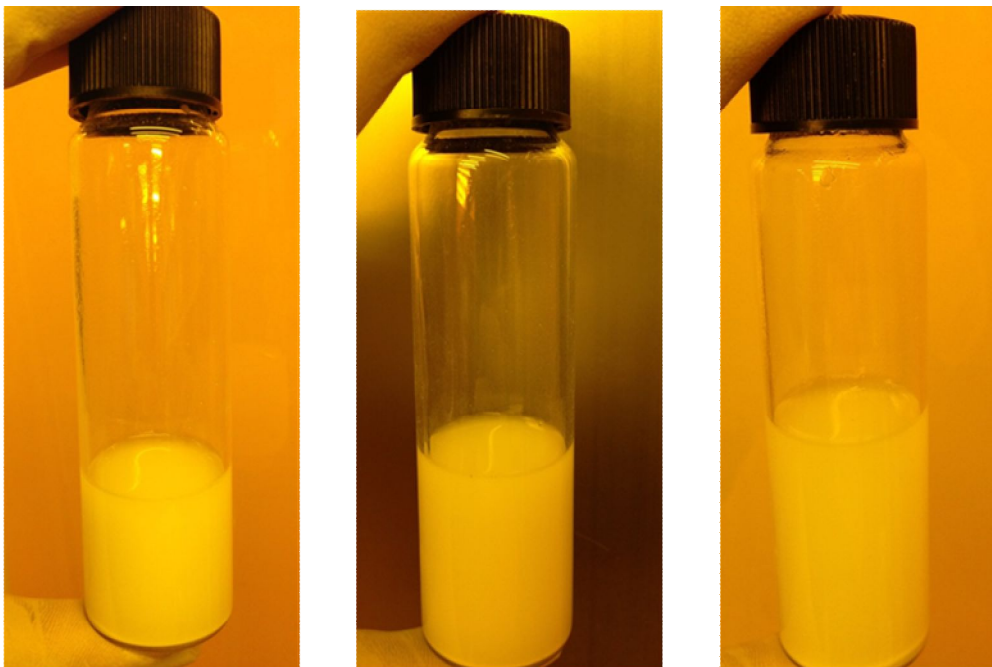
Indium tin oxide (ITO) is a highly transparent, wide band gap semiconducting material with a good conductivity. Owing to its optical band gap of ~ 3.6 eV, ITO has found its application as an advanced transparent semiconducting material in the opto-electronics industry. The high conductivity is observed only in non-stoichiometric form of ITO resulting from the oxygen deficiency and dopant tin (Sn), whereas the stoichiometric form acts as an insulator. Further, the structural, optical and electrical properties also depend on the fabrication techniques adopted and the growth conditions which could be maneuvered. Thus far, ITO thin films have been prepared by a wide range of deposition techniques which include sputtering, reactive thermal evaporation, electron beam evaporation, plasma enhanced metallorganic chemical vapor deposition (PEMOCVD), laser ablation, ion assisted deposition and pulsed laser deposition. Physical vapor deposition techniques have been reported to yield good quality ITO thin films and offer controllability over the thin films produced.

In this present study, we demonstrate the fabrication of ITO thin films through electrohydrodynamic atomization (EHDA) technique which is a cost-effective, room temperature, direct printing process and one of the developing fabrication techniques in the field of printed electronics. The structural, optical and electrical properties of the deposited ITO thin films are discussed in this chapter.

3.2 Experimental

ITO thin films have been produced through electrohydrodynamic atomization at room temperature and atmospheric pressure. The basic principle of EHDA depends on the disruption of liquid into an atomized spray due to the applied electric field. A liquid precursor is fed to a nozzle and on the application of electric field droplets at the nozzle tip form a stable cone-jet also known as Taylor cone. The charged, stable cone-jet of liquid precursor reaches the substrate as spray containing fine, charged liquid droplets. The substrate either carries a charge opposite to the droplet or grounded. EHDA technique can deposit thin films of a wide range of organic, inorganic compounds and synthetic polymers. The process can retain the samples relatively free from damage, as the process is carried out under room temperature and atmospheric pressure. This technique is capable of processing nano particles and fibers to deposit thin films over a large area and can be incorporated with roll-to-roll systems for mass production. Furthermore, depositions and patterns of the particle can be controlled by tuning the process parameters.

ITO ink of three different concentrations namely 5 wt %, 10 wt % and 20 wt % have been synthesized by dispersing ITO nanoparticles in a combination of ethanol and deionized water upon stirring with Triton-100x as the surfactant. The ratio of ethanol to deionized water to surfactant (Triton 100x) was kept at 3:1:2 for all the three different concentrations. Initially the ITO nanoparticles were added to ethyl alcohol and subjected to stirring followed by the addition of deionized water and surfactant. The resultant solution was stirred for 5 hours to achieve a stable, homogeneous dispersion. Flexible polyethersulphone (PES) and glass were used as substrates to deposit the ITO thin films. The substrates have been cleaned using de-ionized water followed by isopropanol in ultrasonic agitator. The cleaned substrates were plasma treated for enhanced adhesion prior to the deposition.



ITO 20 wt%

ITO 10 wt%

ITO 5 wt%

Figure 3-1 ITO ink synthesized at three different concentrations

Two different nozzles with diameter of 430 μ m and 150 μ m have been used to process the 20 wt % concentration of ITO ink. The liquid flow rate was maintained by a syringe pump (Harvard Apparatus, PHD 2000 Infusion) which held the syringe (Hamilton, Model 1001GASTIGHT syringe) containing the ink. A high-voltage regulated DC power supply (NanoNC) connected between the nozzle and the copper plate ground electrode was used to supply the electric field required for the deposition. A high resolution CCD camera (MotionPro N3) capable of operating at high speeds was employed to observe the tip of the nozzle in order to capture the various modes that occurred during the deposition. The process was optimized by varying the liquid flow rate, applied potential and stand-off distance.

The operating envelope for 20 wt% ink obtained with 150 μ m nozzle is shown in figure 3-2. From the operating envelope, the liquid flow rate was set at 250 μ l/hr while the applied potential was fixed at 5.5 kV. The stand-off distance was maintained at 10mm throughout the process. Both glass and PES were used as substrates. The deposited ITO thin films were then annealed at 120 $^{\circ}$ C.

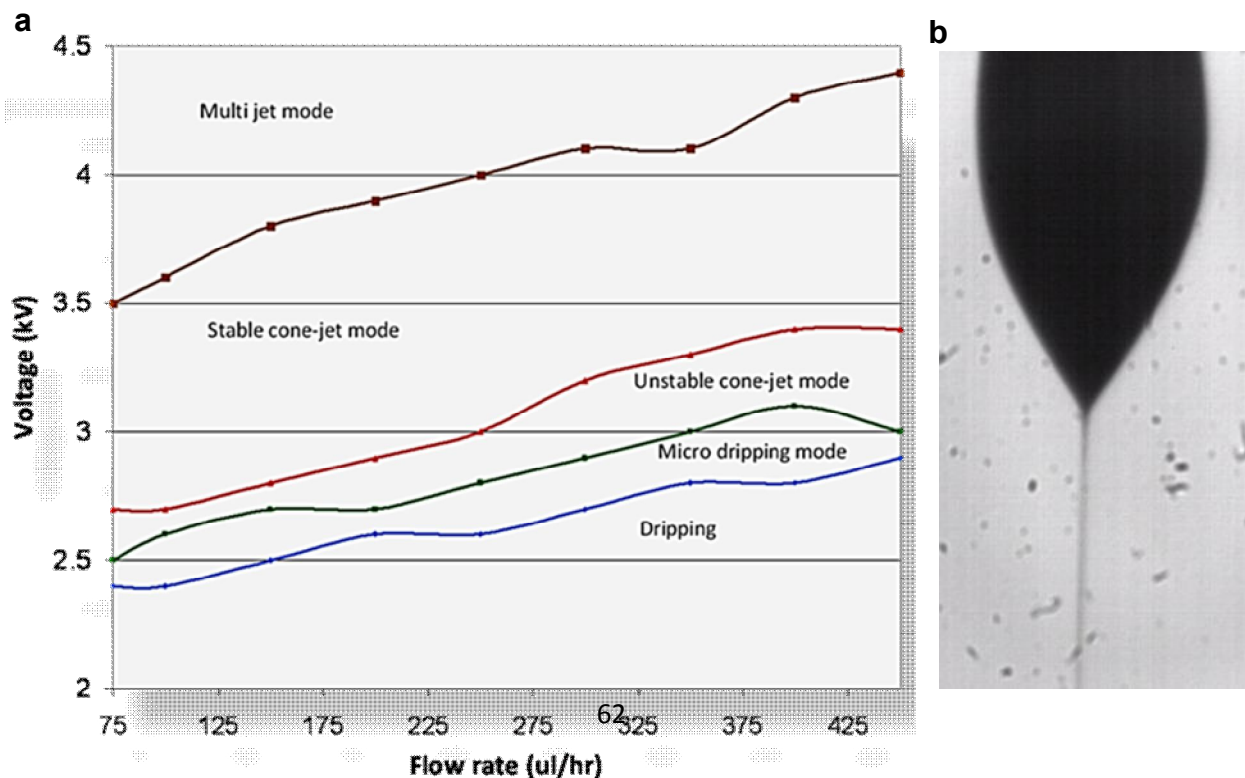


Figure 3-2 (a) Operating envelope (b) Stable conjet of 20 wt% ITO ink

To process 10 wt% ITO ink, stainless steel nozzle with a diameter of 430 μm was used. The optimized value of liquid flow rate was 125 $\mu\text{l/hr}$ whereas the applied potential was fixed at 5.3 kV. The stand-off distance was retained at 9mm.

The operating envelope for 10wt% ink is shown in figure 3-3. The ITO thin films deposited on PES substrates were cured at 120 $^{\circ}\text{C}$.

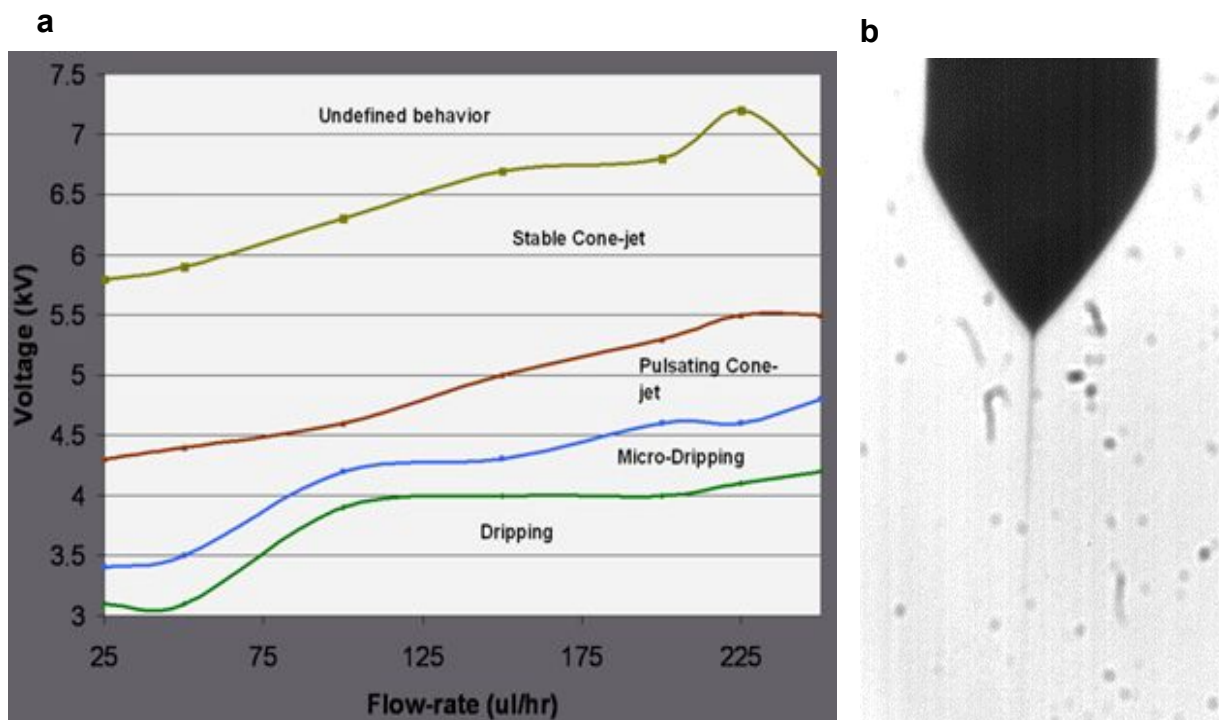


Figure 3-3 (a) Operating envelope (b) Stable conjet of 10 wt% ITO ink

The ITO (5 wt %) ink was sprayed through 150 μm stainless steel nozzle (NanoNC, NNC-DN-2230). A constant flow rate of (100 $\mu\text{l/hr}$) was maintained throughout the deposition and the applied voltage was sustained at 5.1 kV throughout the deposition.

Distance between the substrate and nozzle was maintained at 7mm. PES substrates were used to deposit the ITO thin films and then cures at 120 °C.

The crystallinity and purity of ITO thin films were analyzed using an X-ray diffractometer (Rikagu D/MAX 2200H, Bede model 200). The XRD measurement was performed using a Cu $\kappa\alpha$ radiation source of wavelength $\lambda = 1.5406 \text{ \AA}$. Transmittance of the ITO thin films was recorded by a UV-vis spectrometer (Shimadzu UV-3150) with a wavelength range of 200–800 nm. The surface morphology was examined by a field emission filed emission scanning electron microscope (FE-SEM, JSM-6700F, JEOL Ltd). The current-voltage (I-V) characteristics were measured by a semiconductor device (B1500A, Agilent, USA) parameter analyzer.

3.3 Results and discussion

Figures 3-4 (a) and 3-4 (b) show the FE-SEM micrographs of ITO thin films deposited with 20wt% ink at substrate speeds of 0.5 mm/s and 1mm/s respectively.

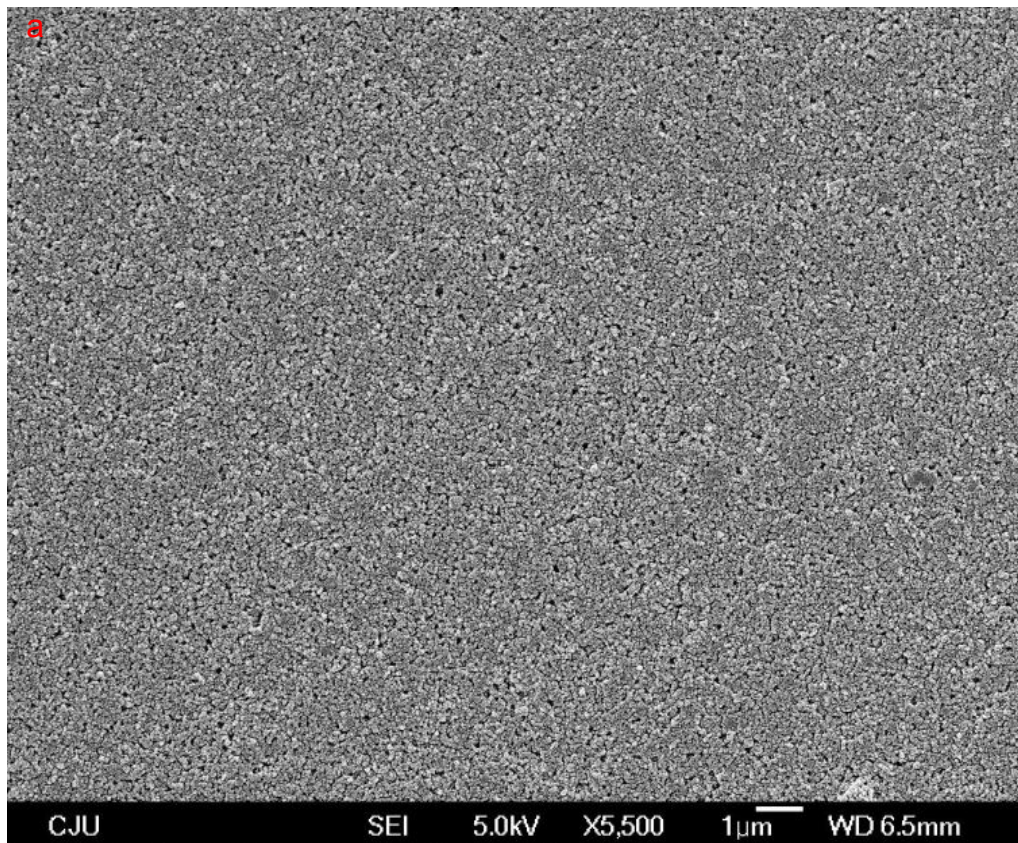


Figure 3-4 (a) FE-SEM micrograph of ITO thin film deposited with 20wt% ink at 0.5 mm/s

The thickness of the film deposited at 0.5 mm/s substrate speed was measured to be 1.5 μ m and the the 1mm/s substrate speed produced 600nm thick ITO thin films.

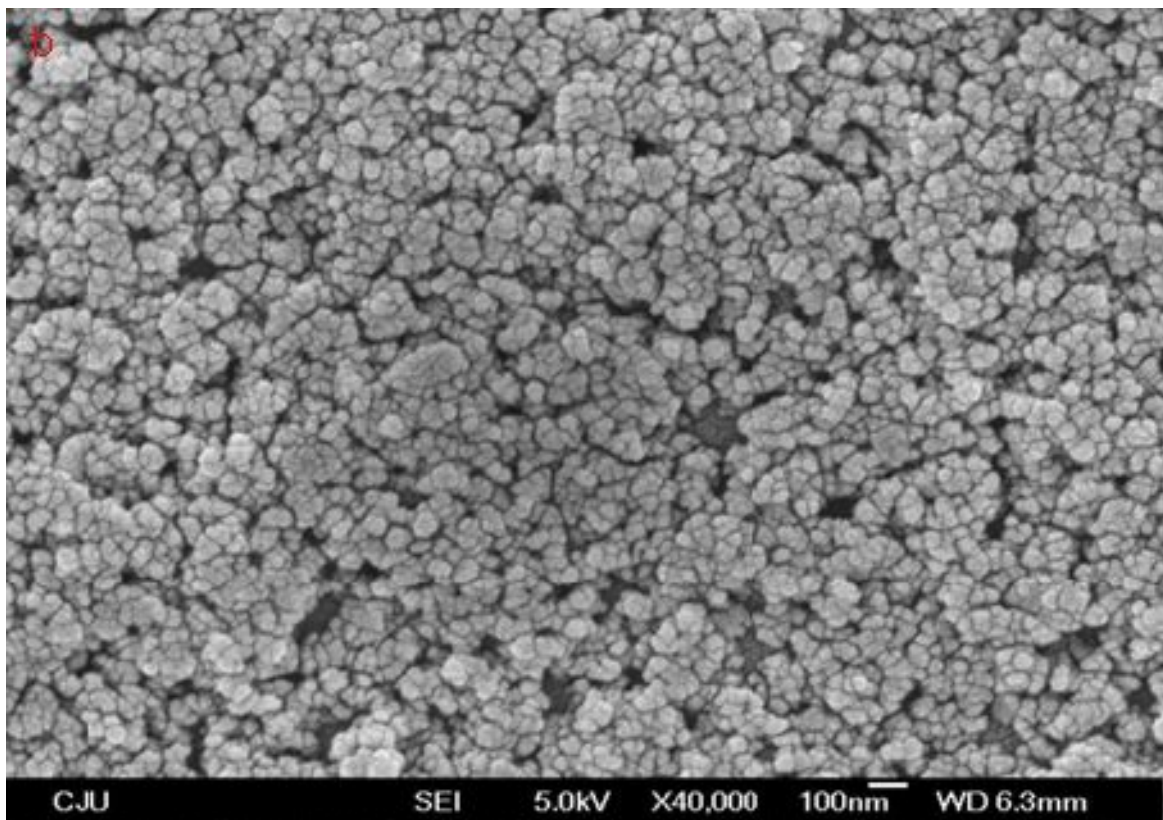


Figure 3-4 (b) FE-SEM micrograph of ITO thin film deposited with 20wt% ink at 1 mm/s

Though the surface morphology of ITO thin films deposited with 20 wt% ink at 0.5 mm/s substrate speed was smooth the thickness was on the higher side. On the other hand, thin films deposited with a substrate speed 1mm/s were discontinuous and nonuniform in nature. Figure 3-5 represents the FE-SEM micrographs of ITO thin films produced with ITO ink of 10 wt% particle concentration at substrate speeds of 0.5 mm/s and 1 mm/s respectively. The thickness of the thin films deposited at 0.5 mm/s was 5 μ m whereas thin films deposited at 1mm/s substrate speed was 2 μ m.

The relatively higher thickness of 10 wt% ink in comparison with the 20wt% is a result of the difference between the nozzle diameters (150 μ m for 20 wt% and 430 μ m for 10 wt %).

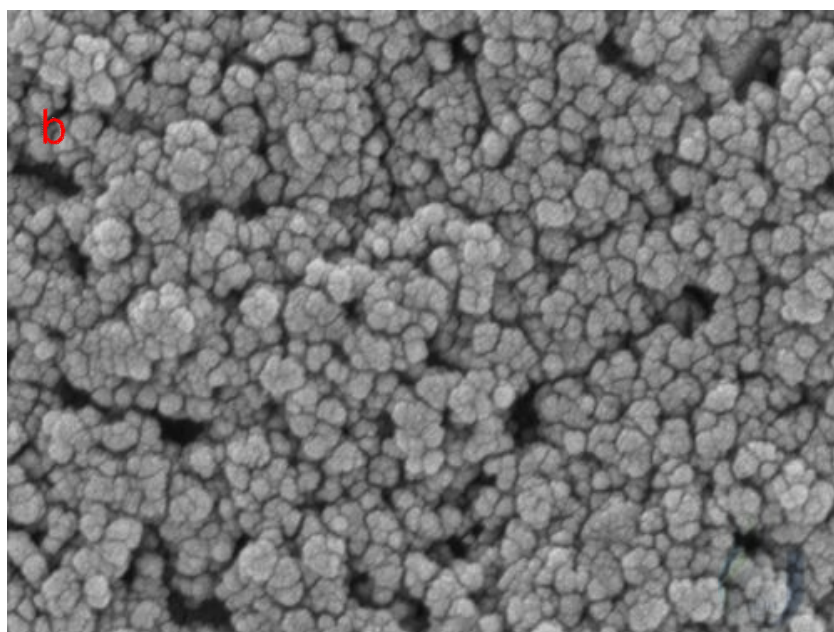
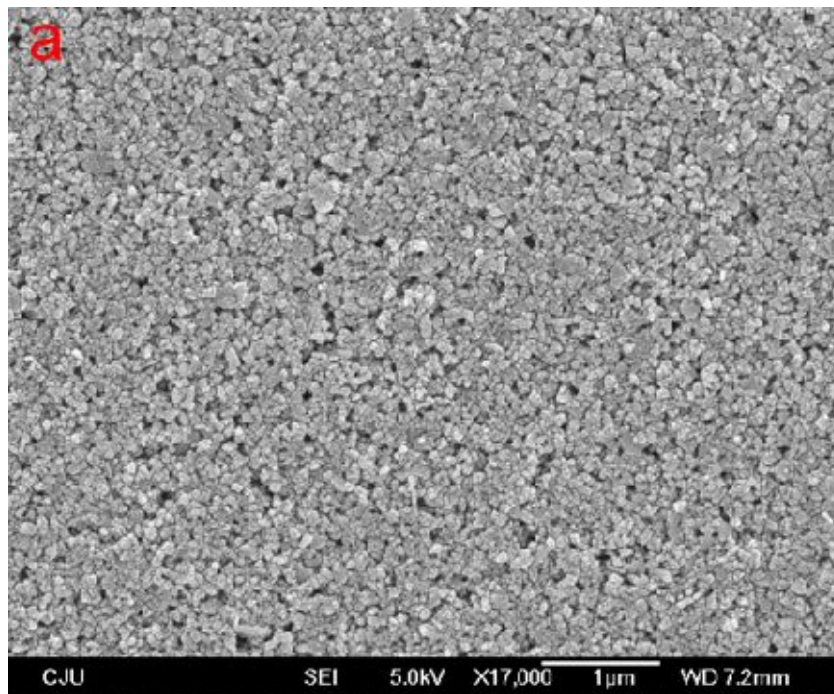
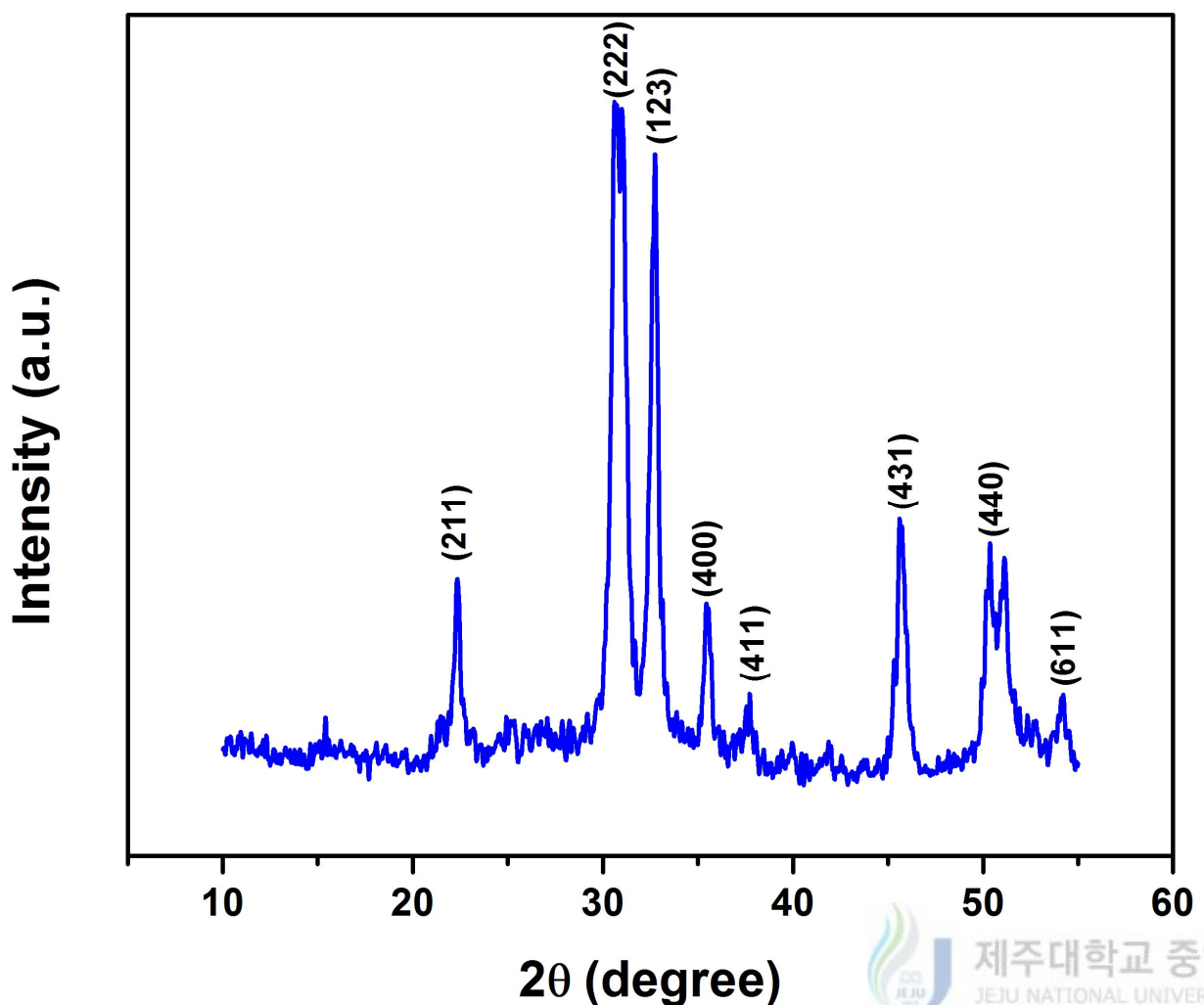


Figure 3-5 FE-SEM micrographs of ITO thin films deposited with 10 wt% at substrate speeds of (a) 0.5 mm/s and (b) 1mm/s

Figure 3-6 shows the X-ray diffraction pattern of ITO thin films fabricated through EHDA with 5 wt% ink. The predominant plane was (222) in addition to the peaks of (211), (400) and (440) which verify the cubic structure of In_2O_3 . The peak (123) corresponding to the cassiterite phase of SnO_2 could also be seen in the diffractogram with low intensity peaks of ITO phase namely (411), (431) and (611). The XRD spectrum validates the purity and



crystallinity of ITO thin films fabricated through EHDA despite the process being carried out at room temperature.

Figure 3-6 X-ray diffraction pattern of ITO thin film

Figure 3-7 shows the FE-SEM micrographs of ITO thin films of 5 wt% ink at different magnifications. The micrographs reveal the surface morphological features of ITO thin films. The thin films found to have well connected nanocrystallites of uniform size. The surface of ITO thin films was densely packed and smooth.

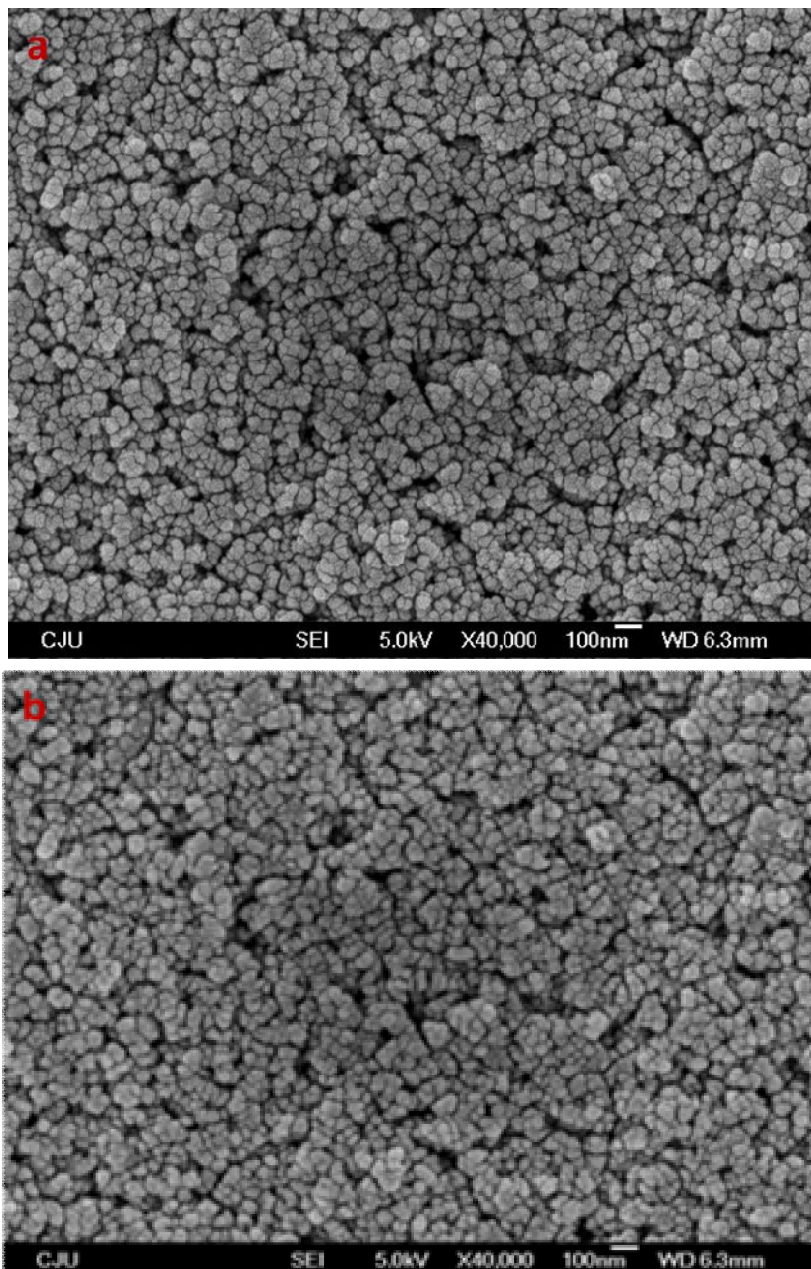


Figure 3-7 FE-SEM micrographs of ITO thin film of 5 wt% ink at (a)microscale (b)nanoscale magnifications

Figure 3-8 shows the transmittance UV-vis spectrum of ITO thin films of 5 wt% ink. The wavelength range was set between 200nm to 800nm to record the transmittance spectrum. The transmittance value of ITO thin films at Fraunhofer sodium D-line (589.59 nm) was found to be 96% which qualifies the deposited ITO thin films as highly transparent. The cut-off wavelength found in the UV-vis spectrum at 50% transmittance was well below 350 nm which substantiates that ITO is completely colorless.

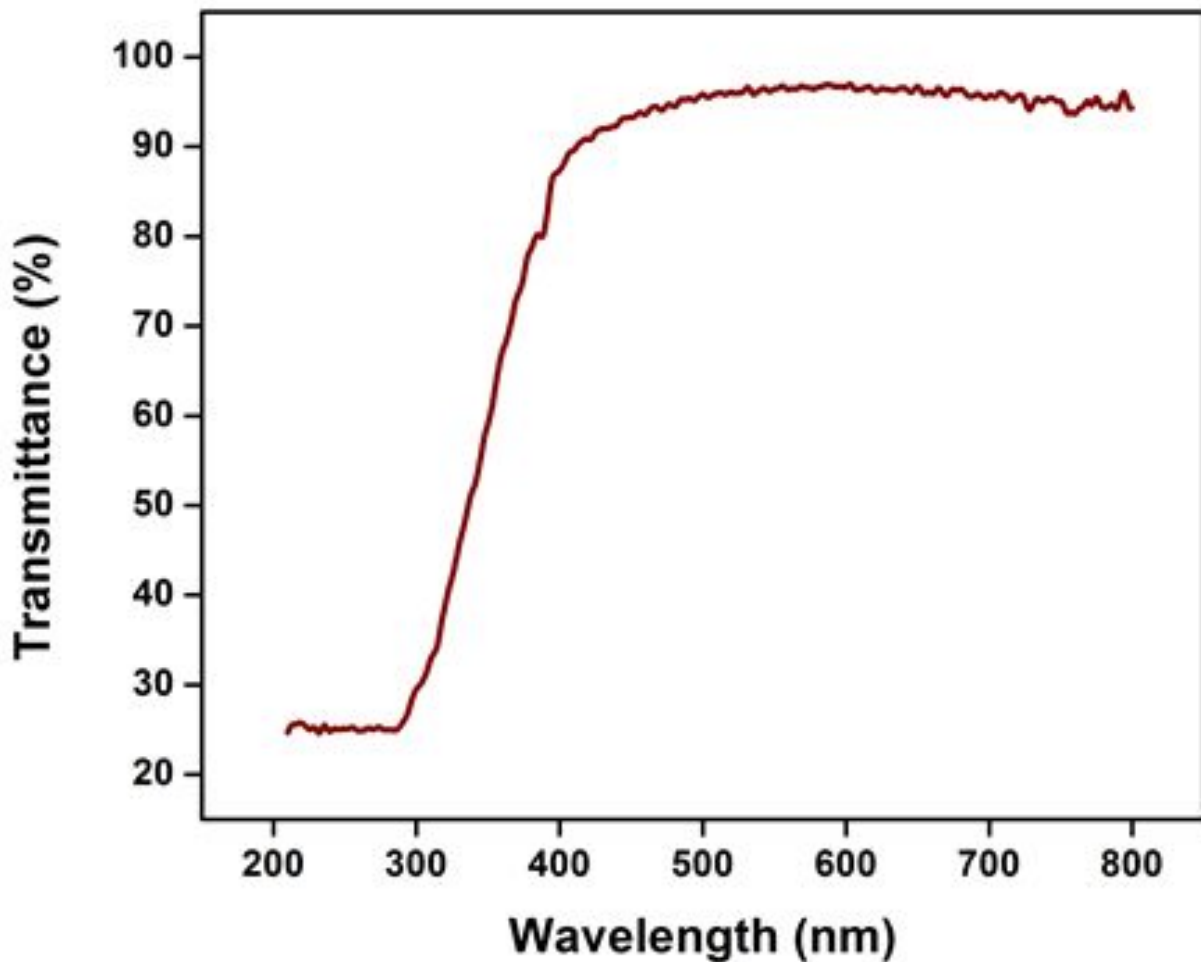


Figure 3-8 Transmittance UV-vis spectrum of ITO thin film

Figure 3-9 shows the I-V characteristics of the ITO thin films deposited with 5 wt% ink. The current-voltage characteristics were studied from -5V to 5V applied voltages. The I-V curves showed perfectly linear behavior through the origin. This Ohmic behavior exhibited by the ITO thin films demonstrates the conducting nature and potential application as electrodes in a wide range of electronic devices.

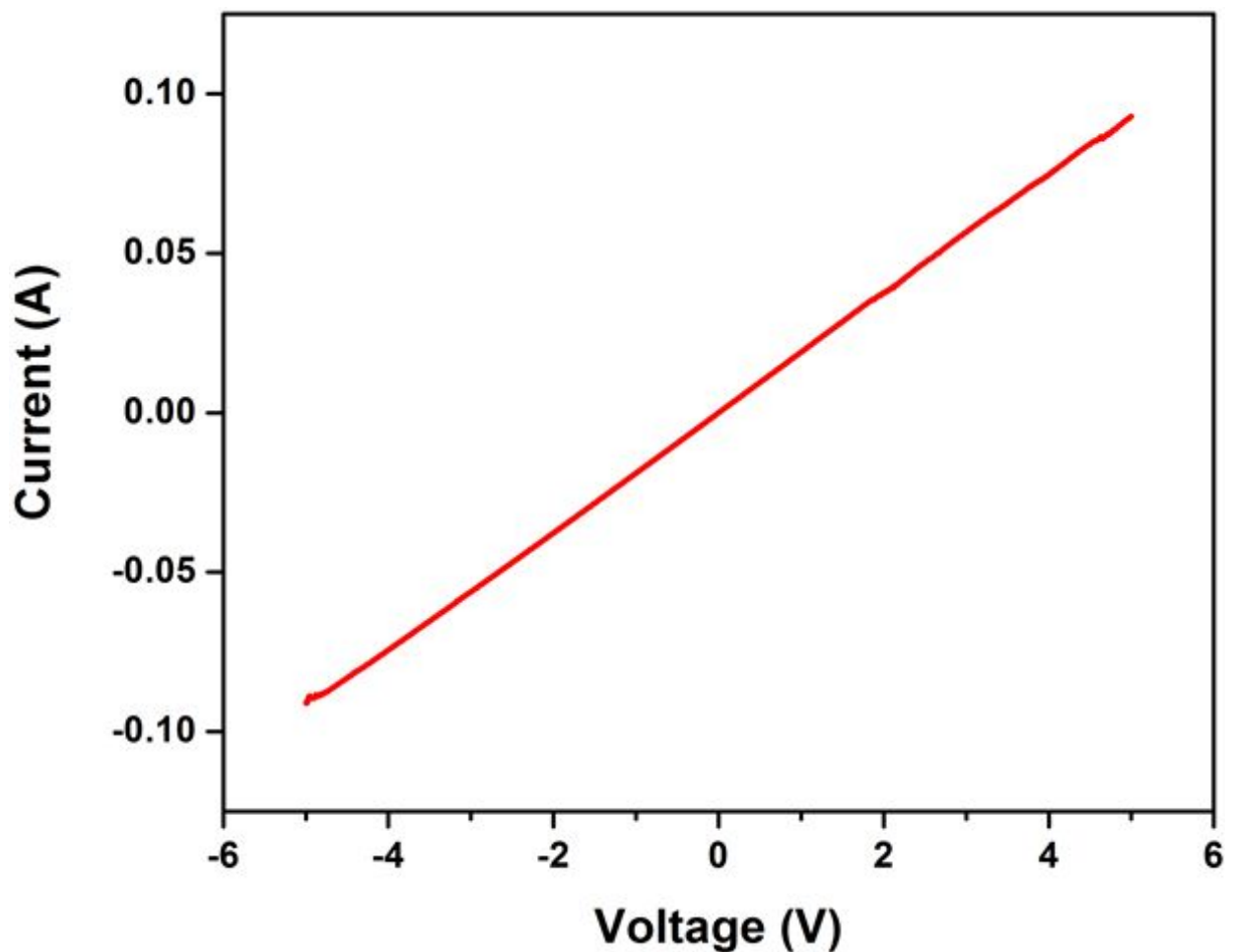


Figure 3-9 I-V characteristics of ITO thin film

3.4 Conclusion

ITO thin films have been fabricated by a cost-effective, room temperature, advanced direct printing technique of EHDA. ITO ink with three different particle concentrations namely 20 wt%, 10 wt% and 5 wt% have been synthesized. Of all the three concentrations, ITO 5wt% has yielded thin films of 120 nm thick whereas the 10 wt% and 20 wt% produced thin films with thickness ranging from 600nm to 5 microns. Subsequently, ITO 5 wt% ink which met the device requirements has been chosen for the fabrication of current collectors. The XRD analysis confirmed the purity and crystalline nature of ITO thin films implying the process introduced no impurities. Surface morphology of the thin films revealed smooth surface with densely packed nanocrystallites of uniform size. The optical studies showed that ITO is colorless and highly transparent with a transparency of 96%. Perfectly Ohmic behavior of current-voltage curve validated the conducting nature of ITO thin films. The electrohydrodynamic atomization technique with its flexibility to incorporate with roll to roll systems has the potential to mass produce feasible, high purity thin films at higher production rates without any need for isolated ambience. The ITO thin film thus produced through this technique is a promising candidate to be used as highly transparent electrodes in energy storage applications, organic photovoltaics, organic light emitting diodes and in sensor modules.

4. Fabrication of flexible SWCNT active layers

4.1 Introduction

Single-walled carbon nanotubes (SWCNTs) have been found to have high mechanical strength, excellent conductivity, high chemical stability and high surface area making them ideal electrode material (Ajayan et al. 1993, Fukushima et al. 2003, Izadi-Najafabadi et al. 2010). Based on chirality, the orientation of graphene lattice with respect to the tube axis, SWCNTs can be metallic or semiconducting in nature. Their thermal conductivity ($3500 \text{ W m}^{-1} \text{ K}^{-1}$) can exceed that of diamond (Xu et al. 2011, Pop et al. 2006). Owing to their intrinsic nature and high energy density, SWCNTs with little bundling exhibit exceptional capacitor performance (Huang et al. 2010, Kimizuka et al. 2008). Due to their attractive properties and wide-spread applications, such as batteries, flat panel displays, hydrogen storage, supercapacitors, etc., SWCNTs are emerging as multi-functional coating material.

There are different types of physical and chemical methods including physical vapor deposition, chemical vapor deposition, etc., employed to design nanostructured films (Chopra et al. 1983, Vargas Gracia et al. 2003). However, these techniques have some limitations such as high cost, low production rate and need for specific ambiance which have a negative impact on large scale production. Consequently, development of advanced fabrication techniques for the deposition of nanostructured thin films has gained more attention in thin film industries. The limitations of the above stated techniques can be overcome by the direct printing

technique of electrohydrodynamic atomization (EHDA) which is a unique, cost-effective, room-temperature process (Muhammad et al. 2011).

The basic principle of EHDA technique relies on the disruption of liquid into an atomized spray containing charged droplets due to the applied electric field (Ganan Calvo et al. 1999). Briefly, a liquid precursor is fed to a nozzle which further results in the formation of droplet at the nozzle. When an electric field is applied, the droplet at the nozzle tip tends to attain a Taylor cone or stable cone-jet due to the ejection of electric field on the liquid droplet. A charged jet of liquid precursor is propelled to the substrate which carries a charge opposite to the droplet or is grounded. This technique offers the production of unique nanostructured thin films on desired substrates and are highly influenced by several physico-chemical properties of the precursor liquid such as viscosity, surface tension, electrical conductivity, and flow rate, etc. In order to achieve stable cone jet, it is highly important to optimize these parameters. It can be achieved by several surface modification processes or by the use of stabilizer. On the other hand, some process parameters have also influenced the nature of thin films such as working distance, applied voltage, substrate velocity and nozzle diameter.

In this work, we have reported the efficacious deposition and investigation of flexible nanostructured thin films of single-walled carbon nanotubes through EHDA technique. The process parameters for achieving homogeneous thin film via Taylor cone formation have been distinctly presented. The morphology and surface chemistry of the deposited SWCNT thin film have been discussed. The electrical study of deposited SWCNT thin film on flexible substrate has been demonstrated with respect to temperature.

4.2 Materials and methods

Materials:

SWCNT ink was procured from Nanostructured and Amorphous Materials Inc., USA. Ethanol (CH₃CH₂OH) was acquired from Sigma-Aldrich, South Korea.

Preparation of Ink:

The original SWCNT (3 wt%) ink was modified for the EHDA process with a combination of ethanol and de-ionized water. Combination of solvents yielded stable, homogeneous solution required for the atomization. In the process of modification, five different combinations have been prepared and studied to make the ink suitable for the EHDA process. Initially, 1 ml of ethyl alcohol was added to 1 ml of ink which was the first combination of 1:1. The second combination had equal amounts of ethyl alcohol, SWCNT ink and deionized water, i.e. a ratio of 1:1:1. The ratio of SWCNT ink to ethyl alcohol to deionized water for third combination was 1:2:1. Ratio of deionized water was made equal to that of ethyl alcohol which was twice that of SWCNT ink for the fourth combination, resulting in ink to ethanol to deionized water ratio of 1:2:2. The fifth combination of ink to ethanol to deionized water was 1:3:2.

The need for all these different combinations originated from the fact that the original ink was water based. As the high surface tension of water was not suitable for the EHDA process, miscible solvent with low surface tension had to be added to reduce the surface

tension. However, just addition ethyl alcohol to the ink made the ink inhomogeneous; to compensate this effect and to make the ink homogenous deionized water was added.

Furthermore, as procured ink was highly viscous and to be processed through EHDA the ink had to be diluted with suitable solvents. For all the aforementioned combinations, ethanol was added to SWCNT ink and stirred at 1000 rpm followed by addition of deionized water drop by drop while the stirring continued. The solution was stirred for 55 minutes for all the five combinations. The fifth combination has produced a stable, homogenous solution suitable for the EHDA process. The obtained solution was filtered through the polymeric filter (PTFE – 0.45 μm) to obtain homogeneous dispersion of SWCNT.

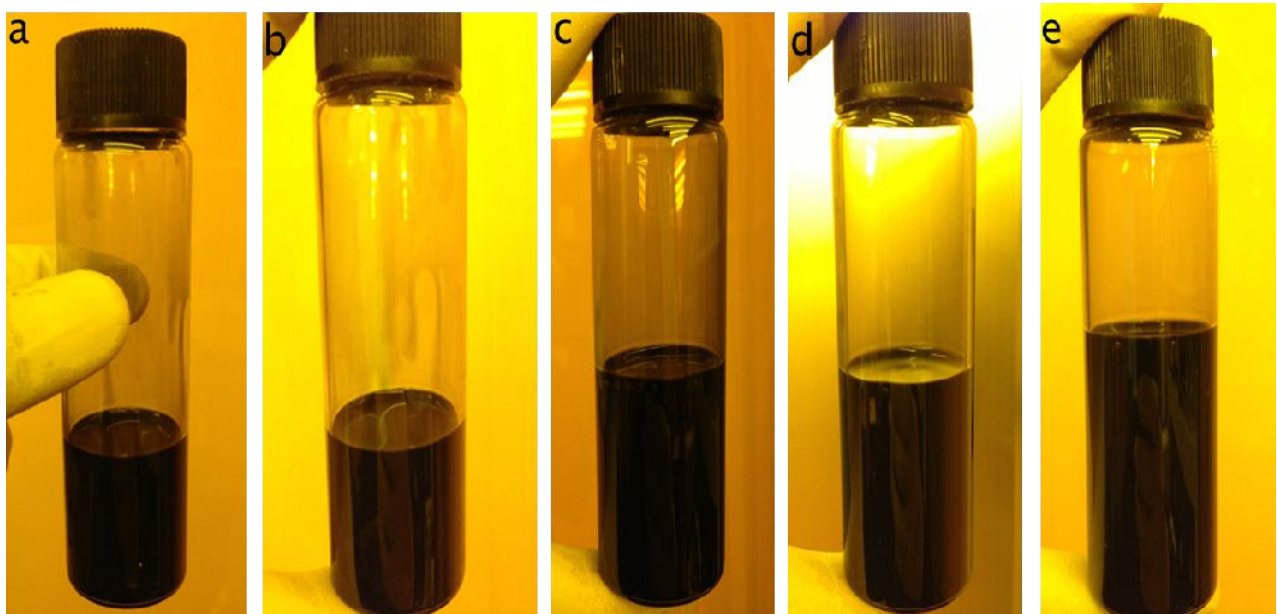


Figure 4-1 Modified SWCNT ink at different combinations (a) SWCNT ink to ethanol, 1:1 (b) SWCNT ink to ethanol to DI water 1:1:1, (c) SWCNT ink to ethanol to DI water 1:1

1:2:1, (d) SWCNT ink to ethanol to DI water 1:2:2, (e) SWCNT ink to ethanol to DI water 1:3:2.

Deposition of SWCNT thin films using EHDA technique:

The EHDA setup consists of a nozzle with 430 μm internal diameter and 610 μm external diameter. The SWCNT solution was electrosprayed through the metallic nozzle with different flow rates and various applied potentials to attain a stable cone-jet. The optimum flow rate for the formation of Taylor cone and successive mono-dispersed spray was ascertained to be from 50 $\mu\text{l/h}$ to 90 $\mu\text{l/h}$. As the voltage varied from 0 to 4.1 kV, different modes of atomization such as dripping, micro-dripping, unstable cone-jet, stable cone-jet and multi-jet appeared. A steady flow rate of 70 $\mu\text{l/h}$ was maintained throughout the experiment for the SWCNT film deposition. Dripping mode appeared up to a potential of 2.3 kV whereas micro-dripping was observed from 2.3 kV to 2.7 kV. Unstable cone-jet began at 2.7 until the vital mode of stable cone-jet emerged at 3.2 kV. The stability of cone-jet sustained until the potential reached a value of 3.7 kV. Multi-jet started at 3.7 kV and remained till 4.1 kV. On increasing the applied voltage further, the jet discharged. For the deposition process a potential of 3.5 kV was retained. Spraying time or substrate speed and the stand-off distance also play a crucial role in determining the thin film thickness and the surface morphology.

During this process, a stand-off distance of 6 mm and a substrate speed of 5 mm/s were sustained. The block diagram of the EHDA is represented in Figure 4-2 and a photograph of the EHDA setup used in the experiment is shown in Figure 4-3 and Figure 4-4. SWCNT thin films thus deposited have been annealed at 90 $^{\circ}\text{C}$ for 1 h. The film thickness

was measured using thin film thickness measurement system (K-MAC ST4000-DLX) at 10 different points on the film and the average thickness of the film came out to be approximately 90 nm.

Taylor cone and spray formation:

The EHDA experiment usually starts from a minimum flow rate and continues to a maximum flow rate with various voltages in order to obtain different atomization modes such as dripping, microdripping, pulsating cone jet, stable cone jet and multi-jet. This process is used to optimize the flow rate and applied voltage for the stable cone-jet mode of spray. Figure 4-5 shows the different modes of atomization captured by a high-speed CCD camera with a constant flow rate of 70 $\mu\text{l/h}$ at different voltages. The dripping and microdripping modes appeared from zero voltage until to 2.3 kV, while the spindle mode started appearing at 2.3 kV. The pulsating cone jet appeared at 2.7 kV. The stable cone jet formed at 3.2 kV and it remained until the multi-jet formed at 3.7 kV. Increasing the applied voltage after 3.7 kV led to jet discharge. A flow rate of 70 $\mu\text{l/h}$ was used throughout the experiment to achieve a homogeneous thin film.

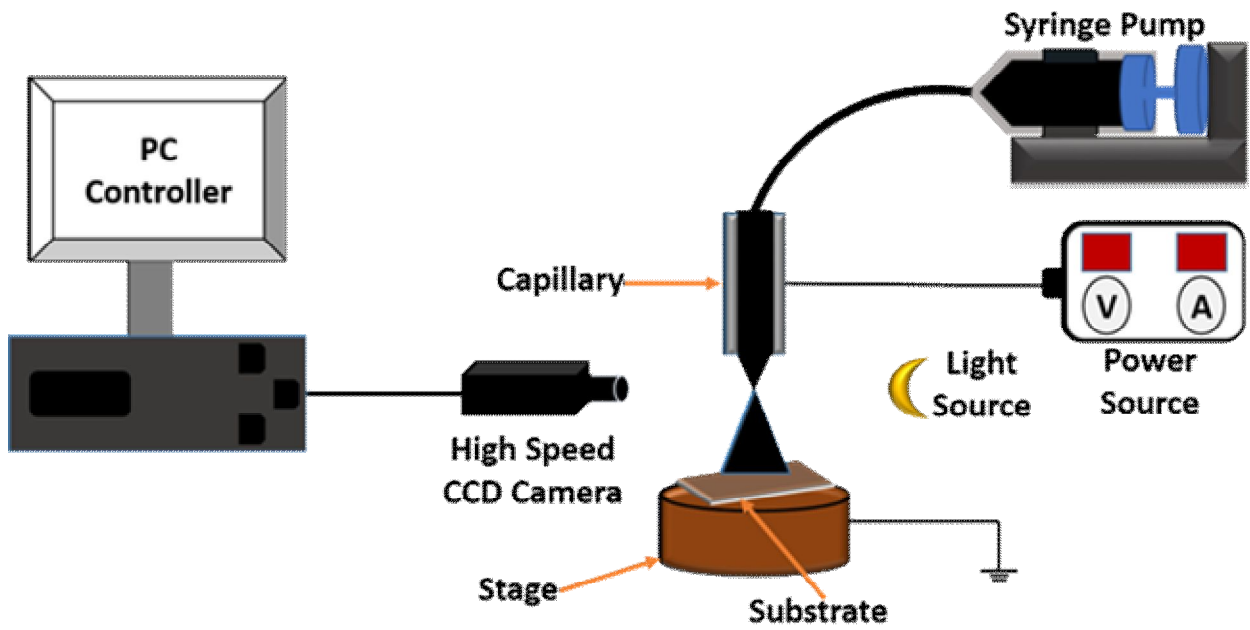


Figure 4-2 Schematic diagram of the electrohydrodynamic atomization system

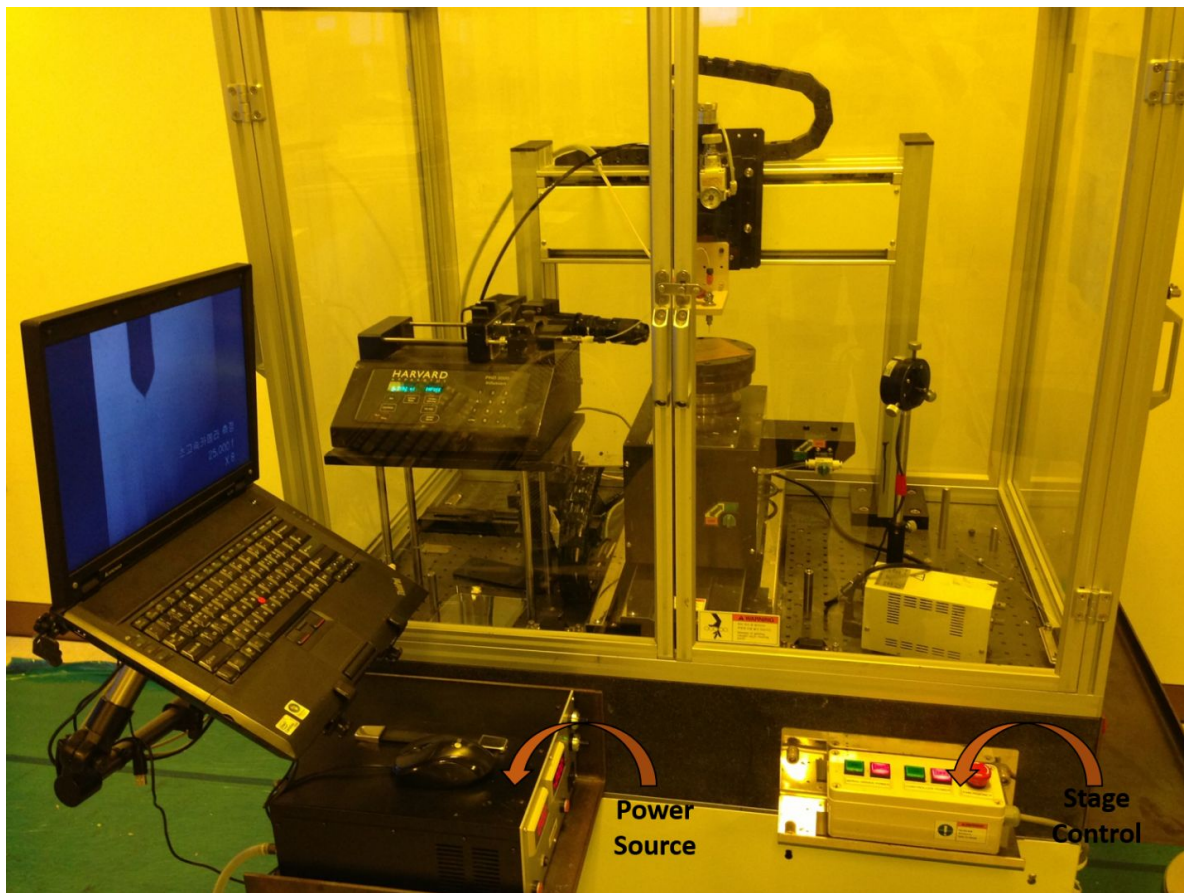


Figure 4-3 Photograph of electrohydrodynamic atomization system

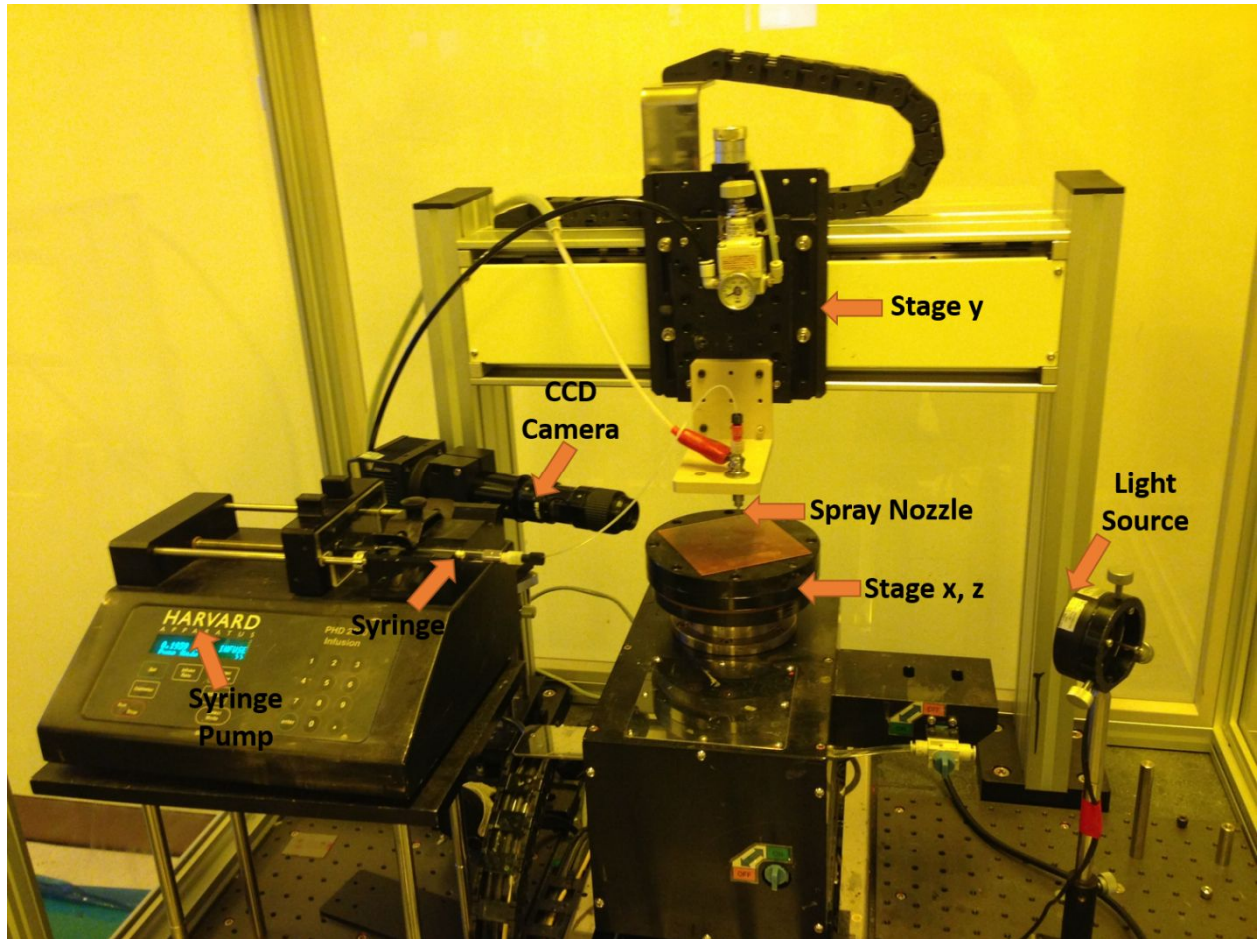


Figure 4-4 Close-up photograph of EHDA system

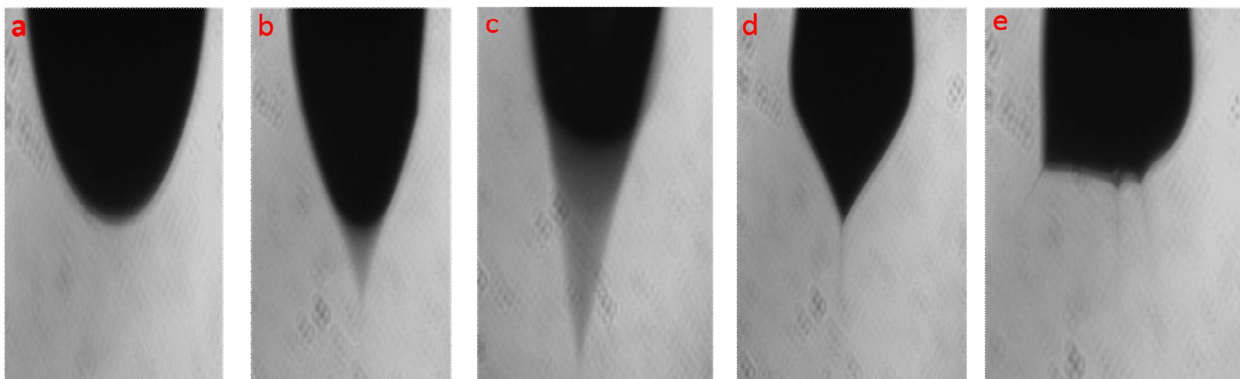


Figure 4-5 Different modes of atomization of SWCNT, a) Dripping, b) Micro-dripping, c) Unstable cone-jet, d) Stable cone-jet, e) Multijet mode

Characterization techniques:

The crystallinity and phase purity of the prepared SWCNT thin films were analyzed using an X-ray diffractometer (Rikagu D/MAX 2200H, Bede model 200). The XRD measurement was performed using a Cu $\kappa\alpha$ radiation source of wavelength $\lambda=1.5406 \text{ \AA}$. FTIR analyzer (Bruker IFS 66/S, Germany) was employed to investigate functional groups present in the film. The surface morphology was examined by a field emission scanning electron microscope (JEOL, JEM1200EX II). The transparency of the films was recorded by a UV/vis/NIR spectrometer (Shimadzu UV-3150) with a range of 200–700 nm.

The current–voltage (I–V) characteristics of the SWCNT thin films were measured by a semiconductor device (B1500A, Agilent, USA) parameter analyzer. The electrochemical characterization of the SWCNT active layers were carried out using an AUTOLAB PGSTAT302N electrochemical work station. A three-electrode cell consisting of a working electrode, platinum foil as counter electrode, and an Ag/AgCl reference electrode, was used for measuring the electrochemical properties of SWCNT active layers. A liquid electrolyte of 1 M Na₂SO₄ solution was used as at room temperature. The cyclic voltammetry (CV) curves of the SWCNT electrode have been obtained for scan rates ranging from 5 through 125 mV s⁻¹ for a potential range of 0–0.8 V. Electrochemical impedance spectroscopy (EIS) measurements were ca using a direct current (dc) bias of 0.1 V with a signal of 10 mV over the frequency range of 0.1 Hz to 100 kHz. The galvanostatic charge-discharge curves were attained over the potential range of 0-0.8 V (vs. a saturated calomel electrode (SCE)) for three different values of current densities, namely 2.5, 5, 7.5, and 10 mA cm⁻².

4.3 Results and discussion

XRD analysis of SWCNT thin films:

The X-ray diffraction is used to investigate the crystallinity of SWCNT thin films. Figure 4-6 (a) shows the X-ray diffraction of the deposited SWCNT thin films. The strong characteristic peak of SWCNT corresponding to the (002) plane could be seen in the figure as reported in previous studies (Chew et al. 2009). No other peaks were observed which validates that the processing of the solution did not introduce any impurities and hence the purity of the deposited SWCNT film is substantiated.

Surface morphology of CNT thin films:

The surface morphology and film uniformity of nanostructured thin films were examined via FE-SEM analysis. Figure 4-6 (b) shows the FESEM micrographs of SWCNT thin films deposited on flexible PES substrates. The surface morphology revealed that the layer is non-porous with closely packed nanotubes. The length and diameters of SWCNT were ~1 μm and ~30 nm, which significantly influences the optical and electrical properties of carbon nanotube based device applications. The occasional bundling up of the nanotubes has been observed which is desirable for energy storage applications.

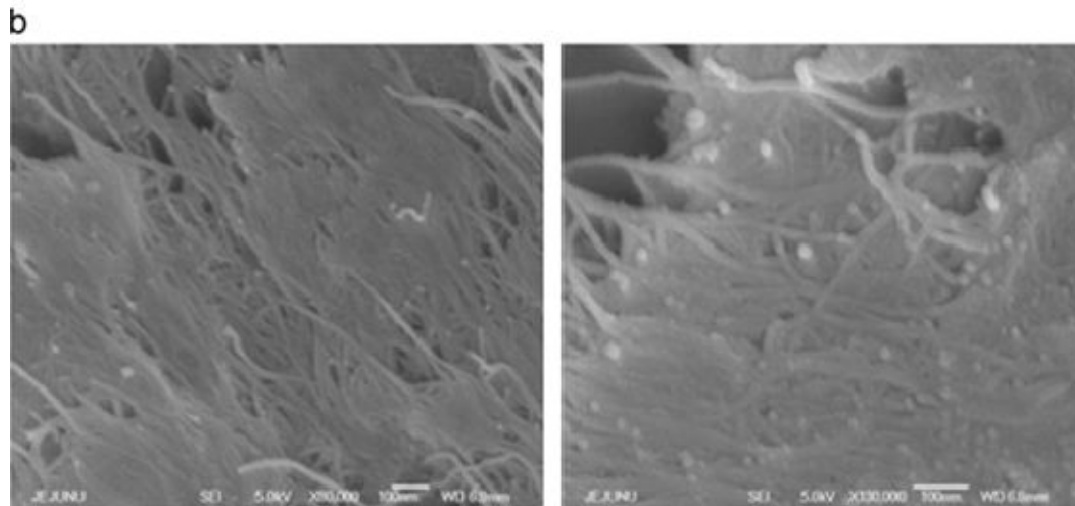
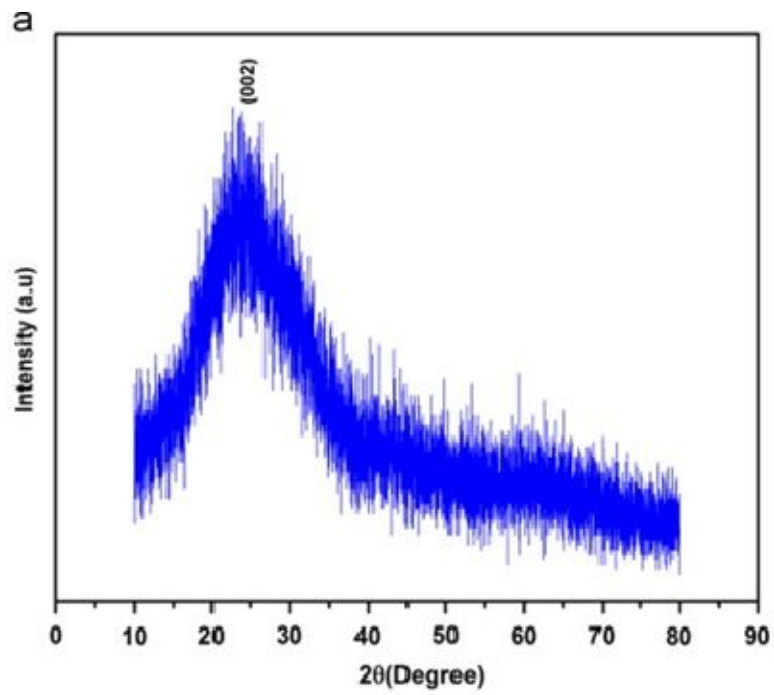


Figure 4-6 (a) X-ray diffraction pattern SWCNT thin films on PES substrates. (b) FE-SEM micrographs of SWCNT thin films

Surface chemistry analysis:

The functional groups present in SWCNTs analyzed through FTIR spectroscopy as shown in Figure 4-7 (a). The peak at $\sim 1257\text{ cm}^{-1}$, 1453 cm^{-1} and 1167 cm^{-1} are attributed to the oxygenated functional groups such as C–O–C, C–OH and C–O. The peak at $1600 \sim 1650\text{ cm}^{-1}$ arises due to the C–C skeletons present in the SWCNT (Wang et al. 2009). In addition, the carbonyl group (C=O) has appeared at $\sim 1730\text{ cm}^{-1}$, which indicate the presence of carboxylic or ester group. The FTIR spectrum of SWCNTs illustrates the presence of C=O (1734 cm^{-1}), C–OH (1453 cm^{-1}), C–O–C (1257 cm^{-1}), and C–O (1167 cm^{-1}) (Titus et al. 2006, Chou et al. 2010). All these functional groups make SWCNTs hydrophilic in nature which lead to homogeneous dispersion and a uniform spray through EHDA.

Optical properties of SWCNT thin films:

Figure 4-7 (b) shows the UV-vis spectroscopy of SWCNT thin film. It shows a maximum absorption peak at 267 nm which corresponds to the $n\text{-}\pi^*$ transitions of the aromatic C–C bonds present in the SWCNT skeleton (Titus et al. 2006). The band gap calculated from the UV-vis absorption spectra was 3.1 eV. The absorption spectra revealed that the SWCNT film has low absorbance in the visible region, which is a characteristic of SWCNT. The transmittance of the SWCNT thin film showed that it has 85% transmittance in the visible region. The high transparency of the SWCNT films is a desirable property in developing flexible, transparent electrodes for various printed electronics devices including batteries and supercapacitors.

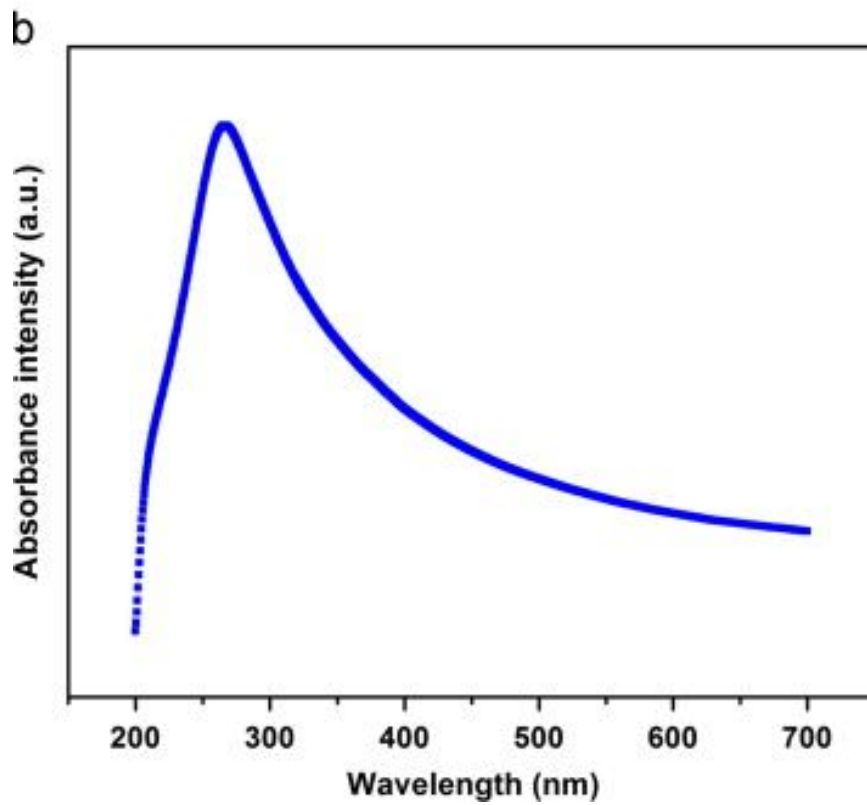
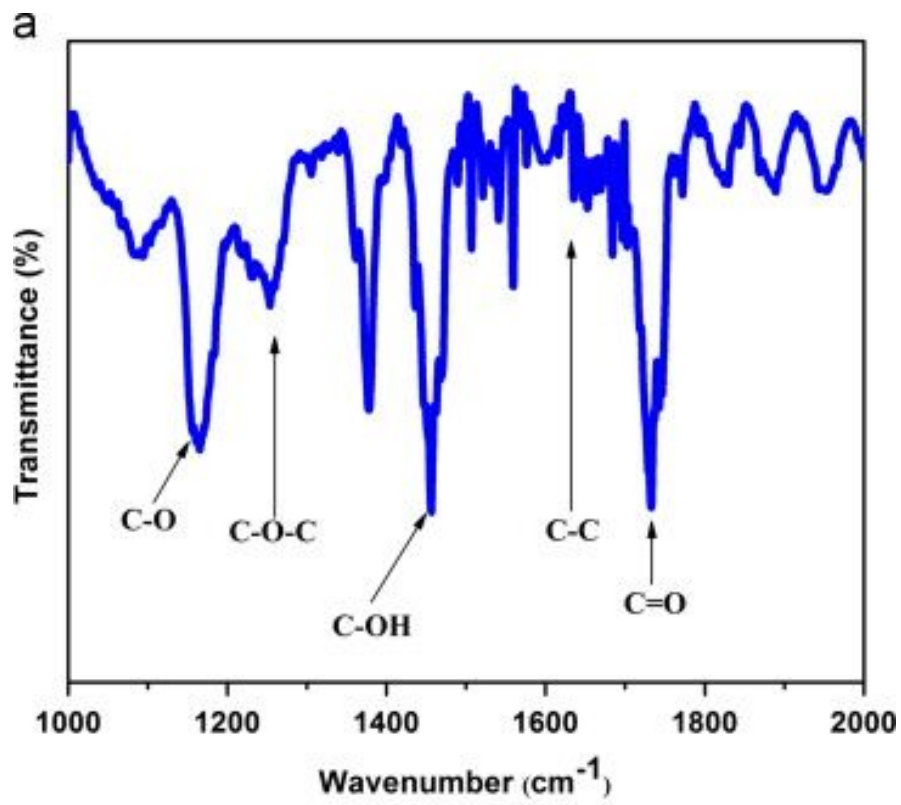


Figure 4-7 (a) Fourier transform infra-red absorption spectra of SWCNTs. (b) UV-vis spectra of SWCNT thin films

Electrical study:

The electrical study of SWCNT thin film was examined through current-voltage (I –V) measurement. Figure 4-8 (a) shows the (I –V) measurement of SWCNT thin films. The I-V characteristics of the SWCNT thin films were studied at different temperatures and voltages. The temperature was gradually increased from a minimum of 10°C to a maximum of 90°C, whereas the voltage values were 0.2 mV, 1mV, 2mV and 5mV respectively. For all the applied voltages linear curves were observed which confirmed the Ohmic behaviour. The thin film exhibited linear behavior at all temperatures, which confirmed the Ohmic behavior of SWCNT thin film (Titus et al. 2006). Figure 4-8 (b) shows the semi-logarithmic scale of thin film. These results reveal that the current density of SWCNT thin film has increased with temperature.

Electrochemical study:

The capacitive performance of SWCNT electrode fabricated through EHDA on flexible PES substrates was evaluated by cyclic voltammetry, electrochemical impedance spectroscopy and galvanostatic charge-discharge techniques. Figure 4-9 shows the CV curves of EHDA deposited SWCNT electrode at scan rates ranging from 25mV s⁻¹ to 125mV s⁻¹ in 1 M Na₂SO₄ electrolyte solution. All of the CV curves observed had a similar trapezoidal shape, which indicated the electrochemical double layer capacitive behavior of the SWCNT electrode. The specific capacitance (Cs) of the SWCNT electrode can be calculated from the CV curves through the following equation,

$$C_s = \frac{\int Idv}{vm\Delta V} \quad (1)$$

Where integrated area under the CV curve I is the response current (A), m is the mass of the active material (mg), v is the scan rate (Vs^{-1}), and ΔV is the potential window (V).

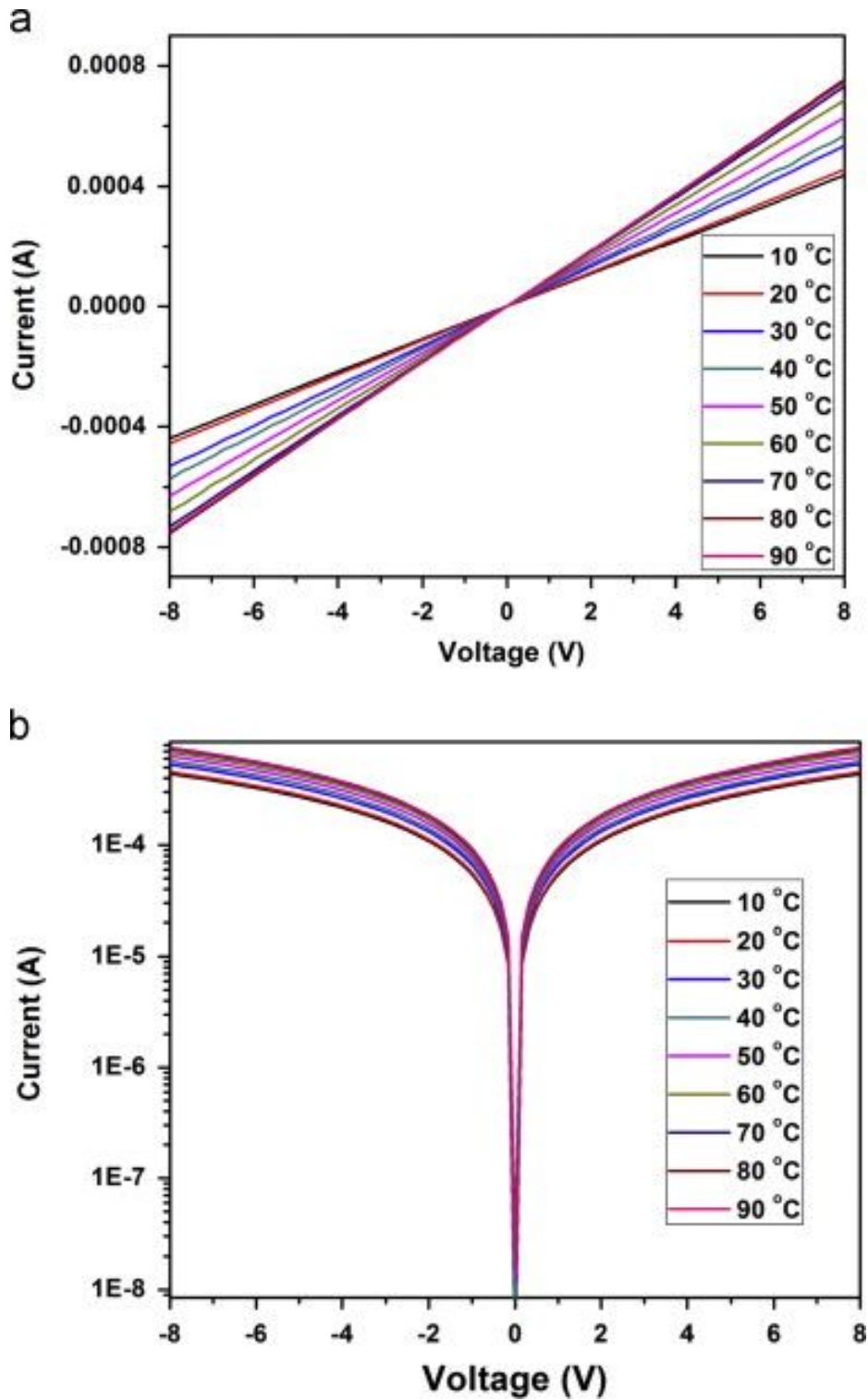


Figure 4-8 (a) I-V characteristics of SWCNT thin films at various temperatures (b) Semi-log of I-V characteristics of SWCNT thin films

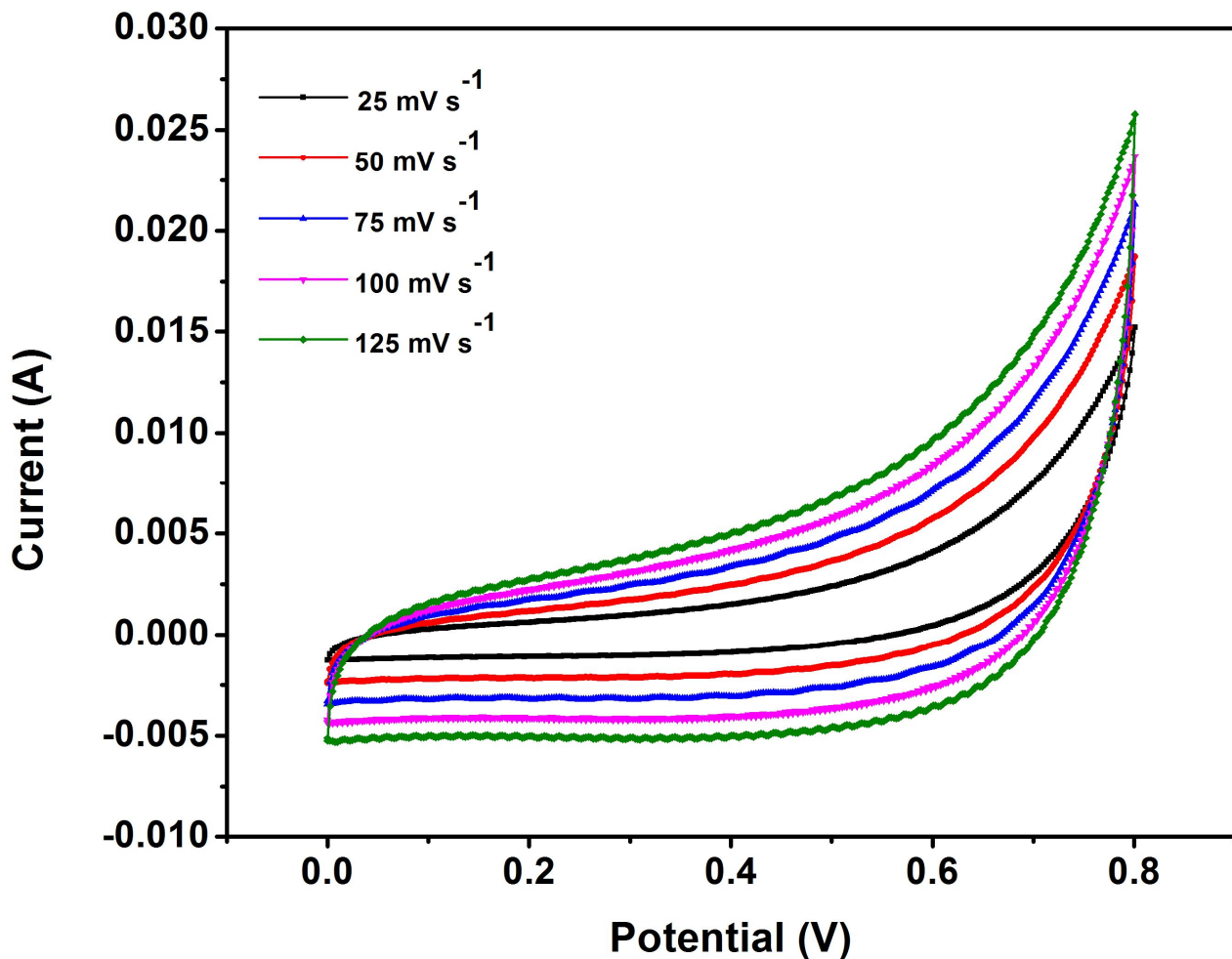


Figure 4-9 CV curves of SWCNT electrode at different scan rates from 25 to 125 mV s⁻¹

The calculated value of C_s of SWCNT from equation (1) is 74 Fg^{-1} at a scan rate of 125 mV s^{-1} . This value is higher than that of the recently reported value (Jha et al. 2012). The trapezoidal shape of the CV curves indicate that there was no reaction, it also substantiates the purity of the EHDA deposited SWCNT active layer and the process is very much suitable to fabricate thin films for applications in a wide range of electronic devices including supercapacitors.

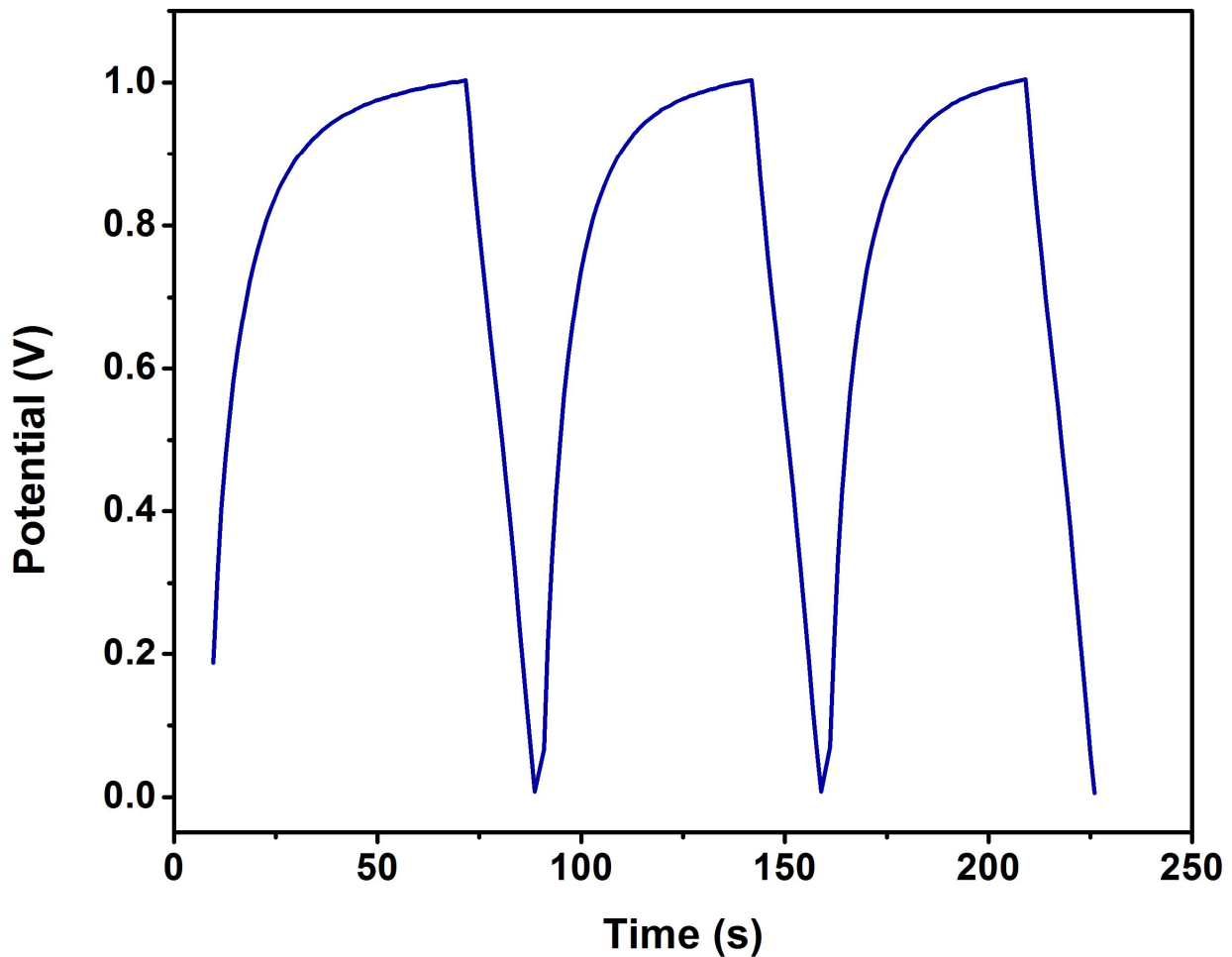


Figure 4-10 Galvanostatic charge–discharge curve of SWCNT electrode at a constant current density of 5 mA cm^{-2} in $1 \text{ M Na}_2\text{SO}_4$ electrolyte solution

To further evaluate the specific capacitance of SWCNT electrode, galvanostatic charge-discharge measurements have been performed in the potential range of 0-0.8 V. Figure 4-10 shows the typical galvanostatic charge-discharge curves of the SWCNT electrode for current density of 5 mA cm^{-2} . All the charge- discharge curves were linear and exhibited typical triangular shapes that reveal good electrochemical capacitive characteristics.

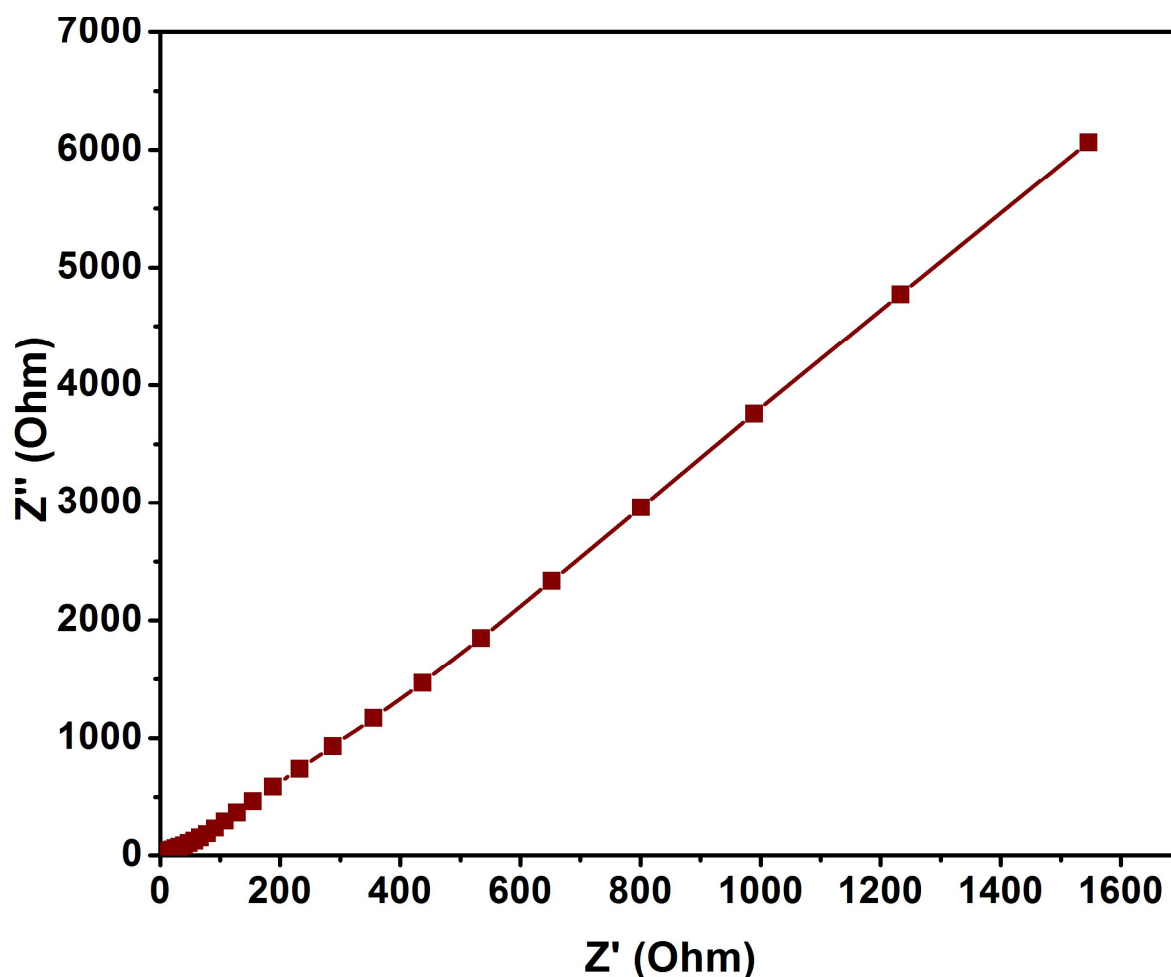


Figure 4-11 Nyquist plots for SWCNT electrode in 1 M Na₂SO₄ electrolyte solution

Electrochemical impedance spectroscopy analysis has been employed to study the vital behavior of the electrode materials for supercapacitors. The analysis was carried out in a frequency range of 0.1 Hz to 100 kHz using an open circuit potential with an AC perturbation of 10 mV. The Nyquist plots of the SWCNT electrode is shown in Figure 4-11. The impedance spectrum was a straight line at the lower frequencies and had slight arc-like curve at the higher frequencies. The straight line at low frequencies is known as Warburg resistance which corresponds to the dependence of ion diffusion on frequency. The arc at high frequencies corresponds to the charge transfer resistance which is very low in this EIS spectrum.

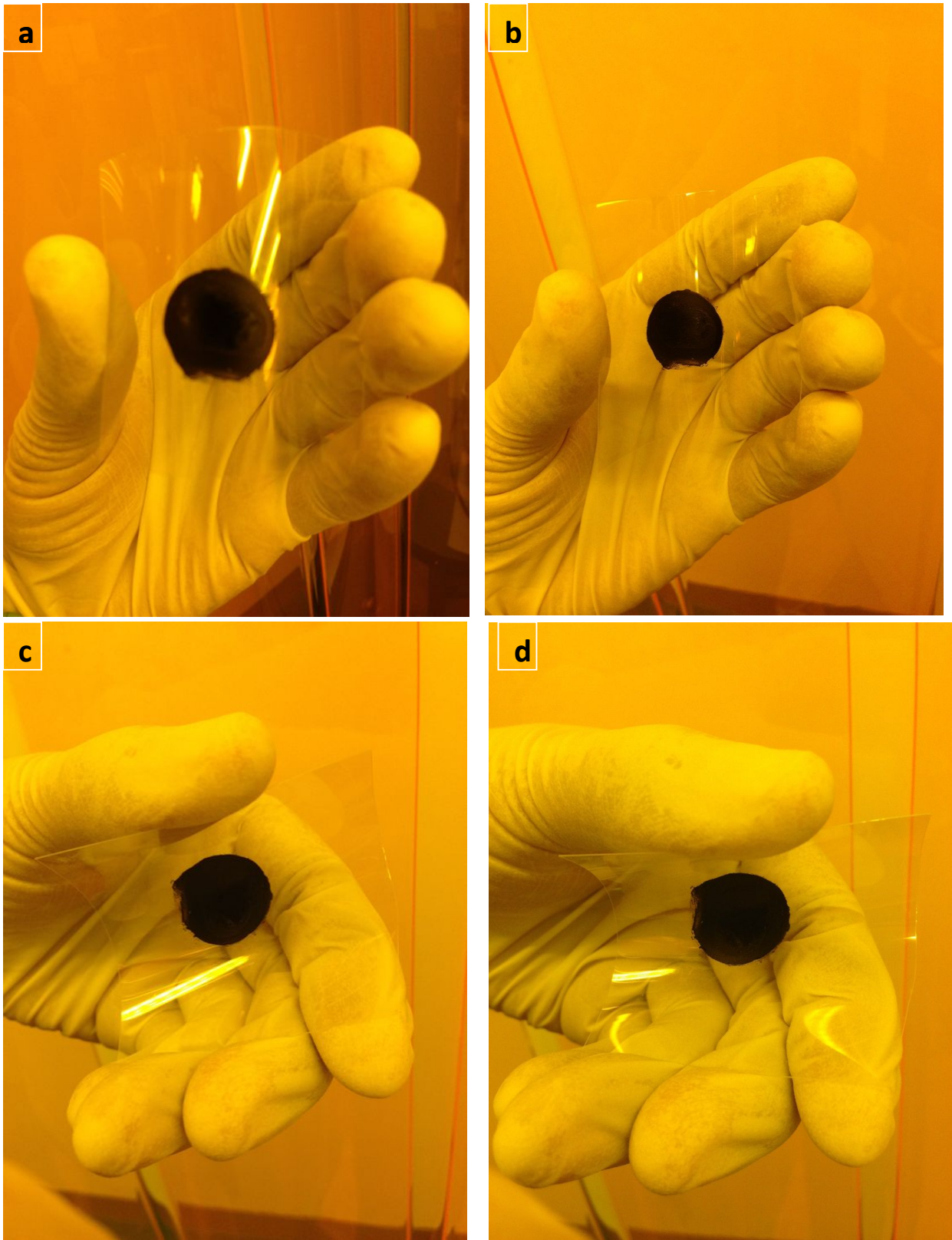


Figure 4-12 SWCNT active layer after (a) 50, (b) 100, (c) 200, (d) 300 flexing cycles

Flexibility test:

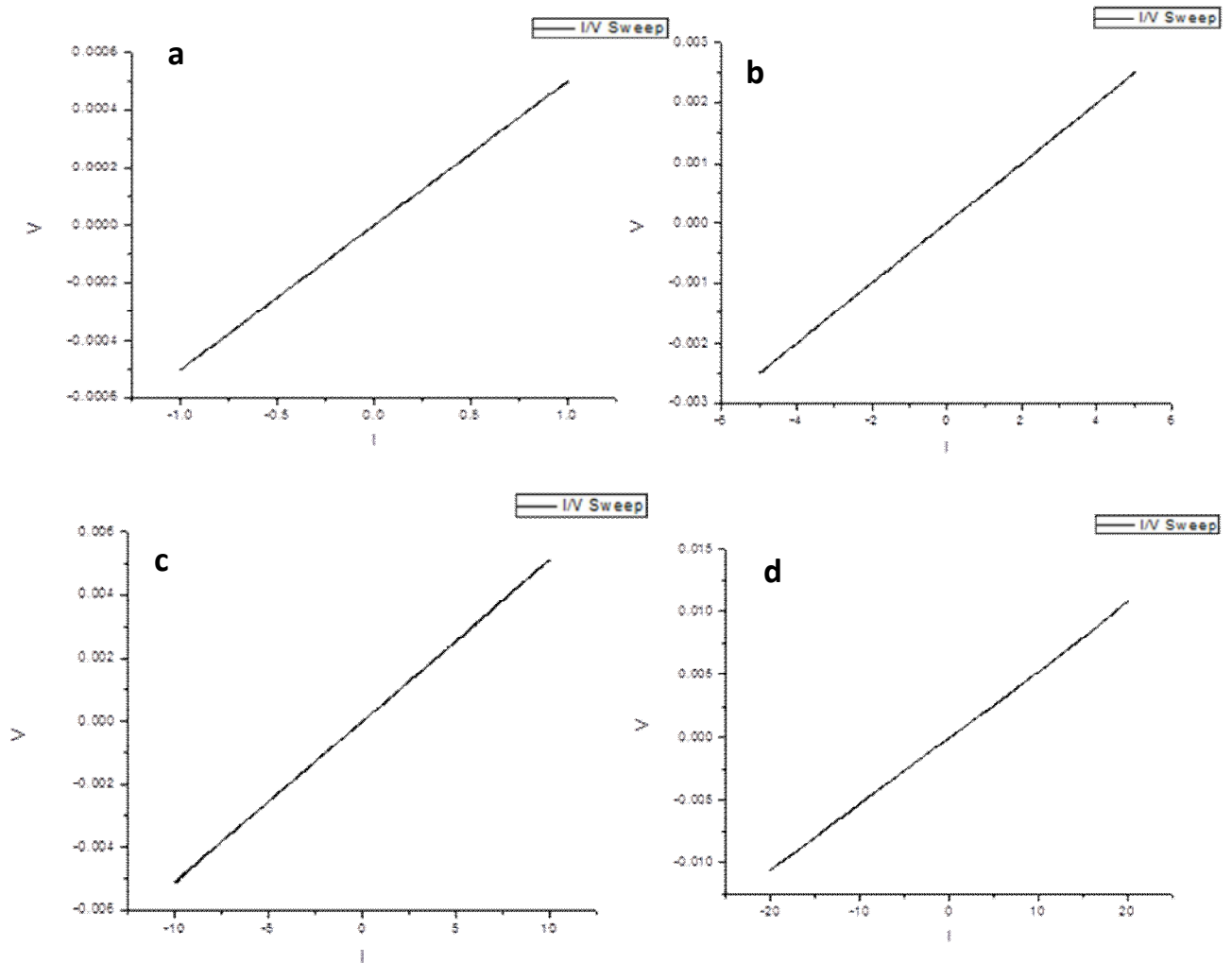


Figure 4-13 I-V characteristics of flexible SWCNT active layer after (a) 50, (b) 100, (c) 200, (d) 300 flexing cycles

I-V characteristics of the SWCNT active layers deposited on flexible PES substrate was analyzed after 50, 100, 200 and 300 flexing cycles. For all the cases, the I-V curves exhibited perfectly Ohmic behavior which implied that the deposited SWCNT active layers had good adhesion and can withstand the effects of flexing thus retaining their properties.

4.4 Conclusion

SWCNT thin films of 90 nm thickness have been fabricated employing EHDA technique which is an efficient, cost-effective, room temperature process suitable for mass production. The process parameters for achieving homogeneous thin films through Taylor cone formation were discussed. The XRD analysis confirmed purity of SWCNT thin films deposited through EHDA. The surface morphology of deposited SWCNT thin film revealed porous free, uniform surface. The optical study confirmed that the SWCNT has absorbance in the UV region and also exhibited good transmittance in the visible region. The band gap calculated was 3.1 eV. Electrical characteristic of deposited thin film shows good ohmic behavior and its current density has increased with temperature. Electrochemical studies revealed that the SWCNT electrodes have a capacitance of 74 Fg^{-1} . The electrodes exhibited excellent electrochemical stability. The flexibility test proved that flexible SWCNT layers produced through EHDA can retain their properties under flexing and suitable for flexible energy storage applications. The results substantiate that EHDA process has the potential to compete with conventional techniques despite being a room temperature process, and the SWCNT thin films thus produced are suitable for energy storage applications such as supercapacitors. Further development of hybrid electrodes and fabrication of stretchable devices are of future research interests.

5. Conclusions and Future Work

5.1 Summary and Major Conclusions

Electrohydrodynamic atomization technique has been successfully employed to fabricate ITO current collectors and SWCNT active layers onto flexible substrates for applications in flexible supercapacitors. The experimental observations of this work lend a hand in the understanding and further development of the EHDA technique. Stabilization of the Taylor cone is the key in this process and a lot of factors come into play. As far as solution/precursor properties are concerned, surface tension, viscosity, contact angle and conductivity are the crucial factors that influence the stability of the cone-jet. Meanwhile, process parameters such as applied electric field, liquid flow rate, nozzle diameter and stand-off distance contribute in determining the cone-jet stability. All these properties need to be taken into account while processing any given material through EHDA as the steady cone-jet transition occurs only within a limited range of operating parameters and liquid properties.

Optimization of the precursor involves achieving stable homogeneous solution/uniform dispersion while keeping other liquid properties (surface tension, viscosity, conductivity, etc.) under the range suitable for EHDA processing. This has been a challenge as the solvents differ for every material that is used. Few solvents, like water, are not suitable for EHDA processing owing to their high surface tension, yet they are desirable in developing eco-friendly devices. To address this issue miscible solvent combinations have been developed (IPA/Ethanol +DI water). The ratio of this combination varies according to the material used and its weight percent.

The surface properties of the substrate also play a major role in defining the quality of thin films and patterns produced by this technique. Comparative studies done on various substrates during the course of process optimization for each material substantiated that the substrates that are hydrophilic in nature yield good quality thin films. Hence, the substrates are subjected to plasma treatment after cleaning and before going in for the fabrication. Substrate speed is yet another parameter that influences the thickness and morphology of the deposited thin films. By the careful manipulation of the above said liquid properties and process parameters, the properties of the thin films/ produced can be controlled.

Nanostructured ITO thin films have been deposited by EHDA technique. XRD analysis confirmed the purity and crystalline nature of ITO thin films implying that the process introduced no impurities. Surface morphology of the thin films was smooth with densely packed nanocrystallites of uniform size. The optical studies showed that ITO is colourless and highly transparent with a transparency of 96%. Perfectly Ohmic behaviour of current-voltage curve validated the conducting nature of ITO thin films. The ITO thin film thus produced through this technique is a promising candidate to be used as highly transparent electrodes in energy storage applications, organic photovoltaics, organic light emitting diodes and in sensor modules.

Single walled carbon nanotube (SWCNT) thin films of 90 nm thickness have been fabricated employing EHDA technique. Purity of SWCNT thin films was verified by the XRD analysis. The surface morphology of deposited SWCNT thin film revealed porous free, uniform surface. The optical study confirmed that the SWCNT has absorbance in the UV region and also exhibit good transmittance in the visible region.

The band gap calculated from UV-vis spectra of SWCNT active layer was 3.1 eV. Electrical characteristic of deposited thin film shows good ohmic behavior and its current density has increased with temperature. The electrochemical studies revealed that flexible SWCNT electrodes fabricated through EHDA are promising candidates for energy storage applications. The specific capacitance measured from the CV curves was 74 Fg^{-1} . There EIS analysis proved that the SWCNT electrode offered little resistance with excellent conductivity at low and high frequencies alike. These results substantiate that EHDA process has the potential to compete with conventional techniques despite being a room temperature process. With the its flexibility to incorporate with roll to roll systems has the potential to mass produce feasible, high purity thin films at higher production rates without any need for isolated ambience.

5.2 Future Work

The future work include development of hybrid/composite electrodes the electrochemical study of flexible SWCNT thin films and extending thin film fabrication to stretchable substrates which is in progress. Fabrication of carbon based composite/hybrid electrodes involving polymers and metal oxides for the flexible and stretchable supercapacitors is of strong research interest. Furthermore, developing flexible and stretchable eco-friendly biosensors through EHDA has a great research scope. In addition to the development flexible and stretchable printed electronics devices, EHDA can be utilized in the fields of medicine as well. In particular, targeted drug delivery through nanoparticles with small molecule drugs and biologics has an attractive research space. EHDA can be employed to control the size, shape, chemical composition and surface characteristics of nanoparticles. Incorporation of synergetic drug combinations and programmed drug delivery can be accomplished.

References

Armand et al., Nature 451, 652 (2008)

Miller et al., Science 321, 651 (2008)

Alotto et al., Renewable and Sustainable Energy Reviews 29, 325 (2014)

Gu et al., Nano Letters 8, 2757 (2008)

Wang et al., J. Phys. Chem. C 113, 13103 (2009)

IEC Report, (2011)

Rayleigh et al., Proc. Royal Soc. 29, 71 (1879)

Poon, Thesis, Princeton University (2002)

Taylor et al., Proceedings of Royal society of London A313, 453(1969)

Calvo et al., Phys. Rev. 79, 217 (1997)

Taylor et al., Proc. Royal Soc. A. 280, 383 (1964)

Zeleny et al., Phys. Rev. 3, 69 (1914)

Chandrasekhar et al., Hydrodynamic and Hydromagnetic Stability, (Dover, New York, 1961)

Saville et al., Phys. Fluids 14, 1095 (1971)

Korkut, Thesis, Princeton University (2008)

Clooupeu et al., J. Aerosol Sci. 25, 1021 (1994)

Hartman, Thesis, Technical University, Delft (1998)

Calvo et al., J Aerosol Sci. 30, 863 (1999)

Wilhem, Thesis, University of Tübingen(2004)

Bonnefoi et al, J Power Sources 80, 149 (1999)

Simon et al., Nat Mater 7, 845 (2008)

Najafabadi et al., Adv. Mater. 22, E235 (2010)

Lu et al., Nanoletter 12, 5376 (2012)

Yuan et al., ACS Nano 6, 656 (2012)

Wu et al., ACS Nano 4, 5835 (2010)

Lu et al., Advanced Materials 24, 938 (2012)

Zhu et al., Science 332, 1537 (2011)

Burke et al., Electrochim. Acta 53, 1083 (2007)

Bao et al., Nano Letter 11, 1215 (2011)

El-Kady et al., Science 335, 1326 (2012)

Ye et al., Inorganic chemistry communications 30, 1 (2013)

Simon et al., Nat. Mater. 7, 845 (2008)

Rudge et al., J. Power Sources 47, 89 (1994)

Toupin et al., Chem. Mater. 16, 3184 (2004)

Zhu et al., Adv. Mater. 22, 3906 (2010)

Hamberg et al., Appl Phys Lett 40, 362 (1982)

Patel et al., Sens Actuators B 96, 180 (2003)

Hartnagel et al., Institute of Physics Publishing, Bristol: UK, (1995)

Senthilkumar et al., Vacuum 84, 864 (2010)

Carvalho et al., J. Non-Cryst. Solids 1208, 299 (2002)

Amaral et al., Surf. Coat. Technol. 125, 151 (2000)

Lee et al., Vacuum 77, 69 (2004)

Balasubramanian et al., J. Phys. D Appl. Phys. 22, 206 (1989)

Park et al., Surf. Coat. Technol. 161, 2 (2002)

Wu et al., J. Appl. Phys. 86, 991 (1999)

Suzuki et al., Thin Solid Films 411, 23 (2002)

Mortan et al., Vacuum Technol. Coat., 53 (2000)

Muhammad et al., Current Applied Physics 11, 68 (2011)

Qin et al., Semicond. Sci. Technol. 27, 04505 (2012)

Ajayan et al., Nature 361, 333 (1993)

Fukushima et al., Science 300, 2072 (2003)

Najafabadi et al., Adv Mater 22, 235 (2010)

Huang et al., J Mater Res 25, 1525 (2010)

Xu et al., Mater Lett 65, 1878 (2011)

Pop et al., Nano Lett 6, 96 (2006)

Kimizuka et al., Carbon 46, 1999(2008)

Chopra et al., Thin Solid Films 102, 1 (1983)

Garcia et al., Sci Technol Adv Mater 4, 397 (2003)

Muhammad et al., Curr Appl Phys 11, S68 (2011)

Calvo et al., J Aerosol Sci 30, S547 (1999)

Cloupeau et al., J Electrostat 22, 135 (1989)

Grace et al., J Aerosol Sci 25, 1005 (1994)

Chew et al., Carbon 47 2976 (2009)

Wang et al., Carbon 47, 1359 (2009)

Titus et al., J Mater Eng Perform 15, 182 (2006)

Chou et al., Adv Powder Technol 21, 542 (2010)

Jha et al., Adv Energy Mater 2, 438 (2012)

APPENDIX

List of Publications

1. Nauman Malik Muhammad, **Sridharan Sundharam**, Hyun-Woo Dang, Ayoung Lee, Beyoung-Hwan Ryu, and Kyung-Hyun Choi, CIS layer deposition through electrospray process for solar cell fabrication, Current Applied Physics 11 (2011) S68-S75.
2. **Sridharan Sundharam**, Jeongdai Jo, Hyun-Woo Dang, Yang-Hoi Doh, and Kyung Hyun Choi, Structural and Electrical Studies of Electrohydrodynamic Atomized ITO Thin Films, Journal of NanoScience and NanoTechnology 1 (2013) 63-66.
3. **Sridharan Sundharam** and Kyung-Hyun Choi, Fabrication of flexible SWCNT thin films through electrohydrodynamic atomization technique and investigation of their electrical properties, Materials Letters 115 (2014) 215–218.

Conference

1. **Sridharan Sundharam**, Nauman Malik Muhammad, Saleem Khan, Hyun-Woo Dang, Sung Jei Hong, Dong Soo Kim and Kyung Hyun Choi, Fabrication of ITO Layers through Electro Spray Deposition Process for Application in OLEDs, THE 7th INTERNATIONAL WORKSHOP ON MICROFACTORIES 24-27 OCT. 2010, DAEJEON, Republic of Korea.